THE DEPOLARIZATION OF RAYLEIGH SCATTERED LIGHT

Thesis for the Degree of Ph. D.
MICHIGAN STATE UNIVERSITY
ROBERT J. ANDERSON
1967

This is to certify that the

thesis entitled

The Depolarization of Rayleigh Scattered Light

presented by

Robert J. Anderson

has been accepted towards fulfillment
of the requirements for

Ph.D. degree in Chemistry

Jack B Kinsinger
Major professor

Date July 24, 1967

O-169

ABSTRACT

THE DEPOLARIZATION OF RAYLEIGH SCATTERED LIGHT

by Robert J. Anderson

The depolarization of light, Rayleigh scattered from pure liquids, binary solutions, and polymer solutions, has been studied by measuring the depolarization ratio, ρ_V, for vertically polarized light. The theory of depolarization by dense fluids has been reviewed, put into a form consistent with the theory of partial polarization, and extended to include the temperature dependence.

The depolarization ratio and its temperature dependence were measured using a helium-neon laser as the light source, a phase sensitive detection system, and a photometer designed to take advantage of the laser output. The results obtained are considered to be the most accurate available, since the methods used in this study have removed the sources of most of the difficulties previously encountered in these measurements.

The experimental techniques are discussed in considerable detail, and potential improvements in the system are included. Moreover, an analysis of the errors inherent in this method yields an indication of the overall accuracy of the result, and shows what limitations are to be expected on measurements of this type.

The results indicate that the depolarization ratio of vertically polarized light has a temperature dependence somewhere between linear and logarithmic. The theory is found to agree well with the experimental results in the case of polar molecules, while for non-polar molecules agreement is poor for those species with a high degree of symmetry. These results have been interpreted as indicating that the hyperpolarizabilities play a significant role in determining the depolarization by pure liquids.

In binary solutions, it is found that the results agree well with theory at intermediate compositions, even when the two pure components do not.

THE DEPOLARIZATION OF RAYLEIGH SCATTERED LIGHT

By

Robert J. Anderson

A THESIS

Submitted to
Michigan State University
in partial fulfillment of the requirements
for the degree of

DOCTOR OF PHILOSOPHY

Department of Chemistry

1967

ACKNOWLEDGEMENTS

The author wishes to acknowledge the assistance of the following persons, without whom this study would have been impossible: Mr. James Grumblatt, electronics technician; Mr. Russell Geyer, machinist; Mr. Andrew Seer, glassblower; Mr. Larry Dosser, for his enthusiastic assistance; and Professor J. B. Kinsinger, for his encouragement and advice.

TABLE OF CONTENTS

TABLE OF CONTENTS (Continued)

CHAPTER Page

LIST OF TABLES

TABLE Page

LIST OF TABLES (Continued)

LIST OF FIGURES

LIST OF FIGURES (Continued)

LIST OF APPENDICES

CHAPTER I

INTRODUCTION

Historical

Recorded light scattering measurements date back to 1802, when Richter[1] observed the scattering from a sol of colloidal gold. Tyndall[2] obtained an artificial blue sky in a mixture of butyl nitrate and hydrochloric acid, and showed that if the incident rays were plane polarized the scattering was only visible in one plane. This so-called "Tyndall Effect" became the starting point of the light scattering investigations of Lord Rayleigh,[3] and in subsequent papers he outlined a complete theory based on induced moments in the scattering particles. Since then, the theoretical and experimental study of light scattering has been steadily pursued, until today it has become a sophisticated tool for the study of molecular properties.

In recent years interest has centered on two distinct areas: linear, or Rayleigh scattering, and non-linear, or Raman scattering. Since the Raman effect is more closely related to spectroscopy, it will not be discussed here, and instead we will concentrate on the treatment of Rayleigh scattering.

Calculations on the scattering of a system may be approached in two ways: quadrature summation of the radiation contributions from each scattering particle, or treatment of the scattering as the result of statistical fluctuations in the bulk dielectric constant of the medium. Actually, these methods are not completely independent, and the exact treatment of a scattering system involves consideration of both approaches. Quadrature summation was originally used by Rayleigh,[3] in the calculation of the scattering from a gas, and has since been extended by Debye[18] to the case of a dilute solution of non-interacting high polymers. The fluctuation theory was developed by Einstein,[4] Smoluchowski, and Gans, and has applications in the scattering from pure liquids as well as solutions of interacting particles.

Rayleigh Scattering

The behavior normally referred to as Rayleigh scattering is actually the sum of three scattering processes:

(1) Scattering of the incident light, ν_o, with no change in frequency, from entropy fluctuations in the medium, giving rise to a narrow, .01cm^{-1}, line.

(2) Scattering of the incident light at some shifted frequency, ν', from density fluctuations propogated at the velocity of sound. This scattering corresponds to modulation of the incident light by a Doppler shift, $\Delta\nu$, such that

$$\nu' = \nu_o \pm \Delta\nu$$

where $\Delta\nu$ is of the order of $.5\text{cm}^{-1}$.

(3) Scattering from orientation fluctuations in the liquid, giving rise to a very broad (tens of cm^{-1}) background centered about the frequency of the incident light. This corresponding to modulation of the incident light by a highly damped rotational Raman effect having, again, both Stokes and anti-Stokes components.

The first process giving rise to the central unshifted line, is the actual Rayleigh (or Tyndall) scattering; the two Doppler shifted sidebands comprise the Brillouin doublet; and the broad background is the Rayleigh wing. Recently, Cummins and Gammon[19] have shown that the Rayleigh and Brillouin lines are highly polarized.

The quantity which is generally of interest in a light scattering measurement is the Rayleigh ratio, $R(\theta)$, where θ is the angle with respect to the incident light at which the observation is made. Using vertically polarized incident light, we may write for pure fluids of small molecules,

$$R_v(\theta) = \frac{2\pi^2}{\lambda^4 N} RT\,\overline{\kappa}\left[\frac{n}{\alpha}\right]^2 \left[\frac{dn}{dT}\right]^2 \left[\frac{3 + 3\rho_v}{3 - 4\rho_v}\right] (1 + \cos^2\theta) \qquad (1\text{-}1)$$

where subscript v denotes the vertical polarization of the incident light, N is Avogadros number, λ the wave length of the incident light, R the gas constant, T the absolute temperature, n the refractive index, $\bar{\kappa}$ the isothermal compressibility, α the coefficient of thermal expansion, and ρ_v the vertical depolarization ratio of the medium. (1-1) may be rewritten, when $\theta = 90°$, as

$$R_v(90) = \left[I_R + 2I_B + 1.75\ I_W\right] \frac{r}{I_o} \tag{1-2}$$

where I_o is the incident intensity, r is the distance to the detector, I_R the intensity of the central, or Rayleigh, line, I_B the intensity of each of the Brillouin sidebands, and I_W the total intensity of the Rayleigh wing.

Moreover, the scattered radiation contains both a vertically polarized, V_v, and a horizontally polarized, H_v, component, such that

$$\begin{aligned} V_v &= I_R + 2I_B + I_W \\ H_v &= 0.75\ I_W. \end{aligned} \tag{1-3}$$

These terms each contain an inverse fourth power dependence on the wavelength, making it necessary, in the past, to perform scattering measurements using blue or green light, and to utilize large light sources. This practice has given rise to ambiguities due to fluorescence in the medium, uncertainty in the wavelength, multiple scattering due to the source size and wavelength, and optical and electronic noise.

The development of the ruby laser by Maiman,[5] and the helium-neon laser by Javan,[6] has largely alleviated these difficulties. The laser emission is highly collimated, monochromatic, and extremely intense, reducing both spatial and temporal uncertainties in the light source. In addition, the longer wavelengths and higher intensities available from lasers allow measurements to be made without fluorescence, and with small enough beams that multiple scattering is minimized. Moreover, the extremely narrow band-pass of the laser output permits observation of the individual components of the Rayleigh scattering. That is, using laser sources, and interferometric techniques, the individual Rayleigh, Brillouin, and Rayleigh wing components may be resolved. In this study, as we are interested in measuring the unresolved scattering, we shall consider the Rayleigh-Brillouin lines, and Rayleigh wing, all to be part of the Rayleigh scattering.

Purpose of this Research

A preliminary study was undertaken to determine the characteristics of the Rayleigh scattered light, using a helium-neon laser operating at 632.8 nm as the source. These experiments utilized a Brice-Phoenix light scattering photometer in its customary configuration, the only modification being the replacement of the mercury lamp by the helium-neon laser. After careful calibration of the instrument (neutral density filters, diffusers, refraction corrections, etc.) it was found, using pure liquids, that the results of the measurement were consistent with published data for this instrument except for the depolarization ratio, ρ_V. The depolarization ratio was observed to be difficult to measure consistently, due to instrumental factors such as uncertainty in the angle of observation, uncertainty in the polarizers and resolvers, stray light within the photometer, and noise in the electronics. Moreover, examination of the light scattering literature (see, for example, Stacey[20]) showed that the same uncertainty existed in values of ρ_V measured elsewhere. Since (1-1) shows that this value is of considerable importance in the Rayleigh ratio, and since examination of the literature showed that the depolarization ratio had not been studied extensively, it was decided to apply the superior characteristics of the helium-neon laser to the study of the depolarization of Rayleigh scattered light. It was decided moreover, to investigate both the theoretical and experimental basis for the existing knowledge of the depolarization ratio, and to extend this basis to include the temperature dependence of ρ_V.

It is hoped that the results of this study will serve to remove some of the uncertainties in the existing light scattering data, and to form the basis of an expanded inquiry into the nature of the depolarization process.

CHAPTER II

THEORY

Electromagnetic Field Properties

Maxwell's Equations

The basic concepts of electrodynamics were formulated in the early part of the nineteenth century, and were summarized by Maxwell in a consistent set of equations known as Maxwell's Equations.

The state of an electromagnetic field may be represented by five field vectors, viz. the electric vector $\overline{E}$, the magnetic vector $\overline{H}$, the electric displacement $\overline{D}$, the magnetic induction $\overline{B}$, and the current density $\overline{J}$. These field vectors are then related by: (ρ being the charge density)

$$\overline{\nabla} \times \overline{H} = \frac{4\pi}{c} \overline{J} + \frac{1}{c} \partial\overline{D}/_{\partial t} \tag{2-1}$$

$$\overline{\nabla} \times \overline{E} = - \frac{1}{c} \partial\overline{B}/_{\partial t} \tag{2-2}$$

$$\overline{\nabla} \cdot \overline{B} = 0 \tag{2-3}$$

$$\overline{\nabla} \cdot \overline{D} = 4\pi\rho \tag{2-4}$$

where, as is customary in optics, we have used Gaussian units. These relations however, are not sufficient to allow a unique determination of the field, and must therefore be supplemented by a set of equations which describe the behavior of a material under the influence of the field. These equations are known as the constitutive relations, and are in general very complicated; however, if the material is at rest and is isotropic they take the form:

$$\bar{J} = \sigma\bar{E} \tag{2-5}$$

$$\bar{D} = \epsilon\bar{E} \tag{2-6}$$

$$\bar{B} = \mu\bar{H} \tag{2-7}$$

where σ is the specific conductivity, ϵ is the dielectric constant, and μ is the magnetic permeability (in vacuum $\epsilon = \mu = 1$).

Field Intensity and the Poynting Vector

Using Maxwell's Equations, we may develop the energy law for an electromagnetic field. We see from (2-1), and (2-2) that

$$\bar{E}.\bar{\nabla} \times \bar{H} - \bar{H}.\bar{\nabla} \times \bar{E} = \frac{4\pi}{c}\,\bar{J}.\bar{E} + \frac{1}{c}\,\bar{E}.\dot{\bar{D}} + \frac{1}{c}\,\bar{H}.\dot{\bar{B}} \tag{2-8}$$

where the dot refers to differentiation with respect to time. This result may be rewritten as:

$$\bar{\nabla}.(\bar{E} \times \bar{H}) + \frac{1}{c}\,(\bar{E}.\dot{\bar{D}} + \bar{H}.\dot{\bar{B}}) + \frac{4\pi}{c}\,\bar{J}.\bar{E} = 0, \tag{2-9}$$

and multiplying by $c/4\pi$, integrating, and applying Gauss's theorem yields

$$\frac{1}{4\pi}\int(\bar{E}.\dot{\bar{D}} + \bar{H}.\dot{\bar{B}})\,dV + \int \bar{J}.\bar{E}\,dV + \frac{c}{4\pi}\int_S \bar{E} \times \bar{H}.\bar{n}\,dS = 0 \tag{2-10}$$

$\bar{n}$ being a unit vector normal to the surface S, of the volume V. Equation (2-10) represents the energy distribution of an electromagnetic field, and is valid for any material. In the case of linear, isotropic media, we may use the constitutive relations to find that,

$$\frac{1}{4\pi}(\overline{E}.\dot{\overline{D}}) = \frac{1}{4\pi}\overline{E}.\frac{\partial(\varepsilon\overline{E})}{\partial t} = \frac{1}{8\pi}\frac{\partial(\varepsilon\overline{E}^2)}{\partial t} = \frac{1}{8\pi}\frac{\partial}{\partial t}(\overline{E}.\overline{D}) \qquad (2\text{-}11)$$

$$\frac{1}{4\pi}(\overline{H}.\dot{\overline{B}}) = \frac{1}{4\pi}\overline{H}.\frac{\partial}{\partial t}(\mu\overline{H}) = \frac{1}{8\pi}\frac{\partial}{\partial t}(\mu\overline{H}^2) = \frac{1}{8\pi}\frac{\partial}{\partial t}(\overline{H}.\overline{B}) \qquad (2\text{-}12)$$

Setting

$$W_E = \frac{1}{8\pi}\overline{E}.\overline{D}$$
$$W_M = \frac{1}{8\pi}\overline{H}.\overline{B} \qquad (2\text{-}13)$$

and

$$W = \int(W_E + W_M)\, dV \qquad (2\text{-}14)$$

where W_E and W_M represent the electric and magnetic energy of the field respectively, equation (2-10) becomes

$$dW/dt + \int \overline{J}.\overline{E}\, dV + \frac{c}{4\pi}\int_S (\overline{E}\times\overline{H})\,.\overline{n}\, dS = 0. \qquad (2\text{-}15)$$

We may now define a vector, $\overline{S}$, and a scalar Q, by the relations

$$\overline{S} = \frac{c}{4\pi}(\overline{E}\times\overline{H}) \qquad (2\text{-}16)$$

$$Q = \int \overline{J}.\overline{E}\, dV = \int \sigma\overline{E}^2\, dV \qquad (2\text{-}17)$$

so that the conservation of energy in the field is expressed by

$$dW/dt = -Q - \int_S \overline{S}\,.\,\overline{n}\, dS \qquad (2\text{-}18)$$

The vector $\overline{S}$ is known as the Poynting Vector, and from (2-18) may be interpreted as the representation of the flow of the energy density. The direction of $\overline{S}$ is the direction of motion of the field, while the magnitude is the energy density of the field per unit time. The term Q represents the dissipation of energy (as Joule heat) at the expense of the field, and for a non-conductor ($\sigma = 0$) is zero. The compounds to be considered in the following are approximately lossless (i.e. transparent) and may therefore be considered to be non-conductors. In this case the conservation law (2-18) may be written in the form of a continuity equation:

$$dW/dt + \overline{\nabla} \cdot \overline{S} = 0 \qquad (2\text{-}19)$$

which is particularly useful in application to geometrical optics.

The intensity of an electromagnetic wave is usually defined as the time average of the absolute value of the Poynting vector, or,

$$I = |\langle\overline{S}\rangle| . \qquad (2\text{-}20)$$

Using equation (2-16) we may then write

$$\langle\overline{S}\rangle = \frac{1}{2T'} \int_{-T'}^{T'} \frac{c}{4\pi} (\overline{E} \times \overline{H})\, dt \qquad (2\text{-}21)$$

where T' is a time interval large compared to the fundamental period of the wave. Then, writing the expression for the time-harmonic field as

$$\left.\begin{aligned}\overline{E}(\overline{r},t) &= \text{Re}\left\{\overline{E}_o(\overline{r})\ e^{-i\omega t}\right\}\\ \overline{H}(\overline{r},t) &= \text{Re}\left\{\overline{H}_o(\overline{r})\ e^{-i\omega t}\right\}\end{aligned}\right. \tag{2-22}$$

we have that

$$<\overline{S}> = \frac{c}{16\pi}\frac{1}{2T'}\int_{-T'}^{T'}\left[\overline{E}_o\times\overline{H}_o e^{-2i\omega t}+\overline{E}_o\times\overline{H}_o^*+\overline{E}_o^*\times\overline{H}_o+\overline{E}_o^*\times\overline{H}_o^* e^{2i\omega t}\right]dt \tag{2-23}$$

or

$$<\overline{S}> = \frac{c}{16\pi}\left(\overline{E}_o \times \overline{H}_o^* + \overline{E}_o^* \times \overline{H}_o\right) \tag{2-24}$$

$$<\overline{S}> = \frac{c}{8\pi}\ \text{Re}\ \left(\overline{E}_o \times \overline{H}_o^*\right) \tag{2-25}$$

Applying a well known result of vector analysis, we now have that

$$I = |<\overline{S}>| = \frac{c}{8\pi}|\overline{E}_o||\overline{H}_o^*| \tag{2-26}$$

The Electromagnetic Plane Wave

In the remainder of this work we shall be concerned primarily with electromagnetic plane waves. Not only do such plane waves represent the simplest electromagnetic field, but, as we shall see later, for the phenomena of interest they represent a valid approximation to the true field distribution. For such waves we have the well known results:

$$\left.\begin{aligned}\overline{E}_o &= -\sqrt{\frac{\mu}{\varepsilon}}\ \overline{s} \times \overline{H}_o\\ \overline{H}_o &= -\sqrt{\frac{\varepsilon}{\mu}}\ \overline{s} \times \overline{E}_o\end{aligned}\right\} \tag{2-27}$$

where $\bar{s}$ is a unit vector in the direction of the Poynting Vector, $\bar{S}$. Scalar multiplication with $\bar{s}$ gives

$$\bar{E}_o.\bar{s} = \bar{H}_o.\bar{s} = 0 \tag{2-28}$$

which shows that $\bar{E}_o$, $\bar{H}_o$, and $\bar{s}$ form a right-handed, orthogonal coordinate system. We also have, from (2-27), that

$$\sqrt{\mu}|\bar{H}_o| = \sqrt{\varepsilon}|\bar{E}_o| \tag{2-29}$$

Using (2-27) and (2-26) we see that the intensity of the plane wave may now be given by

$$I = \frac{c}{8\pi}\sqrt{\frac{\varepsilon}{\mu}}\,|E_o|^2. \tag{2-30a}$$

Thus, we have an expression for the intensity of an electromagnetic plane wave in terms of the spatial portion of the time-harmonic field. In free space, $\varepsilon = \mu = n = 1$ (where n is the index of refraction) so that we may write (2-30) as

$$I = \frac{c}{8\pi}\,[\bar{E}.\bar{E}^*]. \tag{2-30b}$$

Since a dilute gas has a refractive index close to one, (2-30) represents a good approximation to the intensity in a gas.

Coherence Matrix Formalism

Introduction

In this research we propose to study the interaction of polarized radiation with matter, and subsequently generalize this interaction in terms of the theory of partial polarization. In what follows, we shall concern ourselves first with the mathematical formalism that describes the polarization properties of a wave field, and shall see that the formalism introduces considerable simplicity when the polarization properties of a complex system are investigated.

We restrict the wave field to a plane-wave propagating along the positive z-axis of a right-handed space-set of axes. The effect of a given system on the polarization properties of the wave, may then be described as an operation on the incoming wave field to produce the outgoing wave. We must therefore describe the system uniquely with a transformation of the representation of the incoming wave to the representation of the outgoing wave.

Stokes[10] was the first to describe the field in terms of observables, called the four Stokes parameters, which refer to both the total intensity and state of polarization of the field. Jones[11] reconsidered the problem of monochromatic (hence fully polarized) beams and introduced the use of matrix algebra. Jones' matrix elements are not observables of the field however, so that Mueller[12] introduced a transformation of the Jones method such that the matrix elements became the Stokes parameters of the field. The more recent treatments employ the use of correlation functions and "coherence matrices," which were originated by Wiener and Wolf.[12]

Jones Calculus

Jones considered monochromatic (hence fully polarized) fields so that we can describe a wave by its two spatial components, E_x, and E_y, where E_x and E_y are time harmonic. Using vector notation we then have:

$$\overline{E} = \begin{bmatrix} E_x \\ E_y \end{bmatrix} \tag{2-31}$$

and $\overline{E}$ is a unique representation of the field. We can then describe the effect of any linear system on the wave field by a linear operation $\overline{L}$ such that,

$$\overline{L} = \begin{bmatrix} a & b \\ c & d \end{bmatrix} \tag{2-32}$$

The wave field outgoing from the system is then given by,

$$\overline{E}' = \overline{L}\,\overline{E}. \tag{2-33}$$

Using equation (2-30) we see that the total intensity of the wave field is given by, (to within a constant)

$$I = I_x + I_y = |E_x|^2 + |E_y|^2 \tag{2-34}$$

For N operations on the field, the N - operators may be multiplied together to yield a combined operator matrix, $\bar{L}$, for the system (i.e. $\bar{L} = \bar{L}_n \bar{L}_{n-1} \ldots \bar{L}_2 \bar{L}_1$). In reality however monochromatic wave fields are idealizations, and we must consider the more realistic quasimonochromatic approximation to the wave field. The two component representation is now not sufficient to uniquely represent the field however, and we must extend the arguments to a higher order representation of the field.

Coherence Matrices

We now formulate the coherence matrix representation of the wave field by considering a quasimonochromatic light wave of mean frequency $\bar{\nu}$ propagating in the positive z-direction. Wolf[4] has shown that the effect of an optical instrument is the same for the mean frequency as for all Fourier components of the field. Let

$$\begin{aligned} E_x(t) &= a_1(t) \exp\left[i(\phi_1(t) - 2\pi\bar{\nu}t)\right] \\ E_y(t) &= a_2(t) \exp\left[i(\phi_2(t) - 2\pi\bar{\nu}t)\right] \end{aligned} \qquad (2\text{-}35)$$

represent two mutually orthogonal components of the field, at a point x in the field, at time t. Now, the coherence matrix $\bar{J}$ is defined by the direct product,

$$\bar{J} = \langle \bar{E} \times \bar{E}^{\dagger} \rangle = \begin{bmatrix} \langle E_x E_x^{*} \rangle & \langle E_x E_y^{*} \rangle \\ \langle E_y E_x^{*} \rangle & \langle E_y E_y^{*} \rangle \end{bmatrix} = \begin{bmatrix} J_{xx} & J_{xy} \\ J_{yx} & J_{yy} \end{bmatrix} \qquad (2\text{-}36)$$

Where $\overline{E}$ is the two component column vector with elements E_x and E_y given by equation (2-35), and the vector $\overline{E}^\dagger$ is the Hermitian conjugate of $\overline{E}$. The <> stands for the time average. Now, according to the Jones method, when such a beam of light interacts with an instrument described by an operator $\overline{L}$, the outgoing beam is given by, $\overline{E}' = \overline{L}\ \overline{E}$, and therefore the coherence matrix, $\overline{J}'$, of the outgoing beam is

$$\overline{J}' = \langle \overline{E}' \times \overline{E}'^\dagger \rangle \tag{2-37}$$

$$\overline{J}' = \langle \overline{L}\ \overline{E} \times \overline{E}^\dagger \overline{L}^\dagger \rangle \tag{2-38}$$

and since $\overline{L}$ is independent of time,

$$\overline{J}' = \overline{L} \langle \overline{E} \times \overline{E}^\dagger \rangle \overline{L}^\dagger \tag{2-39}$$

and from (2-36) we have,

$$\overline{J}' = \overline{L}\ \overline{J}\ \overline{L}^\dagger \tag{2-40}$$

which is the transformation law for the coherence matrix. The total intensity of the field is given by (2-34) so that we can write

$$I = J_{xx} + J_{yy} = \mathrm{Tr}\ \overline{J}, \tag{2-41}$$

where I is the intensity, and J_{xx} and J_{yy} are the diagonal matrix elements of $\overline{J}$.

Since the matrix elements of the coherence matrix are physical observables, the coherence matrix is Hermitian and is sufficient to supply the state of polarization of the field. Further, the intensity of the outgoing beam can be found from (2-40),

$$I' = \mathrm{Tr}\ \bar{J}' = \mathrm{Tr}\ (\bar{L}\ \bar{J}\ \bar{L}^{\dagger}) \tag{2-42}$$

$$I' = \mathrm{Tr}\ [(\bar{L}^{\dagger}\bar{L})\bar{J}] \tag{2-43}$$

we can therefore treat a cascade of instruments as a lumped parameter, operating on the incoming coherence matrix to produce an output of intensity I'.

Instrument Operators

The instrumentoperator, $\bar{L}$, is easily generated from the physics of any optical instrument since $\bar{L}$ operates directly on the components of the field E_x, and E_y. Let us consider the case of a polarizing element such as a Nicol prism, which passes only a particular component of the field, such as the component making an angle θ with the x-axis. Then we have the relations

$$E_x' = E_x \cos^2 \theta + E_y \sin \theta \cos \theta \tag{2-44}$$

$$E_y' = E_x \sin \theta \cos \theta + E_y \sin^2 \theta \tag{2-45}$$

We then have by inspection that

$$\bar{L} = \begin{bmatrix} \cos^2 \theta & (\sin \theta \cos \theta) \\ (\sin \theta \cos \theta) & \sin^2 \theta \end{bmatrix} = \bar{P}(\theta) \tag{2-46}$$

which is Hermitian and real. $\bar{L}$ is thus represented by a projection operator $\bar{P}(\theta)$, and satisfies the relations,

$$\overline{P}^{\dagger}(\theta) = \overline{P}(\theta) \tag{2-47}$$

$$\overline{P}(\theta)\ \overline{P}^{\dagger}(\theta) = \overline{P}(\theta)\ \overline{P}(\theta) = \overline{P}(\theta) \tag{2-48}$$

Table 2.1 gives the instrument operators of the most usual devices as shown in Wolf.[12]

Coherence Matrices for Cases of Special Interest

Wolf has shown that we may express the intensity of a field in terms of θ and E, the angles of observation and retardation, as,

$$I(\theta,E) = J_{xx} \cos^2\theta + J_{xy} \sin^2\theta + 2 \cos\theta \sin\theta \, \mathrm{Re}(J_{xy} e^{-iE}) \tag{2-49}$$

where Re means the real part of the argument.

TABLE 2.1--The 2 x 2 Coherence Matrix Representation of Certain Optical Instruments

INSTRUMENT	2 x 2 REPRESENTATION
COMPENSATOR: Introduces a phase difference of 2δ	$\overline{C}(\delta) = \begin{bmatrix} e^{i\delta} & o \\ o & e^{-i\delta} \end{bmatrix}$
ROTATOR: Rotates the plane of polarization counterclockwise an angle θ about the z-axis	$\overline{R}(\theta) = \begin{bmatrix} \cos\theta & -\sin\theta \\ \sin\theta & \cos\theta \end{bmatrix}$
POLARIZER: Takes the projection of the E field making an angle ϕ with the x-axis	$\overline{P}(\phi) = \begin{bmatrix} \cos^2\phi & (\cos\phi \sin\phi) \\ (\cos\phi \sin\phi) & \sin^2\phi \end{bmatrix}$
ABSORBER: η_x and η_y are the absorption coefficients in the x and y directions	$\overline{A} = \begin{bmatrix} e^{-\eta x} & o \\ o & e^{\eta x} \end{bmatrix}$

Now, we can determine the coherence matrix for completely unpolarized light, since it must obey the condition

$$I(\theta, E) = \text{Constant} \tag{2-50}$$

This implies that $J_{xy} = 0 = J_{yx}^*$, and $J_{xx} = J_{yy}$, and the coherence matrix is given by,

$$\bar{J} = \frac{I}{2}\begin{bmatrix} 1 & 0 \\ 0 & 1 \end{bmatrix} \tag{2-51}$$

In a similar fashion, the coherence matrices of other polarization states may be found, and are tabulated in Table 2.2.

TABLE 2.2.--The Coherence Matrices of some Special States of Polarization

STATE OF POLARIZATION	$\bar{J}$
Plane of Polarization in xz plane	$\begin{bmatrix} 1 & 0 \\ 0 & 0 \end{bmatrix}$
Plane of Polarization in yz plane	$\begin{bmatrix} 0 & 0 \\ 0 & 1 \end{bmatrix}$
Plane of Polarization at 135° to xz plane	$\begin{bmatrix} 1 & -1 \\ -1 & 1 \end{bmatrix}$
Right Circular Polarization	$\begin{bmatrix} 1 & i \\ -i & 1 \end{bmatrix}$
Left Circular Polarization	$\begin{bmatrix} 1 & -i \\ i & 1 \end{bmatrix}$

Some Equivalent Representations

If several independent light beams are superimposed, the resulting coherence matrix is the sum of the coherence matrices of the individual beams. Conversely, since we may decompose any matrix into the sum of two or more matrices, we may consider a given beam to be a superposition of two or more independent light beams. In particular we may decompose a given $\bar{J}$ in the following way:

$$\bar{J} = \bar{J}_1 + \bar{J}_2, \tag{2-52}$$

where

$$\bar{J}_1 = \begin{bmatrix} A & 0 \\ 0 & A \end{bmatrix} = A\begin{bmatrix} 1 & 0 \\ 0 & 1 \end{bmatrix} \tag{2-53}$$

and

$$\bar{J}_2 = \begin{bmatrix} B & D^* \\ D & C \end{bmatrix} \tag{2-54}$$

$$BC - |D|^2 = 0 \tag{2-55}$$

Wolf[12] has shown that the matrix (2-54) and equation (2-55) are the general equations representing a completely polarized light beam, while $\bar{J}_1$ represents a completely depolarized beam. We can therefore consider a given beam to be the superposition of a completely polarized and completely unpolarized beam.

Theory of Rayleigh Depolarization

Intensity of Radiation from an Induced Dipole

Let us now examine the characteristics of the field radiated in a vacuum by an infinitesimal linear electric dipole, situated at a point $\bar{r}_o$, and vibrating along an axis represented by a unit vector $\bar{n}$. We may express the electric polarization as

$$\bar{P}(\bar{r},t) = p(t)\delta(\bar{r} - \bar{r}_o)\bar{n} \tag{2-56}$$

where p(t) is the dipole moment, and δ the Dirac delta function. Following Sommerfeld,[22] we now define an electric Hertz vector, $\bar{\pi}_e$, such that

$$\bar{\pi}_e = \frac{p(t - R/c)}{R}\,\bar{n} \tag{2-57}$$

where $R = |\bar{r} - \bar{r}_o|$, and the quantity $t - R/c$ is the retarded time. The Hertz vector obeys the homogeneous wave equation (everywhere except the origin) so that we have

$$\nabla^2\bar{\pi}_e = \frac{1}{c^2}\,\ddot{\bar{\pi}}_e \tag{2-58}$$

and in addition it may be shown that

$$\left.\begin{aligned} \bar{E} &= \text{curl curl } \bar{\pi}_e \\ \bar{H} &= \frac{1}{c}\,\text{curl } \dot{\bar{\pi}}_e \end{aligned}\right\} \tag{2-59}$$

Using the vector identity, curl curl = grad div - $\overline{\nabla}^2$, and the homogeneous wave equation, (2-58), we find that,

$$\left.\begin{aligned} \bar{E} &= \text{grad div } \bar{\pi}_e - \frac{1}{c^2}\,\ddot{\bar{\pi}}_e \\ \bar{H} &= \frac{1}{c}\,\text{curl } \dot{\bar{\pi}}_e \end{aligned}\right\} \tag{2-60}$$

Now, if we consider the dipole moment to be time harmonic, we find that

$$\partial p/\partial r = -\frac{1}{c}\,\dot{p},\ \partial^2 p/\partial r^2 = \frac{1}{c^2}\,\ddot{p} \tag{2-61}$$

and using this result and the definition of the Hertz vector we find that

$$\text{div } \bar{\pi}_e = -\left\{\frac{[p]}{R^3} + \frac{[\dot{p}]}{cR^2}\right\}(\bar{n}.\bar{R}) \tag{2-62}$$

$$\text{grad div } \bar{\pi}_e = \left\{\frac{3[p]}{R^5} + \frac{3[\dot{p}]}{cR^4} + \frac{[\ddot{p}]}{c^2R^3}\right\}(\bar{n}.\bar{R})\bar{R} - \left\{\frac{[p]}{R^3} + \frac{[\dot{p}]}{cR^2}\right\}\bar{n} \tag{2-63}$$

$$\text{curl } \bar{\pi}_e = \left\{\frac{[p]}{R^3} + \frac{[\dot{p}]}{cR^2}\right\}(\bar{n} \times \bar{R}) \tag{2-64}$$

where the square brackets denote retarded values (i.e. values taken at time (t - R/c)). The field vectors now assume the values

$$\begin{aligned} \bar{E} &= \left\{\frac{3[p]}{R^5} + \frac{3[\dot{p}]}{cR^4} + \frac{[\ddot{p}]}{c^2R^3}\right\}(\bar{n}.\bar{R})\bar{R} - \left\{\frac{[p]}{R^3} + \frac{[\dot{p}]}{cR^2} + \frac{[\ddot{p}]}{c^2R}\right\}\bar{n} \\ \bar{H} &= \left\{\frac{[\dot{p}]}{cR^3} + \frac{[\ddot{p}]}{c^2R^2}\right\}(\bar{n} \times \bar{R}) \end{aligned} \tag{2-65}$$

which may be converted to spherical coordinates R, θ, and ϕ by the transformations

$$\overline{R} = R\overline{i}_R$$

$$\overline{n} = (\cos\theta)\overline{i}_R - (\sin\theta)\overline{i}_\theta \qquad (2\text{-}66)$$

where the $\overline{i}$ are unit vectors.

We find now that

$$(\overline{n}.\overline{R}) = R\cos\theta$$

$$(\overline{n}\times\overline{R}) = (R\sin\theta)\overline{i}_\phi \qquad (2\text{-}67)$$

and, using the above results and (2-65)

$$\overline{E} = E_R\overline{i}_R + E_\theta\overline{i}_\theta$$

$$\overline{H} = H_\phi\overline{i}_\phi \qquad (2\text{-}68)$$

Comparing (2-68) and (2-65) term by term, we may identify each of the field components and find for the three non-vanishing terms:

$$E_R = 2\left\{\frac{[p]}{R^3} + \frac{[\dot{p}]}{cR^2}\right\}\cos\theta$$

$$E_\theta = \left\{[p]/R^3 + [\dot{p}]/cR^2 + [\ddot{p}]/c^2R\right\}\sin\theta$$

$$H_\phi = \left\{[\dot{p}]/cR^2 + [\ddot{p}]/c^2R\right\}\sin\theta \qquad (2\text{-}69)$$

Of interest in Rayleigh scattering, is the field a long distance from the dipole so that we have

$$R>>c\left|\frac{p}{\dot{p}}\right|, \quad R>>c\left|\frac{\dot{p}}{\ddot{p}}\right| \tag{2-70}$$

Examination of (2-69) shows that at large $\bar{R}$ we may neglect all terms but those in 1/R. In this approximation we have then, that

$$E_R = 0 \tag{2-71}$$

$$H_\phi = E_\theta = \frac{[\ddot{p}]}{c^2R}\sin\theta \tag{2-72}$$

Hence, at large $\bar{R}$, $\bar{E}$ and $\bar{H}$ are of equal magnitude and perpendicular to each other and to the radius vector $\bar{R}$. The field of the linear electric dipole in a vacuum is then that of a plane wave, and the radius vector $\bar{R}$ coincides with the direction of the Poynting vector. Furthermore, at $\theta = 0$ and $\theta = \pi$, the field is zero, so the dipole does not radiate along its axis.

We shall now consider a real molecule, whose dipole moment, p, may be expanded in the form

$$p(t) = p_o + \bar{\alpha}.\bar{E}(\bar{r},t) + \cdot\cdot\cdot \tag{2-73}$$

where we consider only lossless (transparent) media so that the term p_o (permanent moment) is time independent, and $\bar{E}(\bar{r},t)$ is the field inducing a moment in the molecule whose polarizability is $\bar{\alpha}$.

According to (2-22) we may write,

$$p(t) = p_o + \bar{\alpha}.\bar{E}_oe^{-i\omega t} + \cdot\cdot\cdot \tag{2-74}$$

and so

$$\ddot{p} = -\omega^2(\bar{\alpha}.\bar{E}_o)e^{-i\omega t} \tag{2-75}$$

$$\ddot{p} = -4\pi^2\nu^2(\bar{\alpha}.\bar{E}_o)e^{-i\omega t} \tag{2-76}$$

Hence, using 2-72 we see that (assuming the size of the molecule to be small compared to c/ν)

$$E_\theta = \frac{-4\pi^2\nu^2(\bar{\alpha}.\bar{E}_o)e^{-i\omega t}}{c^2 R} \sin\theta \tag{2-77}$$

(while $\bar{E}_\theta$ may be generated by multiplying (2-77) by a unit vector in the coordinates defined by $\bar{S}$ of the scattered light) thus from (2-30),

$$I_\theta = \frac{16\pi^4\nu^4}{c^4R^2} |\bar{\alpha}|^2 I_o \sin^2\theta \tag{2-78}$$

where I_o is the intensity of the incident field. Then at $\theta = 90°$, the scattered intensity per unit solid angle for an ensemble of N_o dipoles is

$$I_{90} = \frac{16\pi^4\nu^4 N_o}{c^4} |\bar{\alpha}|^2 I_o \tag{2-79}$$

$$I_{90} = \kappa|\bar{\alpha}|^2 I_o \tag{2-80}$$

where

$$\kappa = \frac{16\pi^4\nu^4 N_o}{c^4} \tag{2-81}$$

These results are well known from classical scattering theory, and will be used in the subsequent treatment. Actually, (2-79) is correct only for a system of gaseous dipoles, and for condensed systems must be corrected by a factor, $\sqrt{\varepsilon/\mu}$, as in (2-30). In addition the polarization properties of the scattered light are affected by the tensor character of the polarizability, as will be discussed in the next section.

Matrix Treatment of Rayleigh Scattering

Consider a single scatterer oriented at the origin of a right-handed coordinate system (X,Y,Z), along which an electromagnetic wave is propagating in the +Z direction. The scattered radiation will be observed in the YZ plane at some angle θ, and will define a new coordinate system (X', Y', Z') such that the scattered wave is propagated in the $+Z'$ direction. The scattered wave being observed at some distance, r, along the Z' axis. A unit vector in the primed (scattered) coordinate system, $\overline{X}'$, is transformed into a unit vector, $\overline{X}$, in the unprimed system by the transformation

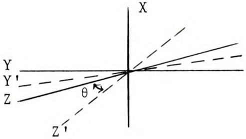

FIGURE 2.1--The Coordinate System

$$\overline{\chi}' = \overline{n}\,\overline{\chi} \tag{2-82}$$

where

$$\overline{n} = \begin{bmatrix} 1 & 0 & 0 \\ 0 & \cos\theta & -\sin\theta \\ 0 & \sin\theta & \cos\theta \end{bmatrix} \tag{2-83}$$

We must now concern ourselves with the generation of a matrix, $\overline{S}$, (not to be confused with the Poynting vector) which will transform the incident wave $\overline{J}$ into the scattered wave $\overline{J}'$. Therefore, we have from (2-36) that

$$\overline{J}' = \overline{S}\,\overline{J}\,\overline{S}^{\dagger} \tag{2-84}$$

or

$$\overline{J}' = \langle\overline{E}' \times \overline{E}'^{\dagger}\rangle \tag{2-85}$$

Then from (2-77), we see that

$$\overline{J}' = \kappa\langle\overline{p}' \times \overline{p}'^{\dagger}\rangle \tag{2-86}$$

where κ is as defined in (2-81), and using the transformation from primed to unprimed coordinates, (2-82), (2-86) becomes

$$\overline{J}' = \kappa\langle\overline{n}\,\overline{p} \times \overline{p}^{\dagger}\overline{n}^{\dagger}\rangle \tag{2-87}$$

$$\overline{J}' = \kappa\langle\overline{n}\,\overline{\alpha}\,\overline{E} \times \overline{E}^{\dagger}\overline{\alpha}^{\dagger}\overline{n}^{\dagger}\rangle \tag{2-88}$$

As we are considering a single scattering center fixed in space

$$\overline{J}' = \kappa\,\overline{n}\,\overline{\alpha}\langle\overline{E} \times \overline{E}^{\dagger}\rangle\overline{\alpha}^{\dagger}\overline{n}^{\dagger} \tag{2-89}$$

and from (2-36)

$$\bar{J}' = \kappa\,\bar{n}\,\bar{\alpha}\,\bar{J}\,\bar{\alpha}^{\dagger}\bar{n}^{\dagger} \tag{2-90}$$

Thus, we see by inspection that

$$\bar{S} = \sqrt{\kappa}\;\bar{n}\,\bar{\alpha} \tag{2-91}$$

where $\bar{\alpha}$ represents the components of the polarizability in the space-fixed coordinate system (X,Y,Z).

$$\bar{\alpha}(N) = \begin{bmatrix} \alpha_{xx} & \alpha_{xy} & \alpha_{xz} \\ \alpha_{yx} & \alpha_{yy} & \alpha_{yz} \\ \alpha_{zx} & \alpha_{zy} & \alpha_{zz} \end{bmatrix} \tag{2-92}$$

Carrying out the operations as indicated yields

$$\bar{S}=\sqrt{\kappa}\left[\begin{matrix} \alpha_{xx} & \alpha_{xy} & \alpha_{xz} \\ (\alpha_{yx}\cos\theta-\alpha_{zx}\sin\theta) & (\alpha_{yy}\cos\theta-\alpha_{zy}\sin\theta) & (\alpha_{yz}\cos\theta-\alpha_{zz}\sin\theta \\ (\alpha_{yx}\cos\theta+\alpha_{zx}\sin\theta) & (\alpha_{yy}\cos\theta+\alpha_{zy}\sin\theta) & (\alpha_{yz}\cos\theta+\alpha_{zz}\sin\theta \end{matrix}\right. \tag{2-93}$$

and since there is no electric field component on the Z axes

$$\bar{S} = \sqrt{\kappa}\begin{bmatrix} \alpha_{xx} & \alpha_{xy} \\ \alpha_{yx}\cos\theta - \alpha_{zx}\sin\theta & \alpha_{yy}\cos\theta - \alpha_{zy}\sin\theta \end{bmatrix} \tag{2-94}$$

This matrix is valid only for the components, $\alpha_{NN'}$, of the polarizability in the space-fixed coordinate system. We may identify a molecule-fixed coordinate system with axes 1,2,3, such that the components of the polarizability in this system are

$$\overline{\alpha}(i) = \begin{bmatrix} \alpha_{11} & \alpha_{12} & \alpha_{13} \\ \alpha_{21} & \alpha_{22} & \alpha_{23} \\ \alpha_{31} & \alpha_{32} & \alpha_{33} \end{bmatrix} \tag{2-95}$$

Furthermore, we may choose the molecule-fixed axes to be the principal axes of polarizability, so that we now have

$$\overline{\alpha}(i) = \begin{bmatrix} \alpha_{1} & 0 & 0 \\ 0 & \alpha_{2} & 0 \\ 0 & 0 & \alpha_{3} \end{bmatrix} \tag{2-96}$$

where the α_i (i = 1,2,3) are called the principal values of the polarizability. A unit vector in the molecule-fixed coordinate system may then be transformed into the space-fixed system by the transformation

$$\begin{bmatrix} \overline{n}_x \\ \overline{n}_y \\ \overline{n}_z \end{bmatrix} = \begin{bmatrix} C_{x1} & C_{x2} & C_{x3} \\ C_{y1} & C_{y2} & C_{y3} \\ C_{z1} & C_{z2} & C_{z3} \end{bmatrix} \begin{bmatrix} \overline{n}_1 \\ \overline{n}_2 \\ \overline{n}_3 \end{bmatrix} \tag{2-97}$$

where the $\overline{n}_i$ (i = 1,2,3,) and $\overline{n}_N$ (N = X,Y,Z) are unit vectors on the molecule-fixed, and space-fixed axes, and the C_{Ni} are the direction cosines of the Euler angles relating the two systems.

We then have that the polarizability components in the space-fixed system are given by,

$$\alpha_{NN'} = \sum_{i=1}^{3} \alpha_i \, C_{Ni} \, C_{N'i} \tag{2-98}$$

The scattering matrix thus generated being valid for a single radiator, fixed in space. For an ensemble of such radiators we must sum the contributions (taking into account the phase relationships), and average the results over all the possible orientations of the ensemble.

Rayleigh Scattering from a Perfect Gas

Assuming a dilute gas of independent particles, we see that the α_i will be constants (i.e. there is no need to consider phase relationships due to the distances between molecules), and the summation of scattering contributions is given by the product of the average contribution and the total number of scatterers, N. From the transformation law (2-84) we see that the terms to be averaged will be of the form:

$$\overline{\alpha^2_{NN'}} = \overline{\left[\sum_{i=1}^{3} \alpha_i C_{Ni} C_{N'i}\right]^2} \tag{2-99-a}$$

and

$$\overline{\alpha_{NN}\alpha_{N'N'}} = \overline{\left[\sum_{i=1}^{3} \alpha_i C^2_{Ni} \sum_{j=1}^{3} \alpha_j C^2_{N'j}\right]} \tag{2-99-b}$$

(where the bar denotes the spatial rather than the time average), and since the α_i are constants in the averaging we may write

$$\overline{\alpha^2_{NN'}} = \sum_{i=1}^{3} \alpha_i^2 \overline{C^2_{Ni} C^2_{N'i}} + \sum_{i \neq j} \alpha_i \alpha_j \overline{C_{Ni} C_{N'i} C_{Nj} C_{N'j}} \tag{2-100-a}$$

$$\overline{\alpha_{NN}\alpha_{N'N'}} = \sum_{i=1}^{3} \alpha_i^2 \overline{C^2_{Ni} C^2_{N'i}} + \sum_{i \neq j} \alpha_i \alpha_j \overline{C^2_{Ni} C^2_{N'j}}. \tag{2-100-b}$$

In this approximation (i.e. independent scatterers) the scattering from any physical system may in principle be treated by appropriately averaging the direction cosines (C_{Ni}) over all the possible orientations of the system.

In this case, the gas molecules are free to assume all possible orientations, with respect to the observer's axes, with equal probability. The averaging process then becomes particularly simple because the diagonal term (i.e. N = N') takes the form,

$$\overline{C^4_{Ni}} = \overline{\cos^4 \theta} = \frac{1}{4\pi} \int_0^{\pi} \int_0^{2\pi} \cos^4 \theta \sin \theta d\theta d\phi \tag{2-101}$$

$$\overline{C^4_{Ni}} = 1/5.$$

Then, from (2-97), we see that we may write

$$\bar{n}_i . \bar{n}_i = |n_i^2| = C^2_{xi} + C^2_{yi} + C^2_{zi} = 1 \tag{2-102}$$

or

$$\overline{|n_i^2|^2} = 3\,\overline{C^4_{Ni}} + 6\,\overline{C^2_{Ni} C^2_{N'i}} = 1 \quad (N \neq N') \tag{2-103}$$

so that combining (2-101) and (2-103) yields the off-diagonal term

$$\overline{C_{Ni}^2 C_{N'i}^2} = 1/15. \quad (N \neq N') \tag{2-104}$$

In the same manner we obtain

$$\overline{|n_i^2||n_j^2|} = 3\,\overline{C_{Ni}^2 C_{N'i}^2} + 6\,\overline{C_{Ni}^2 C_{N'j}^2} = 1 \tag{2-105}$$

where N ≠ N', and i ≠ j, and combining (2-104) and (2-105) we obtain,

$$\overline{C_{Ni}^2 C_{N'j}^2} = 2/15. \quad N \neq N',\ i \neq j \tag{2-106}$$

Finally, using the orthogonality condition,

$$\bar{n}_i \cdot \bar{n}_j = C_{xi}C_{xj} + C_{yi}C_{yj} + C_{zi}C_{zj} = 0 \tag{2-107}$$

and

$$\overline{|\bar{n}_i \cdot \bar{n}_j|^2} = 3\,\overline{C_{Ni}^2 C_{Nj}^2} + 6\,\overline{C_{Ni}C_{N'i}C_{Nj}C_{N'j}} = 0 \tag{2-108}$$

we see that

$$\overline{C_{Ni}C_{N'i}C_{Nj}C_{N'j}} = -1/30. \tag{2-109}$$

We may now compute the components of the coherence matrix of the scattered radiation (i.e. $\bar{J}'$) using the preceding results, and equations (2-100). The non-vanishing terms are easily seen to be

$$\overline{|\alpha_{xx}^2|} = \overline{|\alpha_{yy}^2|} = \frac{3}{15}\sum_{i=1}^{3} \alpha_i^2 + \frac{2}{15}\sum_{i<j} \alpha_i\alpha_j \tag{2-110}$$

$$\overline{|\alpha_{xy}^2|} = \overline{|\alpha_{xz}^2|} = \ldots = \frac{1}{15}\sum_{i=1}^{3} \alpha_i^2 - \frac{1}{15}\sum_{i<j} \alpha_i\alpha_j \qquad (2\text{-}111)$$

$$\overline{\alpha_{xx}^*\alpha_{yy}} = \overline{\alpha_{yy}^*\alpha_{xx}} = \frac{1}{15}\sum_{i=1}^{3} \alpha_i^2 + \frac{4}{15}\sum_{i<j} \alpha_i\alpha_j . \qquad (2\text{-}112)$$

Making the customary use of the spherical part of the polarizability, α, and the anisotropy, β, where

$$\alpha = \frac{1}{3}\sum_{i=1}^{3} \alpha_i \qquad (2\text{-}113)$$

and

$$\beta^2 = \frac{1}{2}\left[(\alpha_1 - \alpha_2)^2 + (\alpha_2 - \alpha_3)^2 + (\alpha_3 - \alpha_1)^2\right] \qquad (2\text{-}114)$$

we see that the non-zero terms are given by,

$$\overline{|\alpha_{NN'}^2|} = \begin{cases} \dfrac{45\alpha^2 + 4\beta^2}{45} & (N = N') \\ \dfrac{3\beta^2}{45} & (N \neq N') \end{cases} \qquad (2\text{-}115)$$

$$\overline{|\alpha_{NN}\alpha_{N'N'}|} = \frac{45\alpha^2 - 2\beta^2}{45} \qquad (2\text{-}116)$$

Depolarization of Vertically Polarized Light

We are now in a position to examine the properties of light scattered from a dilute gas of independent particles.

Consider first, the scattering of light linearly polarized in the X-direction. In this case, the incident beam has a coherence matrix (where I_o is the intensity)

$$\bar{J}_v = I_o \begin{bmatrix} 1 & 0 \\ 0 & 0 \end{bmatrix}. \qquad (2\text{-}117)$$

Where the subscript v refers to the vertical polarization, and the scattering system is represented by (at θ = 90°)

$$\bar{S}(90°) = \sqrt{\kappa} \begin{bmatrix} \alpha_{xx} & \alpha_{xy} \\ -\alpha_{xz} & -\alpha_{yz} \end{bmatrix}. \qquad (2\text{-}118)$$

Then, using (2-84) the scattered radiation is given by the coherence matrix

$$\bar{J}'_v = I_o\kappa \begin{bmatrix} \overline{|\alpha^2_{xx}|} & \overline{-|\alpha_{xx}\alpha_{xz}|} \\ \overline{-|\alpha_{xx}\alpha_{xz}|} & \overline{|\alpha^2_{xz}|} \end{bmatrix} \qquad (2\text{-}119)$$

and from (2-115)

$$\bar{J}'_v = \frac{I_o\kappa}{45} \begin{bmatrix} 45\alpha^2 + 4\beta^2 & 0 \\ 0 & 3\beta^2 \end{bmatrix}. \qquad (2\text{-}120)$$

The intensity of the light scattered at θ = 90°

$$I_v = \mathrm{Tr}\, \bar{J}'_v = \frac{16\pi^4\nu^4 N_o}{45C^4} \left[45\alpha^2 + 7\beta^2\right] I_o. \qquad (2\text{-}121$$

The vertically polarized component of the output is

$$\bar{J}_v'^{v} = \begin{bmatrix} 1 & 0 \\ 0 & 0 \end{bmatrix} \begin{bmatrix} 45\alpha^2+4\beta^2 & 0 \\ 0 & 3\beta^2 \end{bmatrix} \begin{bmatrix} 1 & 0 \\ 0 & 0 \end{bmatrix} \frac{\kappa I_o}{45} \qquad (2\text{-}122)$$

$$= \frac{\kappa I_o}{45} \begin{bmatrix} 45\alpha^2+4\beta^2 & 0 \\ 0 & 0 \end{bmatrix}, \qquad (2\text{-}123)$$

and the intensity of the vertical component is

$$V_v = \frac{16\pi^4\nu^4 N_o}{45C^4} \left[45\alpha^2 + 4\beta^2\right] I_o. \qquad (2\text{-}124)$$

Similarly, the horizontal intensity may be shown to be

$$H_v = \frac{16\pi^4\nu^4 N_o}{45C^4} \left[3\beta^2\right] I_o. \qquad (2\text{-}125)$$

It is now obvious that the total intensity is given by

$$I_v = V_v + H_v = J_{xx}^v + J_{yy}^v \qquad (2\text{-}126)$$

where subscript (and superscript) v refers to vertically polarized incident light. The depolarization ratio for vertically polarized light is defined as

$$\rho_v = H_v/V_v = J_{yy}^v/J_{xx}^v, \qquad (2\text{-}127)$$

and, using (2-124) and (2-125), we achieve the desired result,

$$\rho_v = \frac{3\beta^2}{45\alpha^2 + 4\beta^2} \; . \qquad (2\text{-}128)$$

Noting that for an isotropic molecule $\beta^2 = 0$, the scattered intensity is given by (from 2-121)

$$(I_{iso})_v = \frac{16\pi^4\nu^4 N_o}{C^4}[\alpha^2]I_o. \tag{2-129}$$

Then, solving (2-128) for β^2, we have that

$$\beta^2 = \frac{45\alpha^2\rho_v}{3 - 4\rho_v}, \tag{2-130}$$

and combining (2-130), (2-129), and (2-121) we obtain

$$I_v = (I_{iso})_v\left[\frac{3 + 3\rho_v}{3 - 4\rho_v}\right]. \tag{2-131}$$

Thus, an expression for the isotropic scattering of vertically polarized light from a molecule must be corrected for anisotropy by the second term in equation (2-131). This correction factor is the well known Cabannes factor for vertically polarized light as discussed by Stacey.[20]

Depolarization of Unpolarized Light

The coherence matrix of unpolarized light is given by

$$\bar{J}_u = \frac{I_o}{2}\begin{bmatrix} 1 & 0 \\ 0 & 1 \end{bmatrix}, \tag{2-132}$$

where I_o is the intensity, and the scattering system is (as before) given by,

$$\overline{S} = \sqrt{\kappa}\begin{bmatrix} \alpha_{xx} & \alpha_{xy} \\ -\alpha_{xz} & -\alpha_{yz} \end{bmatrix}. \tag{2-133}$$

Again using (2-84) the coherence matrix of the scattered radiation is given by

$$\overline{J}_u' = \frac{I_o\kappa}{2}\,[\overline{S}\,\overline{J}\,\overline{S}^{\dagger}] \tag{2-134}$$

$$\overline{J}_u' = \frac{I_o\kappa}{2}\begin{bmatrix} \overline{|\alpha_{xx}^2|} + \overline{|\alpha_{xy}^2|} & -\overline{|\alpha_{xx}\alpha_{xz}|} - \overline{|\alpha_{xy}\alpha_{yz}|} \\ -\overline{|\alpha_{xx}\alpha_{xz}|} - \overline{|\alpha_{xy}\alpha_{yz}|} & \overline{|\alpha_{xz}^2|} + \overline{|\alpha_{yz}^2|} \end{bmatrix} \tag{2-135}$$

and using the results (2-115)

$$\overline{J}_u' = \frac{I_o\kappa}{90}\begin{bmatrix} 45\alpha^2 + 7\beta^2 & 0 \\ 0 & 6\beta^2 \end{bmatrix}. \tag{2-136}$$

Thus, the total scattered intensity is, at $\theta = 90°$,

$$I_u = \mathrm{Tr}\,\overline{J}_u' = \frac{8\pi^4\nu^4 N_o}{45c^4}\,[45\alpha^2 + 13\beta^2]I_o \tag{2-137}$$

and the depolarization ratio for unpolarized light,

$$\rho_u = J_{yy}^u / J_{xx}^u \tag{2-138}$$

is seen to be,

$$\rho_u = \frac{6\beta^2}{45\alpha^2 + 7\beta^2}. \tag{2-139}$$

We may now compute β^2 and find that,

$$\beta^2 = \frac{45\alpha^2\rho_u}{6 - 7\rho_u}, \tag{2-140}$$

so that combining (2-137), (2-140), we obtain

$$I_u = (I_{iso})_u \left[\frac{6 + 6\rho_u}{6 - 7\rho_u}\right], \tag{2-141}$$

where $(I_{iso})_u$ is the total scattered intensity when $\beta^2 = 0$ (isotropic). The second term in (2-85) is again the well known Cabannes factor, in this case for unpolarized light.

The Horizontal Depolarization Ratio

In this case the coherence matrix of the incident beam is

$$\bar{J}_h = I_o \begin{bmatrix} 0 & 0 \\ 0 & 1 \end{bmatrix}, \tag{2-142}$$

and using (2-133) and (2-84) we find that the coherence matrix of the scattered beam is

$$\bar{J}_h' = I_o\kappa \begin{bmatrix} \overline{|\alpha_{xy}^2|} & 0 \\ 0 & \overline{|\alpha_{yz}^2|} \end{bmatrix} = \frac{I_o\kappa}{45} \begin{bmatrix} 3\beta^2 & 0 \\ 0 & 3\beta^2 \end{bmatrix}, \tag{2-143}$$

and the scattered intensity is seen to be

$$I_h = \frac{16\pi^4\nu^4 N_o}{45c^4} [6\beta^2] I_o. \tag{2-144}$$

Obviously, if the molecule is isotropic ($\beta^2 = 0$) there is no scattering of horizontally polarized light, and even in the anisotropic case the scattering is weak due to the numerical factor in the denominator of (2-144). The horizontal depolarization ratio is defined as

$$\rho_h = V_h/H_h, \tag{2-145}$$

and is therefore given by

$$\rho_h = 3\beta^2/3\beta^2 = 1. \tag{2-146}$$

From (2-146), (2-139), and (2-128), we obtain the well known result

$$\rho_u = \frac{1 + 1/\rho_h}{1 + 1/\rho_v}. \tag{2-147}$$

We may now seek to apply these results to some real systems, and extend the development to include interactions between molecules.

Depolarization by Dense Fluids of Spherical Molecules

Having examined the details of scattering and depolarization by dilute gases of independent scatterers; we are now in a position to extend these results to the case of dense fluids of interacting particles. In this case we shall assume that the isolated molecules are spherically symmetric so that,

$$p_o = 0 = \beta^2, \tag{2-148}$$

and from (2-128) we see that $\rho_V = 0$. We must now account for two phenomena that were ignored in the approximation of the previous sections; that is

(1) The field at a particular scattering center is the sum of the incident wave and the field due to all the other scattering centers.

(2) In summing the intensity contributions, the cross product terms must be included (with appropriate phase factors) due to the proximity of the molecules in the fluid.

In the following, we shall use alphabetic superscripts to identify molecules while subscripts will refer to coordinates. As before, lower case subscripts refer to molecular-fixed axes, while upper case subscripts refer to space-fixed coordinates. We shall identify the field at molecule a due to other molecules by $\overline{F}^a$, while the field due to the incident wave at molecule a is $\overline{E}^a$. The field expression shall be written in the form

$$\overline{E}^a = E_o \exp(-i\omega t + ik\overline{z}) \tag{2-149-a}$$

where $k = \frac{2\pi}{\lambda}$ is the wave number, and $\overline{z}$ the projection of $\overline{r}$ in the direction of propagation. The field of the incident wave at molecule b is obviously given by

$$\bar{E}^b = \bar{E}^a \exp\,[ik(\bar{r}(b) - \bar{r}(a)).\bar{n}_z] \qquad (2\text{-}149\text{-}b)$$

We shall now write the dipole moment in the form

$$p_i = p_{oi} + \alpha_{ij}\,[E_j + F_j] \qquad (2\text{-}150)$$

and define a new polarizability, a_{ij}, such that

$$a_{ij} = \frac{\partial p_i}{\partial E_j} = \alpha_{ik}\left[\delta_{kj} + \frac{\partial F_k}{\partial E_j}\right] \qquad (2\text{-}151)$$

where the α_{ij} are the polarizability tensor elements of the molecule, and δ_{kj} is the Kronecker delta. Assuming the electric field to induce only dipoles, it may be shown that (Sommerfeld[22]);

$$\frac{\partial F_k}{\partial E_j} = -\sum_{b \neq a} \varepsilon_{k\ell}^{ab}\, a_{j\ell}^{b} \exp\,[ik(\bar{r}(b) - \bar{r}(a)).\bar{n}_z]$$

$$= -\sum \varepsilon_{k\ell}^{ab}\, a_{j\ell}^{b} \exp\,[i\psi_{abz}], \qquad (2\text{-}152)$$

where ψ_{abz} is the phase angle and $\varepsilon_{k\ell}^{ab}$ is given by

$$\varepsilon_{k\ell}^{ab} = r^{-5}(ab)\left\{r^2(ab)\delta_{k\ell} - 3r_k(ab)r_\ell(ab)\right\}, \qquad (2\text{-}153)$$

where r(ab) is the distance between molecules a and b.

We may now follow exactly the same procedure as in the preceding sections with the additional requirement that our summation be taken over the individual field components rather than the intensities, so that

$$\sum \overline{\alpha_{NN'}^2} = \sum_{ab} \alpha_{NN'}^a \, \alpha_{NN'}^b \exp(i\psi_{abz}) \tag{2-154}$$

where the $\alpha_{NN'}$ are the polarizability tensor elements in space-fixed coordinates,

$$\alpha_{NN'} = \sum_{i,j} \alpha_{ij} \, C_{Ni} \, C_{N'j} \tag{2-98}$$

Now, since we are dealing with spherically symmetric molecules, we have that

$$\alpha_{ij} = \alpha \delta_{ij} \tag{2-155}$$

so that we find for the perturbed polarizability,

$$a_{ij}^a = \alpha \left[\delta_{ij} - \alpha \sum_{b \neq a} \varepsilon_{ij}^{ab} \exp(i\psi_{abz}) \right] \tag{2-156}$$

Hence, using (2-101) through (2-112) we find that

$$45 \overline{|\alpha_{NN}^2|} = 45\alpha^2 \sum_b \langle \cos \psi_{1b} \rangle + 18\beta^2 \tag{2-157}$$

$$10 \overline{|\alpha_{NN'}^2|} = 3\beta^2 \tag{2-158}$$

where we now have that

$$\beta^2 = \alpha^4 \sum_b \sum_{\substack{c \neq 1 \\ d \neq b}} \langle \sum_{i,j} \varepsilon_{ij}^{1b} \, \varepsilon_{ij}^{dc} \cos(\psi_{bcz} - \psi_{1dy}) \rangle \tag{2-159}$$

Benoit and Stockmayer[23] have shown that

$$\sum_b \langle \cos \psi_{1b} \rangle = 1 + 4\pi \int_0^\infty [g(r) - N/V] r^2 dr$$

$$= RT\bar{\kappa}/\bar{V} \qquad (2\text{-}160)$$

where R is the gas constant, T the temperature, $\bar{\kappa}$ the compressibility and $\bar{V}$ the molar volume. In addition, Buckingham and Stephen[7] have shown that β^2 may be rewritten as

$$\beta^2 = \alpha^2 \left[\frac{MR - MR_o}{MR_o}\right] \qquad (2\text{-}161)$$

where MR_o is the molecular refraction of the molecule in the gaseous state, and MR the molecular refraction in the condensed fluid. Hence we see that

$$\rho_V = \frac{3\left[\dfrac{MR - MR_o}{MR_o}\right]}{4\left[\dfrac{MR - MR_o}{MR_o}\right] + 10\dfrac{RT\bar{\kappa}}{\bar{V}}} \qquad (2\text{-}162)$$

and we now have an expression for the vertical depolarization ratio of a dense fluid of spherical molecules.

Temperature Dependence of Depolarization by Dense Fluids

Making use of the result (2-162) we may now examine the dependence of the depolarization, ρ_V, on the temperature. First, however, we take note of the fact that the molecular refraction, MR, given by

$$MR = \left[\frac{n^2 - 1}{n^2 + 1}\right] \frac{M}{d} \qquad (2\text{-}163)$$

where n is the refractive index, M the molecular weight, and d the density, is practically temperature independent, and is a function of the bonds present in the molecule. We shall therefore make the following assumption, which will be justified by experiment:

Assumption: The temperature dependence of the depolarization ratio is due to the diagonal elements of the polarizability tensor (i.e. the term, $10RT\overline{\kappa}/\overline{V}$), so that we may write

$$\rho_v = \frac{3A}{4A + B(T)} \tag{2-164}$$

where A refers to a constant, and

$$B(T) = \frac{10RT\overline{\kappa}}{\overline{V}} \tag{2-165}$$

Now we may write

$$(\partial\rho_v/\partial T)_p = \frac{-3A}{(4A + B)^2}(\partial B/\partial T)_p \tag{2-166}$$

or, rearranging terms,

$$(\partial \ln \rho_v/\partial T)_p = -\frac{1}{4A + B}(\partial B/\partial T)_p \tag{2-167}$$

However, using (2-164), we see that

$$4A = \frac{4B\rho_v}{3 - 4\rho_v} \tag{2-168}$$

so that (2-167) becomes

$$(\partial\ \ell n\ \rho_V/\partial T)_p = -\left[\frac{1/B}{1 + 4\rho_V/(3 - 4\rho_V)}\right]\left(\frac{\partial B}{\partial T}\right)_p \qquad (2\text{-}169)$$

or

$$(\partial\ \ell n\ \rho_V/\partial T)_p = \left[\frac{4\rho_V - 3}{3}\right]\frac{1}{B}\left(\frac{\partial B}{\partial T}\right)_p \qquad (2\text{-}170)$$

Moreover, from (2-165) we have that,

$$(\partial B/\partial T)_p = \frac{10R}{\overline{V}}\left[-\frac{T\overline{\kappa}}{\overline{V}}(\partial\overline{V}/\partial T)_p + \overline{\kappa} + T(\partial\overline{\kappa}/\partial T)_p\right] \qquad (2\text{-}171)$$

and

$$\frac{1}{B}\left(\frac{\partial B}{\partial T}\right)_p = \left[\frac{1}{T} - \alpha_T + \frac{1}{\overline{\kappa}}\left(\frac{\partial\overline{\kappa}}{\partial T}\right)_p\right], \qquad (2\text{-}172)$$

where α_T is the coefficient of thermal expansion,

$$\alpha_T = \frac{1}{\overline{V}}\left(\frac{\partial\overline{V}}{\partial T}\right)_p \qquad (2\text{-}173)$$

Combining (2-170), and (2-172) we have finally, the result

$$(\partial\ \ell n\ \rho_V/\partial T)_p = \left[\frac{4\rho_V - 3}{3}\right]\left[\frac{1}{T} - \alpha_T + \left(\frac{\partial\ \ell n\ \overline{\kappa}}{\partial T}\right)_p\right] . \qquad (2\text{-}174)$$

Hence we now have an expression for the temperature dependence of ρ_V, which depends only on the independently measurable thermodynamic quantities, α_T and $\overline{\kappa}$, as well as

ρ_v. We may further simplify this expression by using the well known relation,

$$C_p - C_v = \alpha_T^2 T \overline{V}/\overline{\kappa} \tag{2-175}$$

and the approximate result

$$[\partial(C_p - C_v)/\partial T]_p = 0 = \alpha_T\overline{V} + \alpha_T T(\partial\overline{V}/\partial T)_p + 2T\overline{V}(\partial\alpha_T/\partial T) - \frac{\alpha_T T\overline{V}}{\overline{\kappa}}\left(\frac{\partial\overline{\kappa}}{\partial T}\right) . \tag{2-176}$$

We then have that

$$(\partial\ \ell n\ \overline{\kappa}/\partial T)_p = \frac{1}{T} + \frac{1}{\overline{V}}(\partial\overline{V}/\partial T)_p + \frac{2}{\alpha_T}(\partial\alpha_T/\partial T)_p , \tag{2-177}$$

and since

$$(\partial\alpha_T/\partial T)_p \simeq \alpha_T^2 , \tag{2-178}$$

combining (2-174), (2-177), and (2-178) we finally obtain

$$(\partial\ \ell n\ \rho_v/\partial T)_p = 2\left[\frac{4\rho_v - 3}{3}\right]\left[\frac{1}{T} + \alpha_T\right] \tag{2-179}$$

This is indeed a very simple relationship between the depolarization and temperature, and involves only the temperature, coefficient of thermal expansion, and depolarization ratio. Equations (2-174) and (2-179) form the basis for the analysis of the experimental data to follow.

Laser Theory

Emission and Absorption of Radiation

Atomic systems, such as atoms and molecules, may exist in stationary states called energy levels. Each energy level corresponds to a definite value of energy, and may be described by a suitable wave function. Transitions between energy levels may occur with attendant emission or absorption of radiation, or with the transfer of energy in some other fashion. Radiative transitions obey the Bohr frequency condition; $h\nu_{12} = E_2 - E_1$, where ν_{12} is the frequency of the absorbed or emitted photon, h is Planck's constant, and E_2 and E_1 are the energies of the states between which the transition takes place.

When radiation impinges on an atomic system, it perturbs the Hamiltonian of the system, and can cause a change from the initial state to some other state. In the transition from one state to the other, the system must then either absorb or emit radiation of the same frequency as the perturbing radiation, depending on whether the system was initially in the lower or higher stationary state. The case in which the system is initially in the higher energy state is particularly interesting since a photon is then emitted due to the influence of the perturbing field, and the emitted photon has the same frequency and phase as the perturbing field. This process is called stimulated emission, and has the interesting property that the perturbing photon and the emitted photon are coherent with one another.

The Boltzmann distribution describes the way a system at equilibrium will distribute its population among the available energy levels, and is given by,

$$N_2/N_1 = \exp\,[(E_1 - E_2)/kT], \tag{2-180}$$

N_2 and N_1 being the populations of the states with energies E_2 and E_1, k the Boltzmann constant, and T the absolute temperature. The subscript 2 refers to the higher energy level. According to the Boltzmann distribution then, a system in a state with energy $E_2 > kT$ is not at equilibrium, and must therefore tend to lose energy whether there is a perturbing field present or not. The loss of energy in this fashion is called spontaneous emission, and since there is no field present the emission is incoherent.

Using time-dependent perturbation theory, it is easily shown that the probability of a transition from a lower to a higher state is given by,

$$P_{12} = \rho_{12}\, B_{12}, \tag{2-181}$$

where ρ_{12} is the radiation density of the appropriate frequency, P_{12} is the probability of absorption, and B_{12} is called the Einstein coefficient for absorption. The probability of transition from a higher to a lower level is given by,

$$P_{21} = A_{21} + \rho_{21}\, B_{21} \tag{2-182}$$

where P_{21} is the probability of transition, A_{21} is the Einstein coefficient of spontaneous emission, ρ_{21} is the radiation density of the appropriate frequency, and B_{21} is the Einstein coefficient for stimulated emission. The relations between the Einstein coefficients is given by,

$$B_{nm} = B_{mn},\ A_{nm} = \frac{8\pi h\nu^3}{C^3} B_{nm} \qquad (2\text{-}183)$$

From these relations it is easily seen that at very low frequencies (eg. radio frequencies), $A_{nm} << B_{nm}$ so that even for very small radiation densities, the transition is almost entirely caused by stimulated emission, and the output is coherent. The coherency properties of low frequency radiators account for the extreme usefulness of these devices as information carriers. To achieve stimulated emission at optical frequencies, we must make the product $\rho_{21}\ B_{21}$ greater than A_{21}. This is done by choosing a level for which A_{21} is not extremely large, and then making ρ_{21} as large as possible.

Consider now an ensemble of atomic systems, and designate the number of atoms per unit volume in state n by N_n. Assuming $n>m$, what is the response of the ensemble to collimated radiation of frequency ν_{nm}, and density ρ_{nm}? The number of emissions from n to m is given by, $P_{nm}\ N_n = (A_{nm} + \rho B_{nm})$, per second, and the number of absorptions is given by, $P_{mn}\ N_m = \rho_m\ B_{mn}\ N_m$. Now since N_n is less than N_m for a system anywhere near thermal equilibrium, the beam will suffer a loss of $(N_m - N_n)\ \rho_{nm}\ B_{nm}$ photons per second. The $A_{nm}\ N_n$ spontaneously emitted photons will be radiated in all directions uniformly, and will therefore be lost from the beam. Thus, a beam passing through a material at or near thermal equilibrium will always lose energy, and will therefore not support stimulated emission since ρ_{nm} will diminish, making spontaneous emission the more probable process.

An ensemble can easily be visualized however, in which N_n is greater than N_m, even though n>m. Examination of the Boltzmann distribution shows that such a material is certainly not in thermal equilibrium and indeed, since we have that,

$$N_n/N_m = \exp\ [(E_m - E_n)/kT] \qquad (2\text{-}184)$$

the system must exist in a state of negative temperature. This ensemble is then said to contain a population inversion, and will act as an amplifier of radiation of the proper frequency, since a beam will be enhanced on passage through the medium by $(N_m - N_n)\ \rho_{nm}\ B_{nm}$ photons per second. The amplified radiation is coherent since the amplification is by stimulated emission, and spontaneous emission of the same frequency will appear as amplifier noise. A laser is, by definition, a device that contains such a population inversion, so that it acts as an amplifier of radiation with the property that the output is coherent.

In practice, it is more desirable to use the laser as a source of coherent radiation through oscillation at the appropriate optical frequency. The oscillator is constructed by adding a feedback mechanism, in the form of mirrors, to the light amplifier, so that the laser becomes a saturated amplifier of noise (noise in this case being spontaneous emission of the proper frequency). Laser action is only possible if the material can be placed in a sufficiently large population inversion, and if, in addition, a minimum feedback can be established by means of mirrors. The requirements on the material are therefore very stringent, since the population inversion depends on the rate at which excitation is supplied, and on the rates of relaxation and transition through the levels to be used.

Oscillation and Modes

In their paper on optical masers, Schawlow and Townes[13] pointed out that a Fabry-Perot interferometer may be used as the feedback device for an optical oscillator. Such a device represents a very large cavity however, and will therefore generate a highly complex electromagnetic field within the amplifier, affecting the properties of the coherent light emitted. This field may be regarded as the superposition of a large number of plane waves traveling back and forth in the resonator, with oscillation occurring along those portions of the field that form a standing wave. A particular set of such standing waves, giving rise to oscillation, is a function of the geometry of the resonator and may be referred to as a mode of oscillation.

The electric field distribution of the light emission from such a device is a function of the mode of oscillation, and Figure 2.2 shows the configurations associated with the dominant (TEM_{oo}) circular mode as well as a number of higher-order circular modes. These distributions have the cartesian designation TEM_{mnq} which refers to transverse electric and magnetic fields. The subscript m is an integer giving the number of nodes in the radial direction, while n is the number of nodes in the azimuthal direction. The integer q refers to the number of axial modes and is therefore a very large number given approximately by

$$q = 2L/\lambda \tag{2-185}$$

where L is the length of the cavity, and λ the wavelength of oscillation. The arrows in Figure 2.2 indicate the phase of the field while lines indicate the nodes.

Each mode of oscillation corresponds to a specific resonance of the Fabry-Perot interferometer, and therefore represents a particular frequency component in the output. The frequency separation between modes is given by:

$$\Delta(1/\lambda) = \left[\frac{1}{2L}\,\Delta q + \frac{1}{16}\left(\frac{L\lambda}{D^2}\right)(2m\Delta m + \Delta m^2 + 2n\Delta n + \Delta n^2)\right] \tag{2-186}$$

where D is the field aperture, and the quantity $N = (D^2/\lambda L)$ is the Fresnel number of the aperture. It can be seen from

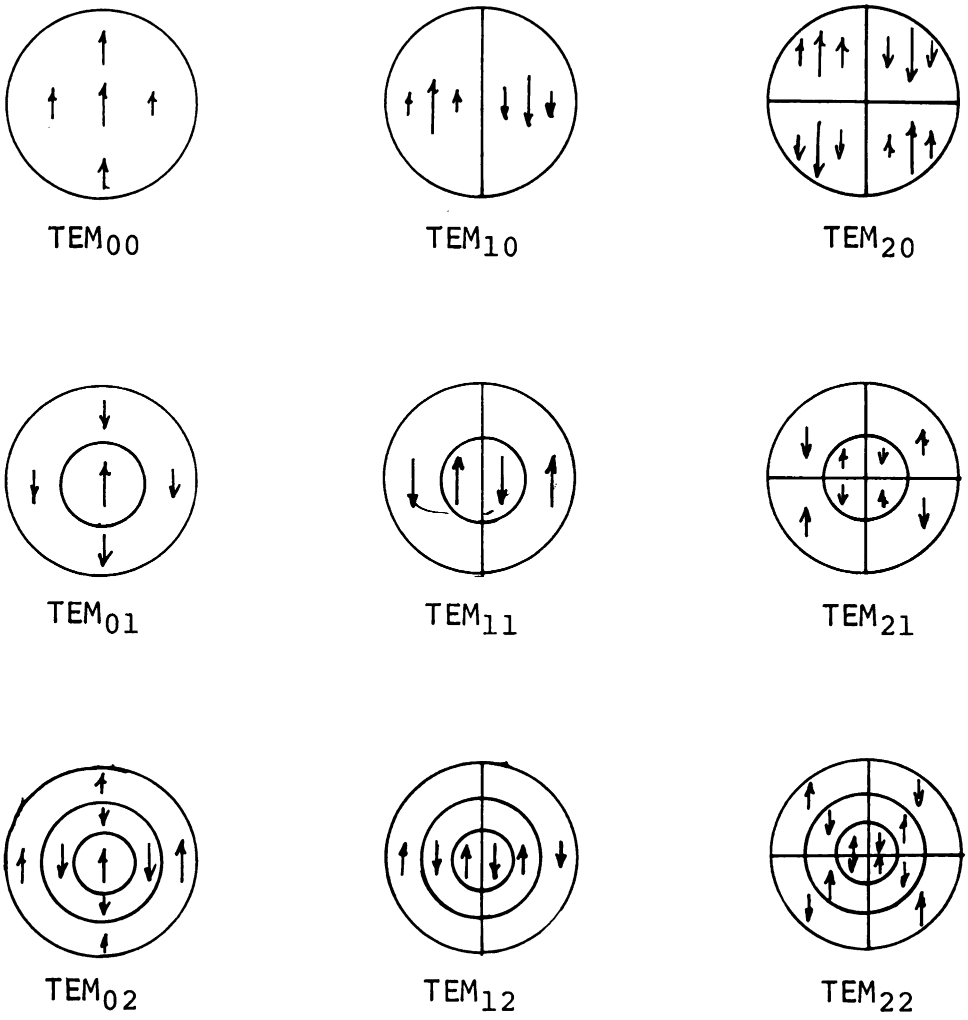

TEM_{00} TEM_{10} TEM_{20}

TEM_{01} TEM_{11} TEM_{21}

TEM_{02} TEM_{12} TEM_{22}

FIGURE 2.2.--Modes in a Laser Interferometer.

(2-186) that the frequency difference between two modes of the same type (i.e. same m and n) is given by,

$$\Delta\lambda = \lambda/q \tag{2-187}$$

or, combining (2-185) and (2-187) we have

$$\Delta\lambda = \lambda^2/2L \tag{2-188}$$

and rearranging terms we now find that,

$$\nu_{q+1} - \nu_q = \Delta\nu = C/2L, \tag{2-189}$$

A resonator formed by two spherical reflectors of equal curvature is of particular interest when the reflectors are separated by their common radii (i.e. the confocal configuration). The variation of the electric field over the surface of the reflector is given by,

$$\frac{E_{xy}}{E_o} = H_m\left[x\left(\frac{2\pi}{\lambda L}\right)^{\frac{1}{2}}\right] H_n\left[y(2\pi/\lambda L)^{\frac{1}{2}}\right] \exp\left(-\pi\frac{x^2 + y^2}{L\lambda}\right) \tag{2-190}$$

where H_m and H_n are Hermite polynomials of degree given by the mode integers m and n, and x and y are the coordinates of the point on the surface. From (2-190) we now see that the field in the TEM_{oo} mode is Gaussian, and falls to 1/e of its maximum value at a radius given by,

$$r_s = [L\lambda/\pi]^{\frac{1}{2}}. \tag{2-191}$$

The surfaces of constant phase are spherical, with radii of curvature given by

$$R = \left|\frac{R^2 + 4Z^2}{4Z}\right| \qquad (2\text{-}192)$$

where R is the radius of curvature of the reflector, and Z is the distance from the center of the resonator to the point at which the observation is made.

The resonant wavelength of the confocal system is given by

$$\lambda = 2L/(1 + q + m + n). \qquad (2\text{-}193)$$

General Description of Lasers

Maiman[5] first achieved laser action with a ruby crystal consisting of a 2 cm long cylinder of pink ruby containing 0.05 percent chronium. The end faces were plane and parallel to a high degree. One end face was made completely reflecting and the other partially reflecting. The population inversion was achieved by irradiating the crystal with a burst of very intense white light from a flashlamp through which a capacitor was discharged. Total input energy was 1000 to 2000 joules in a pulse of a few milliseconds duration. The blue-green output of the flashlamp was absorbed by the crystal, and this energy transferred to a narrow metastable state around 694.3 nm. Laser oscillation then occurred from this level to the ground state, with the emission of 694.3 nm coherent light. A simple laser of this type produces several kilowatts per square centimeter flux density, in a spectral line about 0.01 nm wide, centered about 694.3 nm. By way of contrast, a black-body at 417° K has its maximum output at 694.3 nm and emits only 1700 watts/ cm^2 in its entire spectrum, while emitting only 0.016 watts/ cm^2 in a 0.01 nm pass band at 694.3° nm.

Laser action in gases is more difficult to attain since there are no broad fluorescent levels available for optical pumping to a population inversion. Excitation by electron collision may be used however, since, when a discharge takes place in a gas, ions and free electrons are formed. The free electrons are then accelerated by the field that creates the discharge. In low pressure discharges, the average kinetic energy of the free electrons usually greatly exceeds that of the atoms or ions in the discharge. In a steady discharge, within a short time, the electrons establish a Maxwell-Boltzmann energy distribution among themselves that is characterized by an electron temperature T_e, proportional to the mean electronic kinetic energy. Inelastic collisions between atoms and electrons then occur, in which the atoms distribute themselves among their energy levels according to the Boltzmann distribution, where the temperature is now T_e. Then the number of atoms in state i is given by $N_i = N_o e^{-E_i/kT_e}$.

When more than one gas is present, excitation is exchanged between atoms of different kinds, provided that they possess energy levels near one another. The probability of such an exchange is given by

$$P_{ex} = \exp\,[-\Delta/kT] \qquad (2\text{-}194)$$

where Δ is the energy difference between the levels, and T is the temperature of the gas mixture. This process is called the resonant exchange of energy, and is particularly interesting when the excited level of one gas is metastable, since resonant exchange provides a means of relaxation from the crowded long-lived state.

Javan[6] achieved population inversion at 1.15μ in neon, by using resonance exchange in a gas discharge through a helium-neon mixture. Figure 2.3 shows the energy level diagrams of helium and neon. The lowest excited state of helium is the 2^3S which is metastable, and therefore long-lived. When helium atoms in the 2^3S state collide with neon atoms in the ground state, the excitation may be transferred to one of the 2S states of neon, which lie only 300 cm^{-1} below the helium level. Radiative transitions then take place from the four 2S levels to the ten 2P levels. The 1S terminal levels are quenched by collisions with the walls of the discharge tube. Whether a population inversion will occur depends on the relative abundances of helium and neon, the excitation rate, gas pressure, and diameter of the discharge tube. Laser action at 632.8 nm in helium-neon mixtures is possible because of the degeneracy of the 2^1S level in helium with the 3S levels in neon.

The general appearance of helium-neon lasers is shown in Figure 2.4. The mirrors are generally spherical,

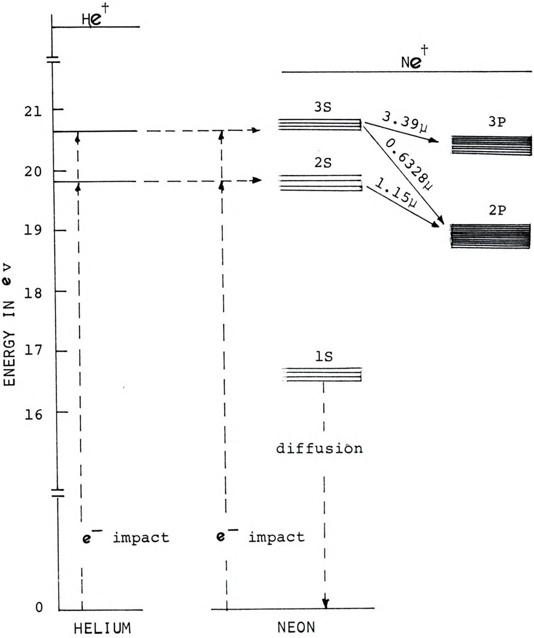

FIGURE 2.3.--Energy Levels in a Helium-Neon Laser.

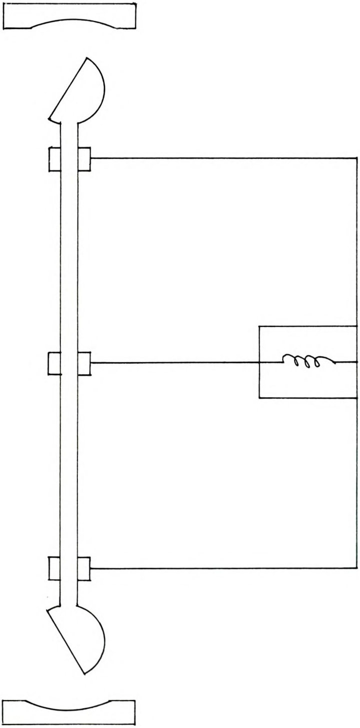

FIGURE 2.4.--Outline of a Helium-Neon Laser.

and coated with a highly reflective dielectric. The windows on the discharge tube are oriented at the Brewster angle to minimize losses and unwanted longitudinal reflections. The optimal tube diameter and length depend on the application. The discharge may be excited by high voltage dc applied to internal electrodes, or radio-frequency power applied to external electrodes.

Oscillation in the helium-neon laser occurs at, or near, the peaks of those cavity resonances that fall within the linewidth of the Doppler broadened atomic line in neon. Cavity resonances occur at frequencies given by,

$$\nu_n = \nu_{n-1} + \Delta\nu \tag{2-195}$$

where $\Delta\nu = c/2L$. Here L is the separation between the mirrors, and the n refers to the number of nodes in the standing wave pattern. For one meter separation, $\Delta\nu = 150$ MHz, and since Doppler line is about 1000 MHz wide, several modes may be excited at one time. The linewidth of a single mode is immeasureably small by spectroscopic techniques, however beat frequency measurements show that it is less than 20 Hz over a short term. The coherence length, measured interferometrically, is of the order of thousands of miles for even unstabilized gas lasers of this type.

CHAPTER III

EXPERIMENTAL

Laser Design Considerations

Introduction

The output characteristics of a laser oscillator are functions of the properties of the active medium (i.e. atomic linewidth, pressure, gas mixture) and the configuration of the optical resonator (length, aperture, reflectivity, etc.). Since the application involved constrains a number of these parameters to predetermined values, it is necessary to adjust the remaining variables to optimal positions. Unfortunately, the extreme sensitivity of the laser output to the cavity configuration precludes the possibility of a general relationship between the variables of the system. However, since most lasers are operated in extremes of either single-mode or highly multi-mode cavities, it is possible to make simplifying assumptions, and arrive at relationships between system parameters that are valid in these limiting cases. Smith[14,15] has developed a set of such relationships describing the output characteristics of the laser in terms of variables of the system, hence making possible the optimization of the output for any desired application.

Power Output

The power output of a helium-neon gas laser in single-mode cw (continuous wave) operation is

$$P = \frac{2\pi}{5}\left(\frac{d}{2}\right)^2 w_o\, G_M[(tw_1)_{opt}/w_o\, G_M] \qquad (3\text{-}1)$$

where $(tw_1)_{opt}$ is the maximum single-mode output intensity per pass (found graphically in (15)), w_o is the gas saturation parameter (found graphically in (14)), G_M is the incremental gain of the amplifier, given by

$$G_M = 3.0 \times 10^{-4}\, \ell/d \qquad (3\text{-}2)$$

where ℓ is the discharge length (cm) and d the diameter (cm). In the limit of extreme multi-mode operation, the output power becomes

$$P = \frac{2\pi}{5}\left(\frac{d}{2}\right)^2 Aw_o\, G_M\left(1 - \sqrt{\frac{a}{G_M}}\right)^2 \qquad (3\text{-}3)$$

where Aw_o = 30 (watts/cm^2) and a is the loss per pass in the resonator, and is found to be 0.2 percent for the mirrors and 0.05 percent for each Brewster angle window.

Gas Mixtures and Pressures

It has been found[14,15,16] that a range of helium-neon mixtures varying from 5:1 to 10:1 yield good results at 6328Å. Moreover Mielenz and Nefflen report that for a rf-excited discharge, a mixture of 7:1 helium-neon is optimal for most tube diameters. Best results are generally obtained however, when tubes are filled to a pressure p, given by

$$p = 0.4/d \tag{3-4}$$

where d is the tube diameter in cm.

Resonator Configuration

The properties of the laser output are defined to a large extent by the curvature and reflectivity of the reflectors used in the optical resonator, as well as by the length and aperture of the cavity. The reflectors used in optical resonators are of extremely high surface quality, and are coated with multiple layers of dielectric materials such that they may achieve virtually any desired reflectivity in any given spectral region. Generally one of the reflectors in the resonator is made as reflective as possible, while the other is chosen to have a reflectivity so that the power out of the cavity is maximized.

The choice of the geometry of the resonator (i.e. curvature and length) has a significant influence on both the spatial and temporal characteristics of the output. Moreover, the geometry may affect both the available power output and stability of the devices. The four most useful and stable configurations are shown in Figure 3.1 and are called the "large-radius," confocal, spherical, and hemispherical resonators.

If the mirrors which define the optical resonator have radii of curvature greater than the length of the

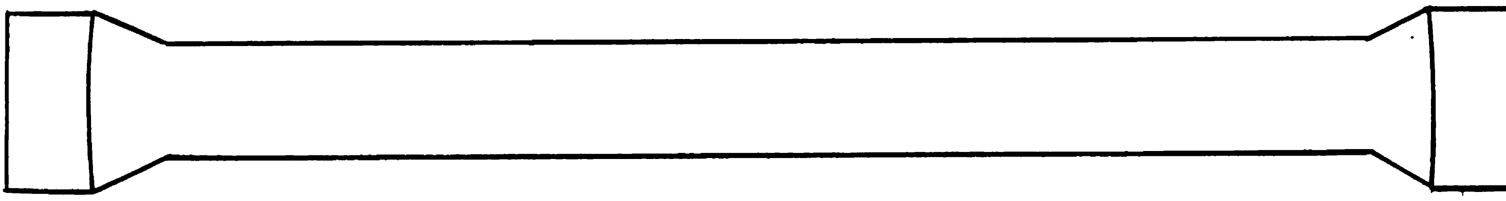

LARGE RADIUS

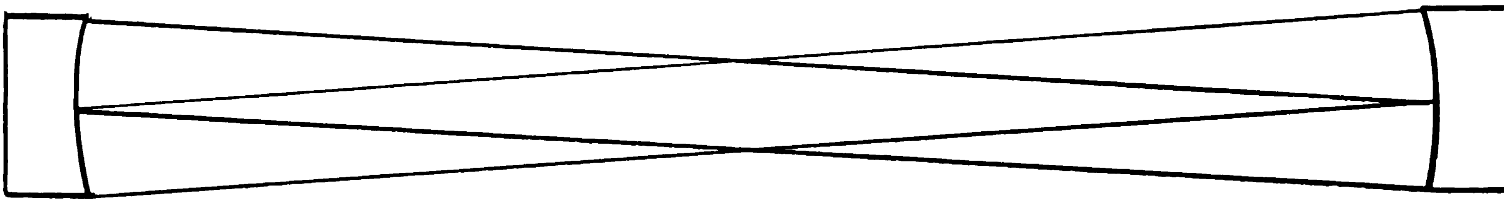

CONFOCAL

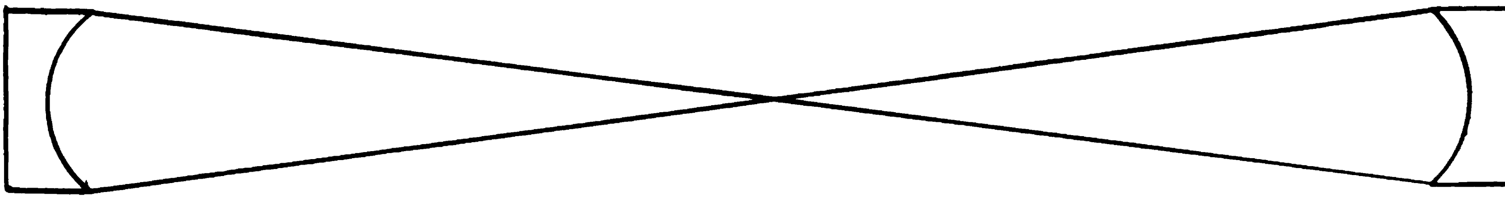

SPHERICAL

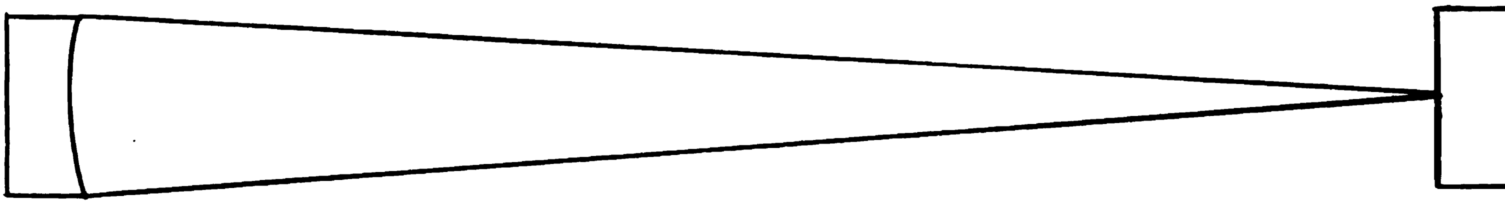

HEMISPHERICAL

FIGURE 3.1.--Resonator Configuration

cavity, the "large radius" configuration is obtained. This configuration is stable, and yields a relatively high power output provided that the radii are not extremely large (i.e. plane mirrors have $r = \infty$). When the mirror radii are three or four times the cavity length, the curvature of the mirrors corresponds to the curvature of the wave front yielding relatively good collimation as well as stable power output.

The confocal resonator (radii of curvature equal to the cavity length) represents the most common configuration for multi-mode operation. It is inherently stable and is extremely easy to align, although the power output is not as great as in the "large radius" configuration. If the radii of curvature of the two mirrors are not identical, the near-confocal configuration is unstable when the cavity length is between the two radii, so in practice the confocal arrangement is modified to keep the cavity length somewhat greater than the radii of the mirrors.

If the cavity length becomes twice the radii of curvature of the mirrors, the spherical cavity is obtained. This represents an extremely useful configuration for single-mode operation, although only about one-third the available gas discharge is used. Alignment of the spherical cavity is somewhat more difficult than the confocal, and the configuration becomes unstable when the cavity length is greater than twice the radii of curvature.

A special case of the spherical cavity is obtained when a curved mirror of radius equal to the cavity length is used in conjunction with a flat mirror to achieve a hemispherical resonator. The properties of this configuration are much the same as the spherical case, however alignment is much easier, and the output is considerably more stable. The hemispherical resonator is the most common configuration for single-mode output.

Laser Characteristics

General Description

High intensity, beam stability, and a high degree of collimation are prime requirements when observing Rayleigh scattering. We have therefore constructed two complete laser systems to fulfill the following design criteria:

(1) Maximize output power.

(2) Stabilize output power.

(3) Obtain a high degree of collimation.

(4) Maintain a beam diameter of less than 0.25 inches.

Since a very narrow band pass is not necessary, multi-mode (high intensity) operation was used whenever possible.

Radio frequency excitation via external electrodes was chosen since it is convenient and provides a relatively stable power output after an initial warm-up period.

The mirrors used in the optical resonators were supplied by Perkin-Elmer Corporation, and were made of either high quality borosilicate glass or fused quartz. The mirrors were coated with multiple layers of dielectric material deposited in vacuum to the specified reflectivity at 6328 Å.

Laser I was constructed entirely of fused quartz and was supplied by Thermal American Corporation. The discharge tube was 85 cm long with an inner diameter of 0.7 cm and was viewed through high-quality quartz windows (flat to $\lambda/10$) fused to the tube at the Brewster angle. The tube was filled with a 7:1 mixture of helium and neon to a pressure of about 1.5 torr after an initial cleanup and bakeout procedure. The resonator consisted of two spherical mirrors with radii of curvature of two meters in a cavity 130 cm long, thereby comprising a "large radius" configuration. One mirror was coated to a reflectivity very close to 100 percent, while the output was coupled from the second mirror which had a reflectivity of 99 percent. The output power for this system calculated from (3-3) was 86 milliwatts for multi-mode operation. Observation of the output using an EGG Lite-Mike calibrated at 6328 Å yielded a power of 50 milliwatts with no observable component at 60 Hz. The output power was stable to ± one percent after initial warmup, and the mode structure (observed visually) appeared very stable. The output beam was approximately 0.25 inches in diameter and had a divergence of less than 2 milliradians.

Laser II was constructed with a quartz discharge tube of length 105 cm and inner diameter 0.5 cm, fused by means of graded seals to Brewster angle windows of 7094 pyrex. The tube was supplied by PEK Laboratories and was filled with a 7:1 mixture of helium and neon at a pressure of 1.5 torr. The resonator consisted of a spherical mirror of two-meter radius and reflectivity of 100 percent, and a planar mirror with reflectivity of 99 percent. The mirrors were mounted with a separation of 150 cm, thereby comprising an almost hemispheric cavity. The calculated multi-mode output power for this laser was 90 milliwatts, however the observed output power was only about 20 milliwatts due to the less efficient cavity. The beam diameter at the planar mirror was 0.1 inch or less, and had a divergence of about 4 milliradians.

Because of its greater output power and lower divergence, Laser I was used in most of the depolarization measurements. Laser II was mounted on a bench constructed of Benelex phenolic resin, giving it considerable thermal and mechanical rigidity and allowing it to be moved about for use in measuring refractive indices.

Filling Techniques

Cleaning and filling of the laser tubes was accomplished on a high-vacuum system incorporating a Cenco Hyvac II mechanical pump in series with a CVC oil diffusion pump. Pressure in the vacuum system was measured using CVC ionization and thermocouple gauges up to a maximum of one torr. Pressures above one torr were measured using an RGI mercury flotation gauge with a range of 10 torr in increments of 0.1 torr.

The helium and neon were obtained both as ultrapure gases and as mixtures (7:1 and 10:1), in pyrex bottles with glass break seals, from Linde Division of Union Carbide

Corporation. The gases were used without further purification except for passage through a liquid nitrogen cold trap.

The discharge tubes were prepared by sealing to the vacuum system and pumping to a pressure less than 10^{-6} torr while heating with a heating tape. After a bake-out of 24 hours the tubes were filled to a pressure of about one torr with ultrapure helium, and the gas ionized by radio-frequency energy coupled into the tube via external electrodes. After several minutes of discharge the tubes were again pumped to a pressure of less than 10^{-6} torr, after which they were again filled and discharged. Having repeated this cycle until inspection with a small hand held spectroscope revealed no impurities being outgassed from the glass, the tubes were finally filled with the operating mixture of helium and neon.

Preliminary measurements of power output as a function of gas mixture and pressure were made with the laser attached to the vacuum system. Results indicated that a 7:1 mixture of helium and neon is optimal over a range of pressures from 0.8 to 2 torr (as measured by the flotation gauge), with maximum power output obtained at 1.5 torr. Having been filled to this pressure and removed from the vacuum system, the tubes were used for several hundred hours before refilling.

Power Supply

The gaseous discharge in both Lasers I and II was obtained by coupling radio-frequency energy into the tube by means of external electrodes. The radio-frequency supply was an E. F. Johnson "Viking-Challenger" transmitter, modified to allow continuous operation at 27.1 MHz as well as to permit continuous adjustment of the input power to the laser. Coupling of the low impedance transmitter output to the high input impedance of the laser was achieved by using a parallel tuned, balanced impedance matching network. The matching network and electrodes were adjusted to maximize the power input to the discharge, the power output from the laser then being controlled by adjustment of the transmitter.

Radio-frequency excitation has the advantages of long tube life (since there are no internal electrodes) and an extremely stable discharge, with the chief disadvantage being the necessity of supplying rf shielding. Typically the power output of the laser was maximized with a power input of about 80 watts.

Laser Alignment

The mirrors of the laser resonator were mounted in precision gimbal suspensions supplied by Lansing Research Corporation. These suspensions allow a smooth and continuous rotation of the plane of the mirror about two orthogonal axes perpendicular to the longitudinal axis of the cavity.

To achieve oscillation the mirrors must be made exactly parallel to one another, and perpendicular to the axis of the discharge. Two methods were devised to permit rapid adjustment of the cavity and tube to fulfill these requirements.

(1) A small point source was used as an autocollimator by placing it at the focal point of a telescope eyepiece. The collimated light emerging from the eyepiece was projected along the axis of the tube from outside the cavity, and the mirror at the opposite end of the cavity was then rotated to reflect the light back to the source. The near mirror was then rotated until the images of the primary and secondary beams on the far mirror coincided. The cavity was then well enough aligned to permit oscillation and further mirror adjustments were made to maximize the power output from the laser.

(2) A glass plate was placed inside the optical cavity to inhibit laser oscillation so that the image of the gaseous discharge could be observed in the far mirror, by sighting through the bore of the discharge tube. Satisfactory alignment was assured when multiple reflections from the two mirrors could be seen in the image at the far mirror. The glass plate was then removed from the cavity and laser action would immediately begin. This was found to be a very simple and rapid means of obtaining alignment, but requires considerable experience and practice on the part of the experimenter.

Photometer Design

Introduction

Light scattering measurements involve the detection and precise measurement of extremely low light levels. Therefore, the elimination or minimization of potential sources of noise, both electrical and optical, is of prime importance in the design and fabrication of a system for the measurement of Rayleigh scattering.

The system for the precise measurement of depolarization ratios consists basically of three parts: the light source, the photometer, and the detection system. It is convenient to consider each of these subsystems independently before considering the characteristics of the system as a whole.

Light Source

The light source used in our measurements was Laser I, which was described in the section entitled Laser Characteristics. Preliminary experiments showed that there are four sources of amplitude noise in this laser, which give rise to fluctuations in both the output power and the spatial intensity distributions.

The first noise source was a statistical fluctuation in the gaseous discharge, which superimposed a "white" noise spectrum on the laser output. This problem was easily overcome by modulating the laser output (using a mechanical chopper) and using a narrow band-pass detector operating in coherence with the modulator (as will be discussed in the section entitled Detector). The second source of noise was caused by the presence of dust in the air, and manifested itself as a low frequency ($\sim$1 Hz) fluctuation in the laser output, with a relatively large spectral power density.

Mechanical and thermal stresses caused small shifts in the laser alignment, thereby creating a noise spectrum in the region from 1000 Hz to 0.1 Hz, and finally, fluctuations in the power supply output contributed to both high and low-frequency noise.

Elimination of thermal and mechanical stress as a source of noise was accomplished by mounting the entire laser on a table top made of a slab of "Benelex," a phenolic resin supplied by the Masonite Corporation. The slab was 12 feet long, 3 feet wide, 2 inches thick, weighed approximately 650 pounds, and was mounted on a permanent laboratory table of the same dimensions and weight. The combination of large mass and very small coefficient of expansion effectively damped mechanical and thermal oscillations.

Drift in the power output of the transmitter was minimized by stabilizing the line voltage, allowing a sufficiently long warmup period before operation, and by operating well below maximum output ratings. Moreover, to prevent radiation of the 27.1 MHz transmitter output to other system components, the entire laser assembly was enclosed in an aluminum box, and all cables and plugs were fitted with rf filters.

The only remaining component of amplitude noise in the light source was that due to dust in the air within the cavity. This was not found to be a serious problem however, and by using a long time constant in the output filter of the detector any noise due to this source was minimized.

Photometer

The intensity of Rayleigh scattered light, and in particular the vertical component of the scattering, is a function of the refractive index and temperature of the scattering material. It is therefore imperative in the precise measurement of depolarization that both sample and cell be kept scrupulously clean, and at constant temperature. In addition, the rescattering of Rayleigh scattered light greatly enhances the depolarization, necessitating the consideration of means to minimize such multiple scattering effects. Since the probability of scattering is directly proportional to the path length, it is necessary to keep the sample small while also keeping the light beam as narrow as possible. Obviously, the use of the 6328Å emission from a helium-neon laser is of great significance in reducing multiple scattering effects due to the inverse fourth power wavelength dependence of the scattering, and due to the high intensity available from a relatively small diameter beam.

Elimination of extraneous light in the observation of Rayleigh scattering is a somewhat more difficult problem as there are several potential sources for such light. The principal sources of extraneous light may be tabulated as follows;

(1) Ambient room light leaking into the measurement system.

(2) Reflection of the incident beam from the surfaces of the sample cell.

(3) Reflection of Rayleigh scattered light from the walls of the cell or cell holder.

(4) Reflection of the incident beam from the beam stop at the end of the light path.

and will be considered one at a time in the following.

(1) Ambient room light was excluded from the photometer by enclosing the entire system in a light-tight box (Figure 3.2) constructed of 0.250 inch aluminum, 10.50 inches long, 9.50 inches wide, and 6.75 inches high, machined to tolerances of 0.001 inch. The light path within the photometer was defined by sets of apertures 0.500 inches in diameter. After assembly of the instrument, all the joints were coated with a liquid rubber sealant, and the entire interior was sprayed with several coats of flat black Krylon.

Light was admitted to the photometer through a standard camera shutter attached to a long (6.0 inch) cylindrical barrel whose interior was painted flat black. After entering the system, the beam passed through an aperture and into the compartment containing the cell holder. The cell holder was constructed of a solid copper cylinder, 2.25 inches high and 2.50 inches in diameter, milled to index the position of the scattering cells, and soldered inside a close fitting copper sleeve, 5.0 inches in height. The copper sleeve, into which the scattering cells were set, was wrapped with a coil of 0.125 inch copper tubing, a layer of asbestos, two coils of nichrome heating wire, and several more layers of asbestos.

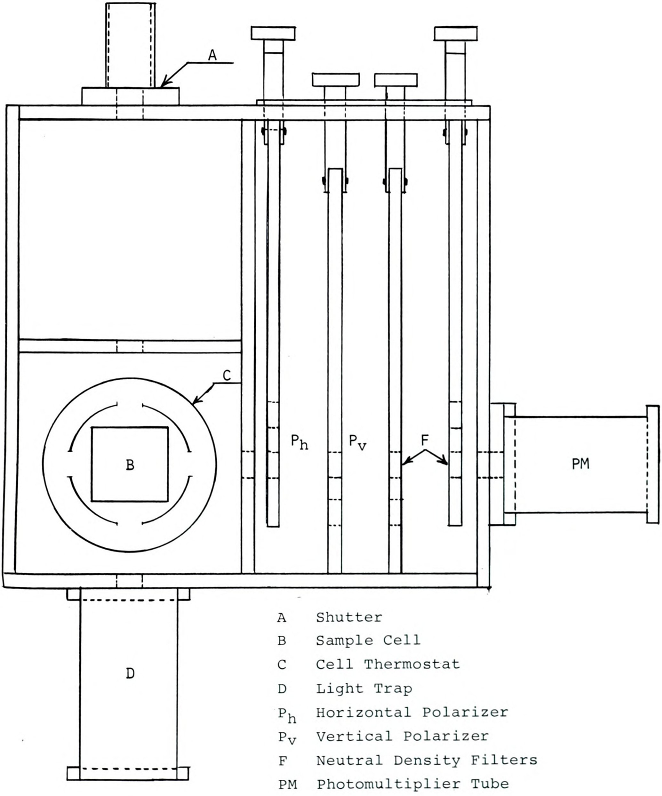

A Shutter
B Sample Cell
C Cell Thermostat
D Light Trap
P_h Horizontal Polarizer
P_v Vertical Polarizer
F Neutral Density Filters
PM Photomultiplier Tube

FIGURE 3.2.--The Polarization Photometer

This entire assembly was painted flat black, and light was admitted through a set of 0.50 inch apertures. The Rayleigh scattered light was observed at 90° to the incident beam through a second set of 0.50 inch apertures in the cell holder.

(2) Reflection of the incident beam from the front surface of the sample cell was eliminated as a source of stray light by careful indexing of the cell within the cell holder, and by indexing the cell holder within the photometer so that such reflections passed back through the entrance apertures and could not reenter the photometer. Reflection from the back surface of the cell could not be eliminated, however use of high quality cells minimized the enhancement of the depolarization due to this source.

(3) Reflection of Rayleigh scattered light from the walls of the cell holder was minimized by the diffuse black surface of these walls. Moreover, the reflection along the viewing axis (90°) was further reduced by allowing Rayleigh scattered light (at -90°) to leave the cell holder through a 0.50 inch aperture opposite the detector aperture, and absorbing it in a black felt light trap.

(4) After passage through the sample cell, the incident beam left the photometer through a 0.50 aperture and entered a specially designed light trap, as shown in Figure 3.3. The trap was constructed of pyrex, and was designed to fit into a photomultiplier housing in place of the photomultiplier tube. Measurement of the incident beam intensity

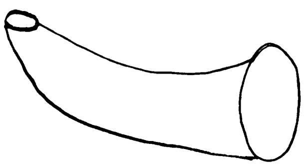

FIGURE 3.3.--Light Trap

could then be accomplished by simply removing the light trap and replacing it with a photomultiplier. The geometry of the trap was such that a beam entering through the 0.50 inch aperture would undergo several reflections from the diffuse surface of the trap and then exit through an aperture, into a closed space with a diffuse black surface. All the surfaces of the trap were painted flat black, and attempts to measure the amount of light reflected back out the front of the trap were unsuccessful, indicating that the design was at least reasonably efficient.

(5) Temperature Control: Constant temperature in the sample was maintained by cementing a thermistor probe to the wall of the cell holder and using this termistor as the sensor for a Thermistemp Model 71 Temperature Controller. The controller operated a Variac Autotransformer connected to the nichrome heating wire on the cell holder. The variac was adjusted to yield approximately equal on-off cycles at the controller, which achieved temperature regulation of better than 0.1°C at 25°C. Any desired temperature from approximately 10°C to 150°C could be maintained by circulating fluid of a slightly lower temperature through the copper

coil surrounding the cell holder, and using the nichrome heating wire to regulate the temperature at the desired point.

(6) Sample Cells: A number of scattering cells of various sizes and shapes were constructed and used in preliminary experiments. It was found however, that best results were obtained using two commercial cells available from Brice-Phoenix Corporation. These cells were square, 1.18 inches on a side, and were 2.375 inches high, containing a volume of about 40 cm^3. They were constructed of optical quality pyrex, and yielded remarkably consistent and identical results.

It was found that with no sample in the cell, no scattered light could be observed by the detection system.

Detector

The detection subsystem (Figure 3.4) included the polarizers for separating the two linear polarization components, neutral density filters for adjusting the intensity level, interference filters for blocking unwanted wavelengths, and the photomultipliers and amplifiers. The principal optical problems in constructing the detection subsystem were maintaining the relative alignment of the optical components, suppression of stray light and fluorescence, and the choice of an optimal geometry.

The Rayleigh scattered light (at 90°), after leaving the cell and cell holder, passed through a 0.50 inch aperture

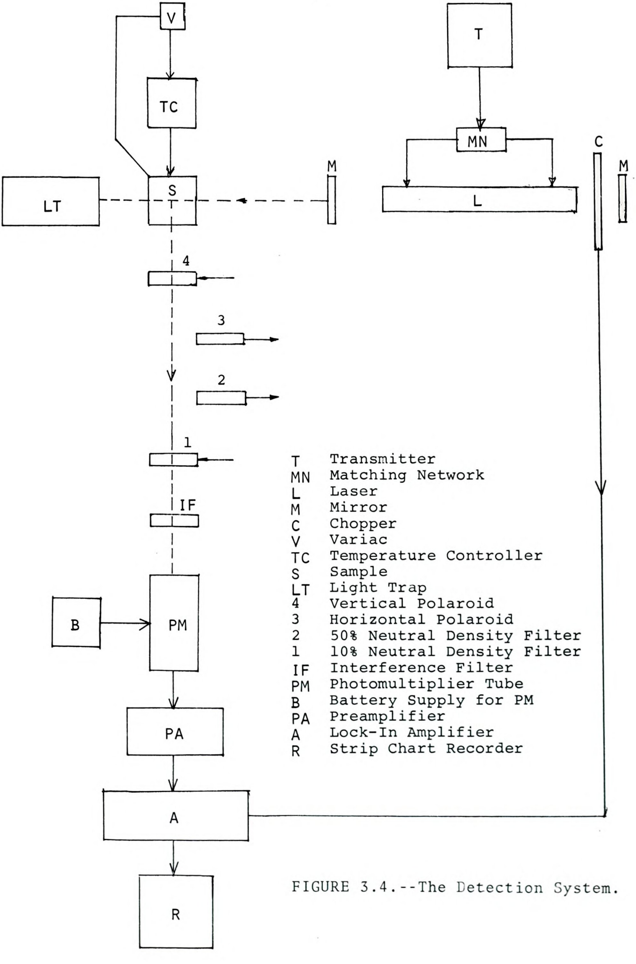

T	Transmitter
MN	Matching Network
L	Laser
M	Mirror
C	Chopper
V	Variac
TC	Temperature Controller
S	Sample
LT	Light Trap
4	Vertical Polaroid
3	Horizontal Polaroid
2	50% Neutral Density Filter
1	10% Neutral Density Filter
IF	Interference Filter
PM	Photomultiplier Tube
B	Battery Supply for PM
PA	Preamplifier
A	Lock-In Amplifier
R	Strip Chart Recorder

FIGURE 3.4.--The Detection System.

into the compartment containing the detection subsystem. The polarizers and neutral density filters were mounted on four plates of 0.125 inch aluminum which were free to move in slots perpendicular to the optical path. Each plate contained two 0.50 inch apertures, one of which was in the optical path when the plate was at either end of its slot. A brass rod was connected to each plate, and projected through a rubber "O"-ring light seal and a double wall of 0.25 inch aluminum to the exterior of the box. One optical element was mounted on each slide, so that the element could be positioned in or out of the light path by pushing on the appropriate rod. The geometry of the light path was not changed by removing or inserting an optical component since the plates were indexed very precisely in their slots. The polarizers were mounted in the first two plates so that no subsequent optical elements could contribute to the depolarization.

The neutral density filters were supplied by Baird-Atomic and were obtained in transmittances of 50 percent, 30 percent, 10 percent, and 1 percent; making available the following transmittances when used one or two at a time: .50, .30, .15, .10, .05, .03, .01, .005, .003, .001. Combinations of neutral density filters were placed in the light path during the measurement of the vertical polarization component, to make its intensity comparable to the horizontal component. It was then unnecessary to make any

electrical changes in the apparatus during a measurement, as the depolarization ratio was simply given by

$$\rho_v = \frac{H_v}{V_v}(T), \tag{3-5}$$

where the subscript v refers to vertically polarized incident light, H_v and V_v are the deflections on the strip chart due to the horizontal and vertical polarization components, and T is the transmittance of the neutral density filter combination. Obviously it is desirable to keep the ratio H_v/V_v as near unity as possible, so a filter combination as near ρ_v as possible must be chosen for best results. In addition, the neutral density filters must be calibrated very carefully to obtain the best possible resolution.

The photomultiplier assembly was a one piece copper cylinder, mounted to the photometer with a light tight "O"-ring seal. The photomultiplier tube was held in place by a nylon bushing, and viewed the scattering volume through 0.50 inch apertures in the photometer wall and the nylon bushing. The inside surfaces of this assembly were also painted flat black, and the nylon bushing was carefully sealed so that light could enter the photomultiplier tube only through the optical aperture. To eliminate any effects due to broadband fluorescence, room light, or incoherent emission from the laser, a narrow band pass interference filter was mounted in the nylon bushing which held the photomultiplier tube in place. This filter had a half-width of 5.2 nm and a maximum transmittance of 75 percent at 632.8 nm. This band-width was sufficient to pass all the components of the Rayleigh scattered light, and yet prevent any fluorescent or extraneous light from being detected.

The photomultiplier tube (RCA 6199 or RCA 7102) was electrostatically and magnetically shielded using mu-metal tube shields, and was wired according to reference data supplied by RCA. Since the RCA 6199 and RCA 7102 are physically identical, they could be rapidly interchanged to provide a broad region of good response characteristics. Photomultiplier power was obtained from a variable voltage battery supply to assure stability of operation and a minimum of 60 Hz noise in the output.

In order to reduce the electrical band-width of the detection subsystem to a value small enough to eliminate most of the noise spectrum, it was decided to use a phase-locked amplification system. In a phase-locked detector, the signal is made to appear at a specified frequency and phase. The receiver is then tuned to the frequency and phase of the signal and ignores any other spectral components accompanying the signal. The receiver is then said to be "phase-locked" to the signal, and will tend to block noise contributions within its band-pass since they are of random-phase.

Amplitude modulation of the cw laser output was achieved by mechanically chopping the beam with a Princeton Applied Research Corporation light chopper operating at

80 Hz, and emitting a reference signal of the same frequency and phase as the modulated light beam. The chopper was placed at the far end of the laser and inside the optical cavity so that the coherent output at 6328 Å was modulated while the incoherent output was not. Hence, only that component of the signal that was actually due to the scattering of coherent light was amplified.

The output of the photomultiplier tube was first preamplified by a Philbrick Associates Model P25A solid state operational amplifier, and was then applied to the signal channel input of a Princeton Applied Research Model JB-5 Lock-In Amplifier. The reference signal from the chopper was applied to the reference channel input of the amplifier, and phase-locked to the signal channel. The amplifier output, as detected by a standard strip chart recorder, was then proportional to that component of the photomultiplier output appearing with the specified frequency and phase. This technique effectively removed those components of the noise spectrum with a frequency greater than 1.5 Hz. Lower frequency noise components, and amplifier noise were reduced by filtering the amplifier output through an RC filter with a 30 second time constant.

Alignment

Alignment of the entire system was perhaps the most critical part of the experiment. To maintain the relative alignment over both long and short periods, the polarization photometer, as well as the laser, was mounted on the Benelex table top described on pages 68 and 69 under Filling Techniques. Defining a right-handed orthogonal coordinate system with the direction of light propagation the Z-axis, the X-axis vertical with respect to the laboratory, and the Y-axis horizontal (Figure 2.1), the system was aligned using a high quality cathetometer whose axis was parallel to the laboratory floor.

The laser was mounted to the table top first, and was aligned such that the Z-axis defined by the laser output was colinear with the optical axis of the cathetometer. Next, the polarization photometer was mounted such that its optical axis was colinear with the Z-axis. The table top was found to be level to better than a degree over its surface, so that the X and Y axes of the laser and photometer were parallel to better than a degree.

Alignment of the plane of polarization of the laser was extremely easy since the Brewster angle windows reflect, in the plane of polarization, a small amount of the light incident on them. Two plumb lines were then dropped from the ceiling to intersect the Z-axis of the system, and the line defined by these two points represented the intersection of the XZ plane with the ceiling. The reflections from the Brewster angle windows were then observed on the ceiling and the discharge tube rotated to bring the reflections onto the line defining the XZ plane. In this way the plane of polarization was adjusted to better than 0.5 cm of arc on a 200 cm radius, or to less than 0.0025 radians.

The polarizers, which were constructed of high-quality Polaroid Corporation Type HN-32 sheet, mounted in aluminum circles, were aligned by measuring their planes of polarization with a conventional optical polarimeter (using light at 632.8 nm). This procedure allowed alignment of the polarizers to within 2° of arc.

System Characteristics

Measurement Techniques

Measurements were made by placing the sample cell in the cell holder and allowing sufficient time for the system to come to thermal equilibrium. Preliminary results indicated that this time was of the order of five to ten minutes, depending on the initial and final temperatures. Three modes of temperature control were available:

(1) Cooling alone.
(2) Coolant plus heat.
(3) Heat alone.

Initial runs were made by first cooling the system to a low temperature limit of 10°C by circulating water, cooled by an ice bath, through the cooling coils around the cell holder. Temperature control was then initiated using both coolant and heat. After a measurement had been obtained, the temperature was increased, generally in increments of five degress centigrade, temperature control being maintained during the course of a particular measurement. At ambient temperatures or slightly above, the coolant supply was disconnected and temperature control maintained in the "heat alone" mode.

The electronic components were optimized by following the recommended procedures outlined in the manufacturers' operating manuals. The photometer shutter was then opened, allowing light to impinge on the sample in the thermostat: care being taken to insure that all the polarizers and filters were in the optical path at this time. The vertical polarizer was then removed, allowing the horizontally polarized component of the signal to reach the photomultiplier.

Phototube voltage, preamplifier gain, and the neutral density filters were adjusted to yield an adequate signal level as indicated by the panel meter on the amplifier, with the output in the "signal" mode; the voltage and gain being balanced so as to yield the best signal to noise ratio as indicated by fluctuations of the panel meter. The amplifier was then switched to the "output" mode and the input level and phase controls used to "peak" the signal within the linear operating range of the amplifier. The system was then operational, requiring only that the appropriate neutral density filters be inserted in the optical path to bring the vertically polarized component of the signal to an on-scale level.

In most cases at least five independent measurements of each component of the signal were taken at each temperature. Furthermore, after the maximum temperature was reached the measurements were repeated while decreasing the temperature in increments of five degrees centigrade. The data were then analyzed statistically using a least-squares treatment.

Temperature Stability and Reproducibility

Throughout the temperature range of the thermostat, the sample temperature was maintained with a stability of better than 0.3°C, as measured by both a thermistor and a sensitive thermometer placed in a sample cell containing water. Reproducibility was a somewhat more difficult matter, requiring calibration of the controls. Using only the permanent dial markings on the controller, the temperature could be set to an accuracy of ±1°C; however, upon calibration this was improved to ±0.5°C. Temperature reproducibility and stability were definitely areas that could bear improvement, however, as we shall see in the results, they were not the accuracy limiting factors.

Photomultiplier Response

The photomultiplier tubes selected for the detection subsystem (i.e. RCA 6199, RCA 7102) have been reported to have uniform response characteristics to various states of polarization. This was verified by rotating the tube while illuminating the photocathode with the linearly polarized output of a Bausch and Lomb grating monochromator using a tungsten lamp as the light source. Over the wavelength region from 550 nm to 700 nm no polarization bias could be observed in either photomultiplier.

In most of the measurements reported here, the RCA 6199 photomultiplier was used because of its higher quantum efficiency at 633 nm and its better noise characteristics. For measurements at 1.15 microns, the RCA 7102 would be the only possible choice due to its S1 photocathode.

Effects of Beam Parameters

Stacey[20] points out that the results of light scattering measurements in general, and depolarization ratios in particular, are affected by the spatial characteristics of the illuminating radiation. Consideration of the scattering process shows that these effects may be due to one of two sources; multiple scattering, or uncertainty in the angle of observation. Use of a helium-neon laser tends to alleviate this spatial dependency, in the first case due to the fourth power wavelength dependence of the Rayleigh scattering, and in the second case due to the extreme collimation and coherence of the source. Preliminary experiments were undertaken to measure the effects of beam parameters using the helium-neon laser, and to compare, when possible, these data with those obtained using a conventional light source (e.g. a mercury lamp).

Beam Diameter: Lontie[24] reports that the depolarization ratio varies linearly as the beam diameter, the slope being very wavelength dependent. The effects of beam diameter in this system (at 633 nm) were measured by using the laser in multimode operation (large beam), and varying the diameter of the iris diaphragm in the photometer shutter. It was found that no diameter dependence could be observed using simple molecules of either high or low depolarization ratio; however, it is to be expected that solutions of strong scatterers (i.e. high polymers) will exhibit diameter dependence due to multiple scattering, in which case a highly collimated laser operating in the TEM_{00} mode would yield the best results.

Single Mode Operation (TEM_{00}): In single mode operation, the laser emits a single well defined frequency, in a very narrow beam with a Gaussian intensity distribution (hence a very low spatial frequency). The "effective" width of the TEM_{00} mode is considerably less than its apparent width due to its intensity profile, making this mode of operation ideal for use when multiple scattering may be a problem. Since simple molecules exhibit little or no diameter dependence, this mode of operation was used to see if the smaller divergence and smaller band-pass would cause a noticeable decrease in depolarization. Results of preliminary experiments showed that this was not the case, and multimode operation was therefore acceptable.

Beam Shape: The effect of beam shape on depolarization is basically the same as that of beam diameter since, for a given intensity, changing the beam shape simply changes the effective scattering volume. Hence, for a given power output, a spherical scattering volume (circular beam) will have the smallest effective size.

Since many beam shapes may be conveniently obtained in a laser by simply operating in an appropriate mode, an attempt was made to observe the affects of changing this parameter. Although no effect could be observed in the scattering from small molecules, it is reasonable to assume that in scattering from high polymers the TEM_{oo} mode should be used exclusively to avoid this problem.

Calibration of the Neutral Density Filters

The range of depolarizations in this study was such (.5 to .02) that two neutral density filters were adequate to cover the range. The 50 percent and 10 percent transmission filters were chosen and mounted in the two slides behind the polarizers.

Careful calibration of the filters is an absolute necessity due to the linear dependence of the depolarization on the filter transmittance. Calibration was accomplished by placing a sample in the cell and operating the instrument as discussed in the preceding sections, except that the deflections were measured for the six possible combinations of filters and polarizers. Over a hundred data were taken in this way under conditions identical to those used in measuring the depolarization. These results are summarized in Table 3.1:

TABLE 3.1.--Calibration Factors for Neutral Density Filters

	F1	F2	F12
Vertical Polarizer	0.1209±0.0005	0.511±.001	0.0644±.0002
Horizontal Polarizer	0.1222± .0005	0.513±.001	0.0645±.0002

where F1 refers to the 10 percent filter, F2 to the 50 percent filter and F12 to the combination of the two. The uncertainties represent the rms deviations of individual measurements from the mean.

Prior to making a measurement with this apparatus, the calibration factors were checked by making a number of calibration measurements. It was found that the factors remained constant over the period of time the apparatus was in use.

Error Analysis and Total Accuracy

Having optimized the various system parameters, the remaining, and limiting source of error is misalignment of the system components. The error accumulated from this source may be analyzed most conveniently by the methods of Chapter II, using the coherence matrix formalism.

Consider the light scattering system as being oriented on a right-handed coordinate system whose origin is the center of the scattering volume, and whose Z-axis is the direction of propagation of the incident beam (see Figure 2.1). We are now interested in observing the polarization components of the light scattered at some distance (r) along the Y-axis ($\theta = 90°$), assuming the incident light to be plane polarized in either the XZ (vertical) plane, or YZ (horizontal) plane. The potential sources of error may now be identified as rotations of this laboratory-fixed coordinate system about the various axes. Denoting a rotation about the Z-axis by ϕ, about the X-axis by θ, and about the Y-axis by γ, we may generate the instrument operator ($\overline{L}$) of the various system components including their alignment errors.

We shall assume the system to consist of a totally unpolarized light source (laser discharge tube), followed by a polarizer (Brewster-angle window), a scattering system, and a resolver which takes the projection of the scattered wave field along some axis. The coherence matrix representation of the unpolarized source is given by:

$$\overline{J} = \begin{bmatrix} 1 & 0 \\ 0 & 1 \end{bmatrix}. \tag{3-6}$$

The instrument operator of the polarizer (Brewster window) is given by (Table 2.1),

$$\overline{P} = \begin{bmatrix} \cos^2 \phi & \sin \phi \cos \phi \\ \sin \phi \cos \phi & \sin^2 \phi \end{bmatrix}$$

where ϕ is the angle the polarizer makes with respect to the X-axis. Now, assuming the polarizer to be oriented along the X-axis, with some small error, we have that,

$$\overline{P}_v = \begin{bmatrix} 1 & \sin\phi \\ \sin\phi & \sin^2\phi \end{bmatrix} \simeq \begin{bmatrix} 1 & \phi \\ \phi & \phi^2 \end{bmatrix} \qquad (3\text{-}7)$$

where the subscript v refers to the vertical axis, and ϕ represents the angular misalignment with respect to the vertical axis.

The instrument operator for the scattering system is given as before by

$$\overline{S} = \begin{bmatrix} S_{XX} & S_{XY} \\ (S_{XY}\cos\theta - S_{XZ}\sin\theta) & (S_{YY}\cos\theta - S_{ZY}\sin\theta) \end{bmatrix} \qquad (3\text{-}8)$$

where

$$S_{NN'} = S_{N'N} = \sqrt{\kappa}\,\alpha_{NN'}$$

Since we are interested in the scattering along the Y-axis, we shall consider the angle θ to be given by,

$$\theta = 90° \pm\Delta\theta$$

where $\Delta\theta$ is the error in alignment in the YZ plane. The scattering matrix now becomes

$$\overline{S}(90) = \begin{bmatrix} S_{XX} & S_{XY} \\ S_{XY}\Delta\theta - S_{XZ} & S_{YY}\Delta\theta - S_{YZ} \end{bmatrix} \qquad (3\text{-}9)$$

Finally, the operators representing the resolvers may be seen (Table 2.1) to be

$$\overline{R}_\beta = \begin{bmatrix} \cos^2 \beta & \sin \beta \cos \beta \\ \sin \beta \cos \beta & \sin^2 \beta \end{bmatrix} \tag{3-10}$$

where β is the angle the resolver makes with respect to the X'-axis. That is, the angle β is zero for a resolver taking the intensity component parallel to the X'-axis, and $\beta = 90°$ for a resolver taking the intensity component parallel to the Y'-axis (where the resolver plane is perpendicular to the Z'-axis). Then, letting γ represent the error in alignment of the resolver we have, for small γ:

$$\overline{R}_v = \begin{bmatrix} 1 & \gamma \\ \gamma & \gamma^2 \end{bmatrix} \tag{3-11}$$

$$\overline{R}_h = \begin{bmatrix} \gamma^2 & \gamma \\ \gamma & 1 \end{bmatrix} \tag{3-12}$$

where subscripts h and v refer to the horizontal and vertical components respectively, and we have assumed the misalignment to be the same for both resolvers.

Using the results of the section entitled Coherence Matrix Formalism in Chapter II, we may generate the instrument operator of the entire system of polarizer, scatterer, and resolver since

$$\overline{L}_h = \overline{R}_h \, \overline{S} \, \overline{P}_v \tag{3-13}$$

and

$$\overline{L}_v = \overline{R}_v \, \overline{S} \, \overline{P}_v . \tag{3-14}$$

Substituting the appropriate expressions, we obtain the result:

$$\overline{L}_h = \begin{bmatrix} \gamma M & \phi\gamma M \\ M & \phi M \end{bmatrix} \quad (3\text{-}15)$$

where

$$M = \gamma S_{XX} + \phi\gamma S_{XY} + \theta S_{XY} - S_{XZ} + \phi\theta S_{YY} - \phi S_{YZ} \quad (3\text{-}16)$$

(replacing $\Delta\theta$ by θ, where θ is now a small error angle) and

$$\overline{L}_v = \begin{bmatrix} N & \phi N \\ \gamma N & \phi\gamma N \end{bmatrix} \quad (3\text{-}17)$$

where

$$N = S_{XX} + \phi S_{XY} + \gamma\theta S_{XY} - \gamma S_{XZ} + \phi\gamma\theta S_{YY} - \phi\gamma S_{YZ} \quad (3\text{-}18)$$

Now, as was shown in Chapter II, the coherence matrix representation, $\overline{J}'$, of the light observed by the detector is given by

$$\overline{J}_h' = \overline{L}_h \, \overline{J} \, \overline{L}_h^{\dagger} \quad (3\text{-}19)$$

where the horizontal resolver is used, and,

$$\overline{J}_v' = \overline{L}_v \, \overline{J} \, \overline{L}_v^{\dagger} \quad (3\text{-}20)$$

when the vertical resolver is used.

Combining (3-6), (3-15), and (3-19) we obtain,

$$\bar{J}_h' = \begin{bmatrix} \gamma^2 & \gamma \\ \gamma & 1 \end{bmatrix} (1 + \phi^2)M^2 \qquad (3\text{-}21)$$

where M is given by (3-16) and the subscript h refers to the fact that the horizontal resolver is being used. Similarly, for the vertical component, we have from (3-6), (3-17), and (3-20):

$$\bar{J}_v' = \begin{bmatrix} 1 & \gamma \\ \gamma & \gamma 2 \end{bmatrix} (1 + \phi^2)N^2 \qquad (3\text{-}22)$$

where N is given by (3-18). Hence, the intensities of the horizontal and vertical components of the scattered radiation are given by, respectively,

$$H_v = \text{Tr } \bar{J}_h' = (1 + \gamma^2)(1 + \phi^2)M^2 \qquad (3\text{-}23)$$

$$V_v = \text{Tr } \bar{J}_v' = (1 + \gamma^2)(1 + \phi^2)N^2 \qquad (3\text{-}24)$$

where the subscript v refers to the vertically polarized incident light. The depolarization ratio, ρ_v, for vertically polarized incident light, is now found by combining (2-71), (3-23), and (3-24); that is,

$$\rho_v = H_v/V_v = M^2/N^2 \qquad (3\text{-}25)$$

where M and N are as defined in (3-16) and (3-18). Performing the squaring operation, dropping cross products of off-diagonal terms ($S_{MM'}$, $S_{NN'}$) which are zero according to (2-115) and (2-116), and dropping terms of fourth degree in γ, θ, and ϕ, (3-25) becomes

$$\rho_V = \frac{S_{XZ}^2+\gamma^2 S_{XX}^2+\phi^2 S_{YZ}^2+\theta^2 S_{XY}^2+\phi\gamma\theta[S_{XX}S_{YY}+S_{XY}^2]}{S_{XX}^2 + S_{XZ}^2 + S_{XY}^2 +\phi\gamma\theta[S_{XX}S_{YY}+S_{XY}^2]} \tag{3-26}$$

and we have derived the desired expression for ρ_V in terms of the angular errors ϕ, θ, and γ.

Assuming now, that the third order term, $\phi\theta\gamma$, is small compared to the second order terms, we have;

$$\rho_V = \frac{S_{XZ}^2 + \phi^2 S_{YZ}^2 + \gamma^2 S_{XX}^2 + \theta^2 S_{XY}^2}{S_{XX}^2 + \phi^2 S_{XY}^2 + \gamma^2 S_{XZ}^2} \tag{3-27}$$

and recalling (2-115), that is,

$$S_{NN'} = \begin{cases} [45\alpha^2 + 4\beta^2]\kappa/45 & (N = N') \\ [3\beta^2/45]\kappa & (N \neq N') \end{cases} \tag{2-59}$$

we see that

$$\rho_V = \frac{3\beta^2(1 + \phi^2 + \theta^2) + (45\alpha^2 + 4\beta^2)\gamma^2}{(45\alpha^2 + 4\beta^2) + 3\beta^2(\phi^2 + \gamma^2)} \tag{3-28}$$

Recalling that the exact value of ρ_V is given by

$$\rho_V = \frac{3\beta^2}{45\alpha^2 + 4\beta^2} \tag{2-128}$$

we see that the measured depolarization ratio, $(\rho_v)_M$, may be written as

$$(\rho_v)_M = \left[\frac{\rho_v + \phi^2\rho_v + \theta^2\rho_v + \gamma^2}{1 + \gamma^2\rho_v + \phi^2\rho_v}\right] \tag{3-29}$$

where ρ_v, is the exact depolarization ratio defined by (2-128). The difference between the measured and exact depolarization ratios is now computed to be

$$\Delta = (\rho_v)_M - \rho_v = \left[\frac{\theta^2\rho_v + \gamma^2(1 - \rho_v^2) + \rho_v\phi^2(1 - \rho_v)}{1 + \gamma^2\rho_v + \phi^2\rho_v}\right] \tag{3-30}$$

and the percentage error, caused by misalignment, is given by the relationship

$$PE = \frac{100\Delta}{\rho_v} = \left[\frac{\theta^2\rho_v + \gamma^2(1 - \rho_v^2) + \rho_v\phi^2(1 - \rho_v)}{\rho_v + \gamma^2\rho_v^2 + \phi^2\rho_v^2}\right] \times 100 \tag{3-31}$$

This is the desired result, and may be used to analyze the errors in the system quantitatively. However, (3-31) also shows some interesting qualitative behavior, which may be used to make some general remarks about the accuracy of these experiments. In the first place, since all the error angles appear as squared terms, the depolarization ratio of vertically polarized incident light is increased by any misalignments. Moreover, the terms γ^2 and ϕ^2 in the denominator of (3-31) tend to decrease the error, thus compensating for the corresponding terms in the numerator. Hence, we may assume that measurements of vertical depolarization ratios tend to be on the high side, and that the error contributions tend to compensate one another.

Error Sources

We are now in a position to quantitatively discuss the various errors present in the system, making estimates of the error magnitudes based on the design parameters discussed in Chapter III.

(1) Rotation of the system components about the Z-axis (direction of propagation of the incident light) corresponds to the error angle ϕ. According to the section on Photometer Design (page 71) there are two potential contributions which must be considered:

  (A) Misalignment of the plane of polarization of the laser, ϕ_1, which we estimate in the section on Alignment (page 84) to be $\phi_1 = 0.0025$ radians.

  (B) The finite area of the scattering volume viewed by the detector, giving rise to an uncertainty, ϕ_2, in the plane of polarization of the laser. From the geometry of the photometer, we see that the angle ϕ_2 is given by the radius of the incident beam divided by the distance from the scattering volume to the photomultiplier (i.e. 12 inches). Thus, the maximum value of ϕ_2 is given by $\phi_2 = 0.188/12 = 0.015$ radians while the average value of

ϕ_2, which is actually the quantity of interest is considerably less ($\simeq$0.004 radians).

The total error angle squared is thus given by

$$\phi^2 = (\phi_1 + \phi_2)^2 = 6.25 \times 10^{-4} \qquad (3\text{-}32)$$

where we have used maximum angles rather than averages, so that ϕ^2 is a maximum.

(2) The term θ corresponds to a rotation of the detection system components about the X-axis (through the center of the scattering volume). This error angle has three potential contributions, as follows:

(A) Rotation of the phototube about the sample, θ_1, estimated from the alignment technique (page 84) to be less than $\theta_1 = 0.034$ radians.

(B) Divergence of the incident beam in the YZ-plane, θ_2, estimated in Appendix under Divergence of the Laser Output to be less than $\theta_2 = 0.002$ radians.

(C) The finite area of the scattering volume viewed by the photomultiplier, θ_3, estimated in the preceding section to be considerably less than $\theta_3 = 0.015$ radians.

Hence, the total angular error component, θ^2, is given by

$$\theta^2 = (\theta_1 + \theta_2 + \theta_3)^2 = 17.6 \times 10^{-4} \qquad (3\text{-}33)$$

where, as before, this must be considered an absolute maximum value for the error.

(3) The term γ corresponds to a rotation of the system components about the Y-axis passing through the center of the scattering volume (i.e. the Z'-axis where the prime refers to the scattered wave as in Chapter II). This term contains four significance contributions as follows:

(A) Rotation of the resolver about the Z'-axis, γ_1, which was estimated in the section on Alignment (page 84) to be $\gamma_1 = 2° = 0.040$ radians.

(B) Rotation of the photometer about the Y-axis, γ_2, which was minimized in the initial alignment procedure so that $\gamma_2 = 0.002$.

(C) The divergence of the incident beam in the XZ plane γ_3, estimated in Appendix under Divergence of the Laser Output to be less than $\gamma_3 = 0.002$ radians.

(D) A contribution due to the inherent resolution of the Polaroid filters, γ_4, such that

$$\gamma_4 \simeq 0.0026$$

as may be seen from Appendix under Inherent Resolution of the Polaroid Filters.

The total angular error component γ^2 is thus given by

$$\gamma^2 = (\gamma_1 + \gamma_2 + \gamma_3 + \gamma_4)^2 = 22.1 \times 10^{-4} \qquad (3\text{-}34)$$

where, as before, (3-34) is to be considered an absolute maximum.

We may now obtain a numerical value for the percentage error, PE, in ρ_V as a function of ρ_V, using the above error components. Combining (3-31), (3-32), (3-33), and (3-34) we find that

$$PE = \left[\frac{\gamma^2 + \rho_V(\theta^2 + \phi^2) - \rho_V^2(\gamma^2 + \phi^2)}{\rho_V + \rho_V^2(\gamma^2 + \phi^2)}\right] \times 10^2$$

$$PE = \frac{1}{\rho_V}[0.221 + 0.239\rho_V - 0.284\rho_V^2] \qquad (3\text{-}35)$$

Furthermore, we may distinguish between two extreme cases in the measurement of ρ_V: the case of large ρ_V ($\rho_V = 1$), and the case of small ρ_V ($\rho_V = 0$). When ρ_V is approximately one we find that (3-35) becomes

$$PE = \theta^2 \times 100 \qquad (3\text{-}36)$$

or

$$PE = 0.176\%.$$

Hence, the limiting error in the case of large ρ_V is given by θ^2, and is caused principally by the uncertainty in the viewing angle, and the diameter of the incident beam. In the case of small ρ_V, we find that

$$PE = \frac{\gamma^2}{\rho_V} \times 100, \qquad (3\text{-}37)$$

or

$$PE = 0.221/\rho_V,$$

and the error is now a function of ρ_V. It is now reasonable to ask what is the minimum value of ρ_V that may be measured by this technique. Taking the maximum permissable error as 20 percent, we see from (3-37) that

$$(\rho_V)_{min.} = 0.221/20 = 0.011.$$

Here again, we take note that this is a maximum error, and in our system we should obtain a percentage error of less than 10 percent at this value of the depolarization. We also note here that the resolution of our system is limited by the error angle γ^2, which is principally due to misalignment of the resolvers. Therefore, to increase the resolution of this system, a more sophisticated means of aligning the polariods is necessary.

The results of this section have been summarized in Figure 3.5, a plot of PE, the percentage error, versus ρ_V, the vertical depolarization ratio. In addition, Table 3.2 summarizes the limiting cases discussed above.

TABLE 3.2.--Limiting Errors for Extreme Values of Depolarization

	$\rho_V = 1.0$	$\rho_V = 0.01$
Percentage Error	0.176	20
Major Error Contribution	θ	γ

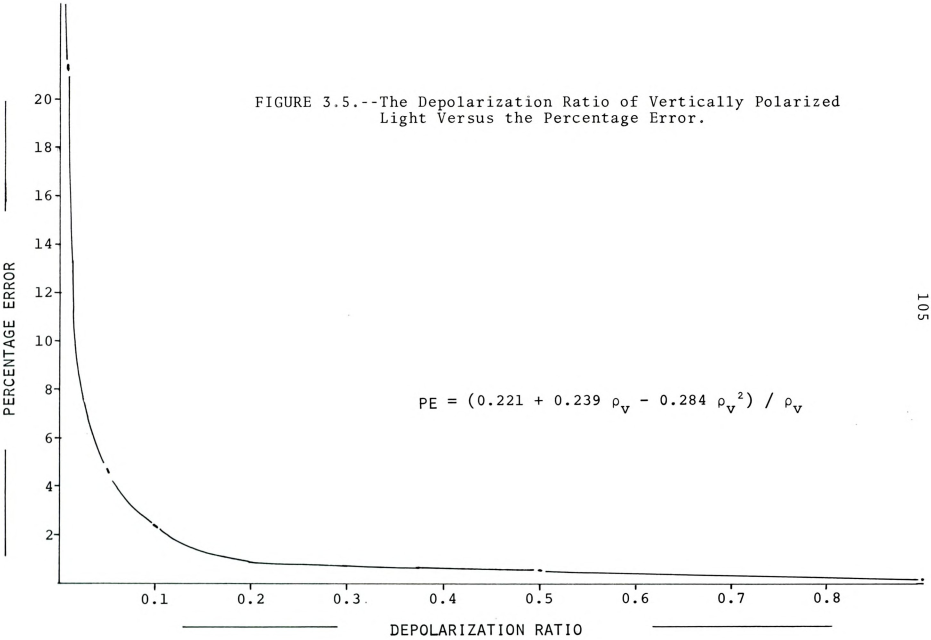

FIGURE 3.5.--The Depolarization Ratio of Vertically Polarized Light Versus the Percentage Error.

$$PE = (0.221 + 0.239\ \rho_v - 0.284\ \rho_v^2)\ /\ \rho_v$$

Preparation of Samples

In any light scattering measurements, the elimination of large impurities, particularly dust, is absolutely essential due to the enormous increase in scattering as the physical size of the scatterer increases. Moreover, the elimination of dust is particularly essential to an accurate measurement of the depolarization, since the specular reflectance from a large particle is highly polarized, giving rise to a decrease in ρ_V.

The benzene used in this study was obtained in both spectroscopic grade and reagent grade. The two grades were handled separately, however, both were fractionally crystallized, and dried by distillation in vacuum. Examination of the small angle scattering using a microscope, and illuminating with a helium-neon laser, revealed no dust particles after filtering through an ultrafine sintered glass filter under pressure from pure, dry, nitrogen gas.

The benzene derivatives were purified by filtration through an activated alumina column, and subsequent distillation under vacuum. The samples were used immediately after distillation by filtration into the cells through ultrafine sintered glass filters.

Carbon tetrachloride, chloroform, methylene chloride, hexane, cyclohexane, and related compounds were obtained in sealed one pint bottles, as reagent grade, and were filtered through activated alumina and distilled over P_2O_5. They were then stored until ready to be used, when they were distilled under vacuum, and then filtered into the cell.

The polymers used in this study were the standard polystyrene samples distributed by the National Bureau of Standards, and by Dow Chemical Company. They were used without further purification, however the solvents used, were purified as described above. The polymer solutions were filtered through ultrafine sintered glass filters before use, to remove dust particles.

The ultrafine filters were cleaned by baking overnight in an annealing oven, and then flushing with hot aqua regia, followed by repeated rinsing with high purity conductance water. The filters were then dried in an oven at 110°C and stored in a vacuum dessicator.

The conductance water used in this study was prepared by passing distilled water through a commerical deionizer, and then redistilling over potassium permanganate. The redistilled water was then distilled once more, and finally stored in a polyethylene bottle until used.

The purity of all the compounds used, was checked by measurement of the index of refraction.

CHAPTER IV

DATA AND RESULTS

Pure Liquids

The depolarization ratios of molecules small compared to the wavelength, were measured using vertically polarized incident light. We shall see that the quantities

$$F = (4\rho_V - 3)/3 \qquad (4\text{-}1)$$

and $(1/T + \alpha_T)$, exhibit relatively small temperature dependencies in the region of interest, so that (2-174), and (2-179), may be used to predict a temperature dependence of ρ_V somewhere between linear and logarithmic. The logarithmic dependence is slightly preferable since the slope is then independent of the temperature; however, to avoid ambiguity, the results will be compared at the standard temperature of 25°C (298°K).

For completeness, values of ρ_u have been included. These were obtained by calculation from (2-147), where ρ_h was assumed equal to unity.

Benzene and Its Derivatives

The study of the depolarization by benzene and its monosubstituted derivatives is of basic interest, due both to the solvent properties of these compounds, and to the degree to which their molecular properties are understood. Moreover, the derivatives chosen represent variations in parameters of importance to the depolarization, such as size and electronegativity.

Table 4.1 presents data obtained with the benzene derivatives at a number of temperatures, where T is the absolute temperature, ρ_v the vertical depolarization ratio, and ρ_u the unpolarized depolarization ratio (assuming $\rho_h = 1$). The data for benzene represent the average of four samples: two obtained from spectroscopic grade benzene, and two from reagent grade. The data for the four samples showed no significant differences in either the total scattered intensity, or the depolarization ratio.

Figure 4.1 is a plot of the natural logarithm of the vertical depolarization ratio versus the absolute temperature, and the slope is given by;

$$Q = \partial \ \ell n \ \rho_v / \partial T = \Delta \ \ell n \ \rho_v / \Delta T. \qquad (4\text{-}1\text{-}b)$$

The approximate linearity of this plot is obvious, however, we may also plot ρ_v versus T, to obtain an approximately linear graph, and evaluate Q from

$$Q = \partial \ \ell n \ \rho_v / \partial T = \frac{1}{\rho_v}(\Delta \rho_v / \Delta T). \qquad (4\text{-}1\text{-}c)$$

The Q evaluated using a logarithmic plot will be denoted by Q(log), and is seen from (4-1-b) to be temperature independent; while the Q evaluated from the linear plot, Q(lin.),

TABLE 4.1.--Depolarization Ratios of Benzene and Its Derivatives.

Compound	T(°K)	ρ_v	ρ_u	Compound	T(°K)	ρ_v	ρ_u
Benzene	293	0.263	0.417	Chlorobenzene	298	0.406	0.578
	298	0.255	0.406		318	0.374	0.544
	308	0.244	0.393		338	0.346	0.514
	313	0.239	0.385		358	0.311	0.474
	318	0.232	0.380				
	328	0.222	0.363				
	338	0.210	0.347	Bromobenzene	298	0.426	0.548
					318	0.395	0.566
					338	0.369	0.539
Toluene	298	0.321	0.486		348	0.353	0.521
	308	0.312	0.476		358	0.340	0.507
	318	0.288	0.447				
	328	0.275	0.431				
	338	0.260	0.412	Iodobenzene	298	0.441	0.612
					308	0.435	0.606
					318	0.420	0.592
Fluorobenzene	298	0.319	0.484		328	0.409	0.580
	308	0.302	0.463		338	0.399	0.571
	318	0.281	0.438		348	0.385	0.556
	323	0.275	0.431		358	0.370	0.540
	328	0.268	0.422				
	338	0.251	0.401				
	343	0.243	0.390	Nitrobenzene	298	0.600	0.750
	348	0.234	0.379		308	0.588	0.743
	352	0.233	0.377		318	0.581	0.735
					328	0.572	0.728

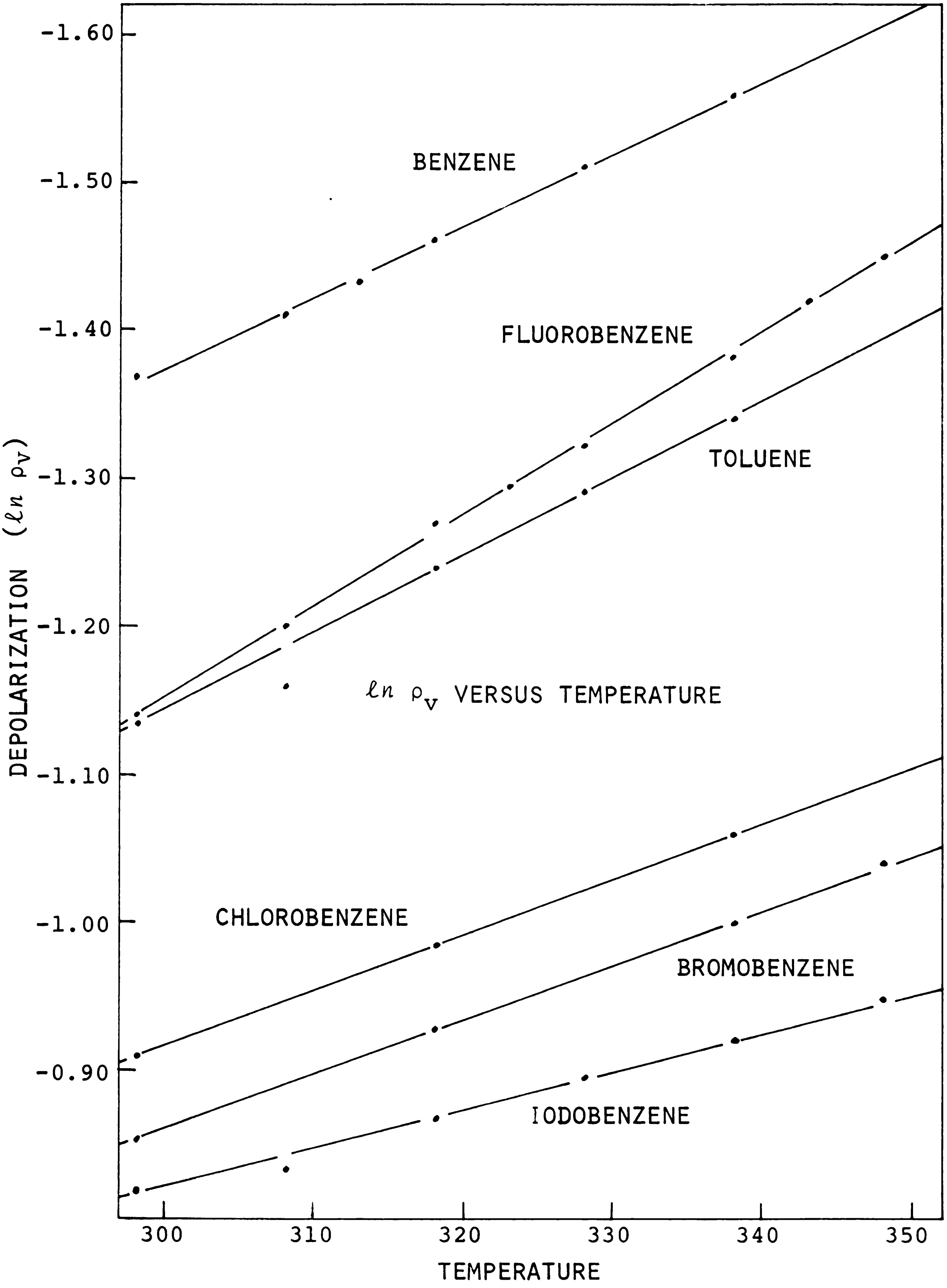

FIGURE 4.1.--Plot of $\ell n\ \rho_V$ Versus T for the Benzene Derivatives.

is obviously dependent on the temperature because of the term, $1/\rho_V$. Figure 4.2 is a plot of ρ_V versus T for the benzene derivatives, and illustrates the approximate linearity of the temperature dependence.

Using equation (2-179), we may examine the temperature dependence of Q, predicted by the theory. Table 4.2 compares the temperature variation in Q obtained using (2-179) with that determined experimentally using (4-1-c) and (4-1-b).

TABLE 4.2.--Temperature Variation of Q Using the Data for Benzene.

Temp (°K)	$-\frac{2}{3}[4\rho_V-3]$	$\alpha_T\times10^3$	$T^{-1}\times10^3$	-Q(Theory)	-Q(lin.)	-Q(log)
298	1.320	1.237	3.356	6.06×10^{-3}	4.61×10^{-3}	4.72×10^{-3}
308	1.352	1.325	3.247	6.17 "	4.83 "	"
318	1.382	1.413	3.145	6.29 "	5.08 "	"
328	1.408	1.504	3.049	6.41 "	5.31 "	"
338	1.440	1.595	2.959	6.56 "	5.62 "	"
			$10^5\times(\Delta Q/\Delta T) =$	1.25	2.5	0

Hence, the theory predicts a temperature variation in the slope, Q, that is midway between that obtained from a linear and a logarithmic depolarization ratio; thereby implying that the data may be analyzed in either way with approximately equal errors. Similarly, using the data for chlorobenzene, we find that:

Theoretical $\Delta Q/\Delta T = -0.78\times10^{-5}$

Experimental $\Delta Q/\Delta T = -1.43\times10^{-5}$ (linear)

Experimental $\Delta Q/\Delta T = 0.$ (log)

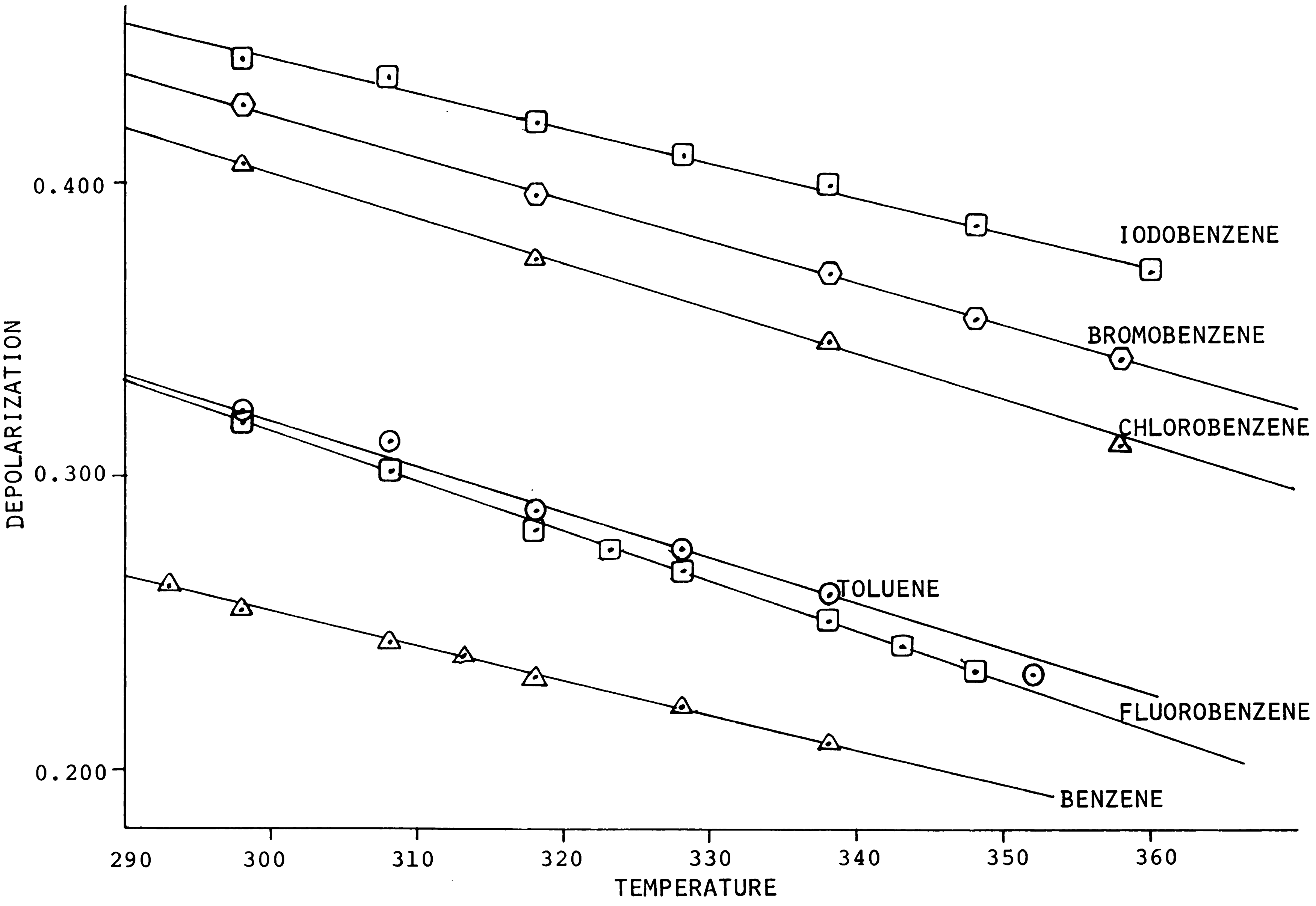

FIGURE 4.2.--Depolarization Versus Temperature for Benzene Derivatives.

Although the errors are approximately the same, the logarithmic analysis may be somewhat preferable to the linear, since the slope is a constant and there is no temperature ambiguity. Moreover, comparison of the results obtained by the two treatments yields information regarding the curvature of the temperature data. That is, the difference in the Q obtained by the two methods may be related to the curvature of the plots.

Recalling equations (2-174) and (2-179),

$$Q(1) = (\partial \ln \rho_v/\partial T)_p = F[1/T - \alpha_T + (\partial \ln \bar{\kappa}/\partial T)_p] \qquad (2\text{-}174)$$

$$Q(2) = (\partial \ln \rho_v/\partial T)_p = 2F[1/T + \alpha_T] \qquad (2\text{-}179)$$

where

$$F = (4\rho_v - 3)/3,$$

and using the data of Table 4.1 and Figure 4.1, we may compile Table 4.3, where the quantities have been evaluated at T = 298°K. The compounds are ordered according to increasing ρ_v, where the values of ρ_v have been interpolated from the data of Table 4.1.

It is apparent that both (2-174) and (2-179) yield reasonably accurate results, despite the approximations used, except in the case of benzene itself. Moreover, the results for benzene are anomalous in that the experimentally determined slope, Q(exp), is considerably smaller than would be expected from the magnitude of ρ_v.

TABLE 4.3.--Comparison of Theory and Experiment for Benzene and Its Derivatives.

Compound	ρ_V	$\alpha_T\times10^3$	$(\partial \ell n\bar{K}/\partial T)10^3$	Q(exp)×10^3 (log)	Q(exp)×10^3 (lin)	Q(1)×10^3	Q(2)×10^3	Dev. Q(1)	Dev. Q(2)
Benzene	0.256	1.237	7.718 [27]	-4.72	-4.60	-6.47	-6.04	-1.75	-1.32
Fluorobenzene	0.320	1.198	6.710 [27]	-5.82	-5.32	-5.10	-5.24	0.72	0.58
Toluene	0.326	0.9221	6.855 [27]	-5.25	-5.23	-5.25	-4.89	0	0.36
Chlorobenzene	0.408	0.979	5.994 [27]	-4.06	-3.86	-3.85	-3.99	0.21	0.07
Bromobenzene	0.425	0.911	5.922 [28]	-3.75	-3.43	-3.62	-3.70	0.13	0.05
Iodobenzene	0.445	0.824		-2.79	-2.74		-3.41		-0.62
Nitrobenzene	0.597	0.828	5.477 [27]	-1.67	-1.63	-1.60	-1.67	0.07	0
							rms deviation =	0.34	0.37

References indicated by superscripts.
Q(1) calculated from (2-174)
Q(2) calculated from (2-179)
Deviations taken with respect to the logarithmic Q(exp).

The deviations between the calculated and experimental (logarithmic) values of Q are recorded in the last two columns of Table 4.3. The rms deviations of Q(1) and Q(2) have been calculated, but do not include the results for benzene, since this data appears anomalous. Thus, Table 4.3 shows agreement between theory and experiment to within 8 percent, using either (2-174) or (2-179), except in the case of benzene itself.

The only other compound exhibiting an appreciable error was iodobenzene. Moreover, the error in this case (as with benzene) was negative, indicating a smaller slope than anticipated. This result could be due to the presence of free iodine in the sample, and indeed the turbidity was observed to increase with time, due perhaps, to photochemical reduction. It is therefore felt that the experimental Q for iodobenzene is about 10 percent low, while the theoretical Q is probably about 10 percent high; the measured ρ_v being about 3 percent low.

Hexane and Related Compounds

The data and results for hexane, cyclohexane, and methylcyclohexane were obtained for the purpose of comparison with their unsaturated analogs: benzene and toluene.

Table 4.4 is a compilation of the depolarization ratios of hexane, cyclohexane, and methylcyclohexane as functions of the temperature, where ρ_u is calculated from (2-147), assuming $\rho_h = 1$.

TABLE 4.4.--Depolarization Ratios of Hexane and Related Compounds.

Compound	T(°K)	ρ_v	ρ_u
Hexane	288	0.0458	0.0877
	298	0.0429	0.0822
	308	0.0398	0.0766
	318	0.0362	0.0699
	328	0.0338	0.0653
	338	0.0305	0.0592
Cyclohexane	298	0.0189	0.0371
	308	0.0179	0.0352
	318	0.0168	0.0331
	328	0.0156	0.0307
	338	0.0146	0.0287
	348	0.0135	0.0266
Methylcyclohexane	298	0.0295	0.0573
	308	0.0278	0.0540
	318	0.0260	0.0507
	328	0.0247	0.0482
	338	0.0232	0.0453
	348	0.0217	0.0425
	358	0.0202	0.0395

Table 4.5 summarizes the results calculated using the data of Table 4.4 and equations (2-174) and (2-179), the data and results for benzene and toluene having been included for purposes of comparison. Figure 4.3 is a plot of the natural logarithm of the vertical depolarization ratio, ρ_v, versus T, for the data of Table 4.4.

TABLE 4.5.--Comparison of Theory and Experiment for Hexane and Related Compounds.

Compound	ρ_V T=298	$\alpha_T \times 10^3$	-Q(log) $\times 10^3$	-Q(lin.) $\times 10^3$	-Q(2) $\times 10^3$	% Error (log)	% Error (lin.)
Cyclohexane	0.0188	1.209	5.56	5.56	8.90	60	60
Methylcyclohexane	0.0293	1.148	5.30	5.30	8.66	62	62
Hexane	0.0427	1.378	8.61	7.30	8.93	4	20
Benzene	0.256	1.237	4.72	4.60	6.04	28	30
Toluene	0.326	0.922	5.25	5.23	4.89	-7	-6

It is obvious from Table 4.5, that the agreement between theory and experiment for the saturated ring compounds is poor. Moreover, there is a rather large difference between the logarithmic and linear treatment of the data in the case of hexane, indicating a good deal of curvature in this data. Least squares analysis indicates, in this case, that the logarithmic fit is the preferred one however.

The results are extremely interesting in another respect, which may best be illustrated by reference to Table 4.6; a comparison of the slopes, Q, for saturated and unsaturated compounds. It is apparent that although benzene, cyclohexane, and methylcyclohexane yield Q values that do not agree well with the theory, the ratios of their values agree reasonably well with the predicted ratios. Moreover, the Q for toluene, which agrees well with theory, is not in agreement with the Q ratio found for cyclohexane and methylcyclohexane. It is therefore apparent, due to the good

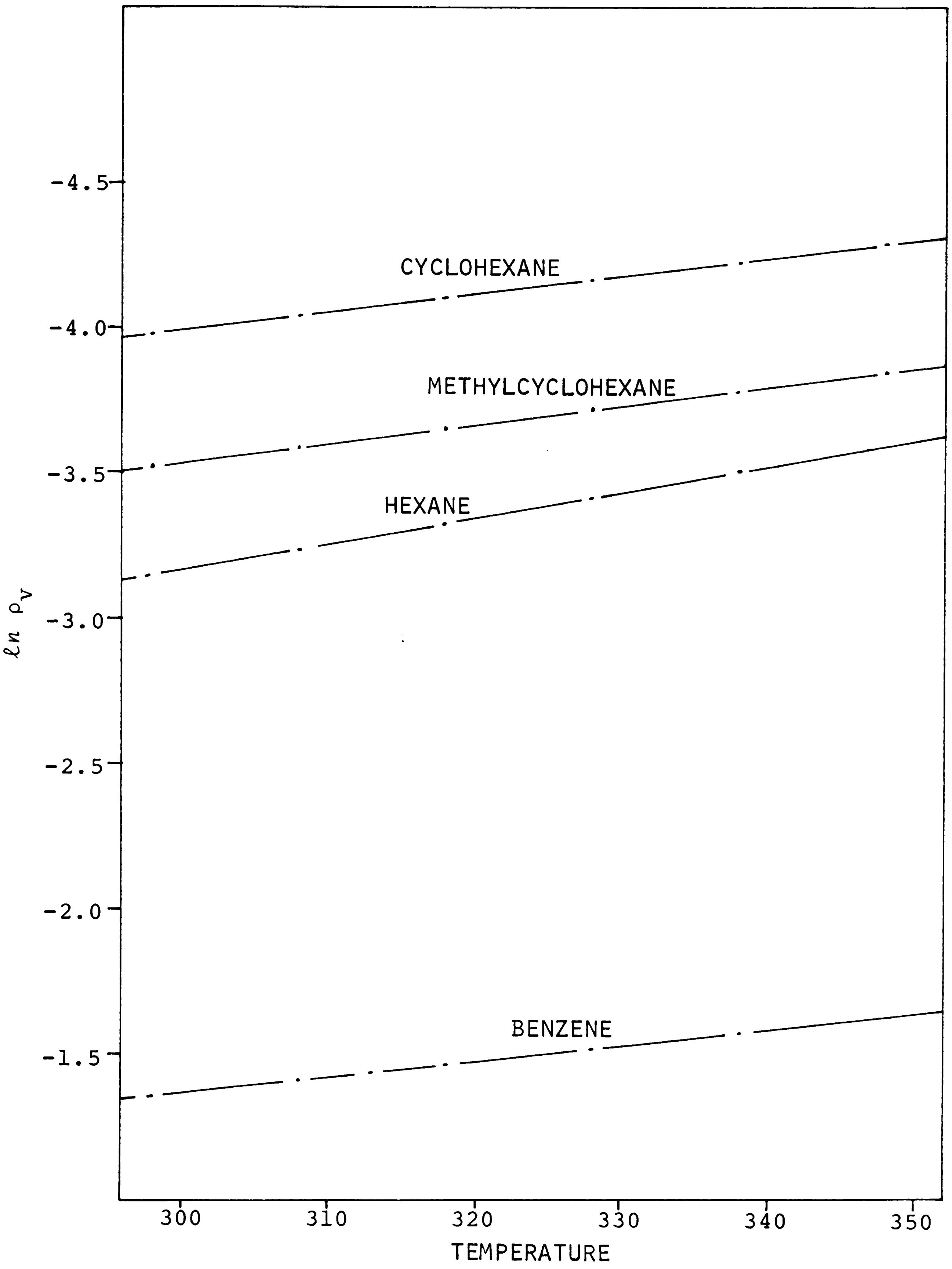

FIGURE 4.3.--$\ln \rho_V$ Versus T for Hexane and Related Compounds.

TABLE 4.6.--Comparison of Saturated and Unsaturated Ring Compounds.

Ratio	Exp. (log)	Theory
Q(CH)/Q(MCH)	1.03	1.03
Q(B) /Q(T)	0.90	1.23
Q(CH)/Q(B)	1.21	1.47
Q(MCH)/Q(T)	1.03	1.76

CH = cyclohexane
B = benzene
MCH = methylcyclohexane
T = toluene

agreement between theory and experiment for hexane, that the ring closure has altered the behavior, in the liquid state, of the hexane related hydrocarbons. It is also apparent from the measurement of the depolarization ratios, that in the case of benzene, ring closure (and loss of six hydrogen atoms) has resulted in an increased anisotropy as compared to hexane, whereas in the case of cyclohexane, ring closure has resulted in a decreased anisotropy. In either case however, the dipole moment has remained zero (except for toluene which has a moment (p_o = 0.36D). Comparison with the results of the previous section shows a definite error decrease with increasing dipole moment. It is therefore evident that the theory predicts good results for molecules with non-zero dipole moments; however the results are poor when the dipole moment vanishes, regardless of the total anisotropy of the liquid. It is also worthwhile to note that the measured Q is smaller than the

predicted Q for molecules of zero dipole moment, indicating a relatively large temperature dependence in the magnitude of the horizontal component of the scattered light, and with a slope opposite that of the vertical component.

It also seems apparent that agreement with the theory becomes worse as the sphericity of the molecule increases. Thus benzene exhibits an error of 30 percent while cyclohexane has an error of 60 percent. It would seem therefore that the relatively good agreement between theory and experiment in the case of hexane is due in part to the rod-like character of the molecule.

Hence, we are led to the obvious conclusion that, in dense fluids of molecules with a very high symmetry, the anisotropy contribution due to intermolecular interactions of the polarizability is of the same order as the anisotropy contributions due to the hyperpolarizability interactions. Thus the hyperpolarizability interactions cause a temperature dependence in the anisotropy such that the anisotropic scattering is increased as a function of the temperature. Returning to the section on Temperature Dependence of Depolarization by Dense Fluids (page 43) we see that, with respect to temperature, and assuming a temperature dependent anisotropy, A, (2-170) becomes

$$Q = (\partial \ln \rho_V/\partial T) = F(\partial \ln B/\partial T) - F(\partial \ln A/\partial T) \qquad (4\text{-}2)$$

where F is as defined in (4-1). Thus we see that an increase in A with respect to T causes a decrease in Q, as observed in the case of the ring hydrocarbons.

The Chlorinated Methane Derivatives

The chlorinated methane derivatives are now of particular interest, since the results obtained with the previous series of compounds imply that, due to spherical symmetry, the measured Q for carbon tetrachloride should be considerably smaller than that predicted by (2-174) or (2-179), however, the slopes measured for chloroform and methylene chloride should agree well with the theoretical predictions.

The data obtained for this group of compounds are summarized in Table 4.7, where, as before, ρ_u has been calculated from (2-147) assuming a horizontal depolarization ratio, ρ_h, equal to one.

Figure 4.4 is a linear plot of the natural logarithm of the vertical depolarization ratio, ρ_v, versus the absolute temperature; and Table 4.8 is a comparison of the experimental and predicted results using the values of Table 4.7.

It is apparent from the results of Table 4.8, that the anticipated behavior is indeed correct. Moreover, it appears that there is, again, a direct relationship between the dipole moment, spherical symmetry, and slope of the vertical depolarization ratio.

TABLE 4.7.--Depolarization Ratios of the Chlorinated Methane Derivatives

Compound	Temperature (°K)	ρ_v	ρ_u
Carbon Tetrachloride	298	0.0166	0.0327
	308	0.0160	0.0315
	318	0.0151	0.0297
	328	0.0147	0.0289
	333	0.0146	0.0287
Chloroform	298	0.108	0.195
	308	0.101	0.184
	318	0.0916	0.168
	328	0.0847	0.157
Methylene Chloride	288	0.146	0.255
	298	0.136	0.239
	308	0.126	0.224

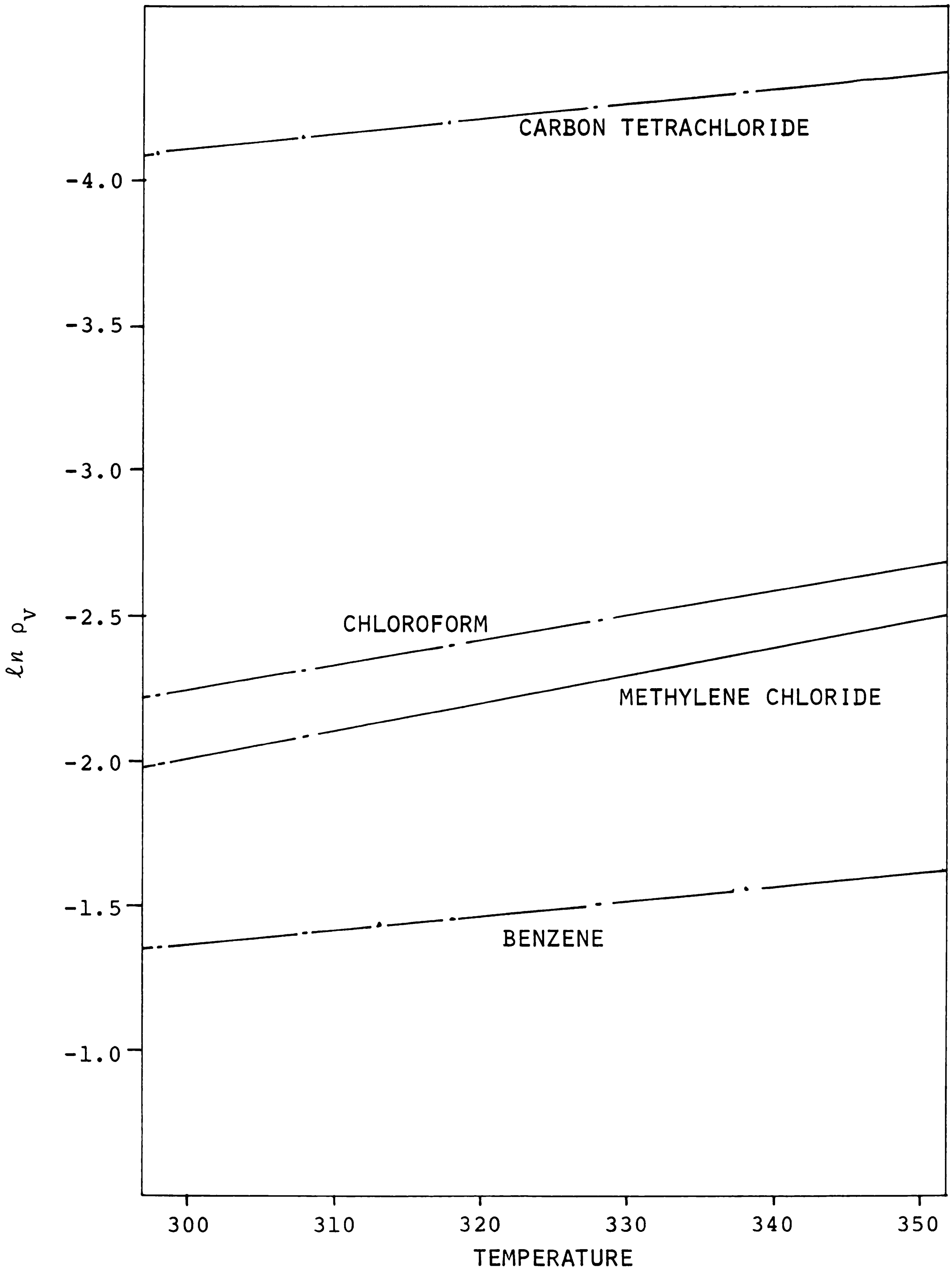

FIGURE 4.4.--*ℓn* ρ_V Versus T for the Chlorinated Methane Derivatives.

TABLE 4.8.--Comparison of Theory and Experiment for the Chlorinated Methane Derivatives.

Compound	ρ_V	$\alpha_T \times 10^3$	$\partial \ell n \bar{\kappa}/dT$ $\times 10^3$	$-Q \times 10^3$ (log.)	$-Q \times 10^3$ (lin.)	$-Q(1) \times 10^3$	$-Q(2) \times 10^3$	$\overset{*}{\text{Dev.}}$ Q(1)	$\overset{*}{\text{Dev.}}$ Q(2)
Carbon Tetrachloride	0.0166	1.236	7.722	4.24	3.44	9.55	8.98	5.31	4.74
Chloroform	0.1075	1.273	8.390	7.97	7.19	8.98	7.93	1.01	-0.04
Methylene Chloride	0.136	1.366	--	7.60	7.35	--	7.72	--	0.12

*Deviations taken with respect to the logarithmic Q.

It seems especially signifigant moreover, to point out that the assumptions of the theoretical section are, perhaps, best fulfilled by the tetrahedral symmetry of carbon tetrachloride. Hence, it becomes apparent that the temperature dependence of the anisotropic portion of the scattered light (i.e. the Rayleigh Wing) is of especial importance for such symmetric cases. In addition, it is significant that the Rayleigh Wing is extremely dependent on the flow properties of the fluid, since its physical basis is a highly damped rotational Raman effect. Hence, the study of the anisotropic scattering may be especially useful in studying the intermolecular structure of isotropic molecules, and thereby allow measurement of the hyperpolarizability tensor elements.

Temperature Dependent Depolarization in the Chlorinated Toluene Isomers

The study of the temperature dependent depolarization by ortho- and para-chlorotholuene is of particular interest, since these two compounds present a considerable change in dipole moment, with substantially similar physical properties.

The dipole moments are seen to be[30],

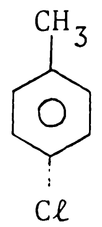

2.07 D

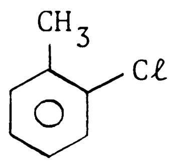

1.55 D

while the physical properties are given in Table 4.9.

TABLE 4.9.--Physical Properties of the Toluene Derivatives.

	ortho-chlorotoluene	para-chlorotholuene
boiling point	159.2°C	162.5°C
melting point	-37.0°C	7.5°C
density	1.082^{20}	1.070^{20}
viscosity	1037×10^5	1030×10^5

The temperature dependent depolarization ratios of these compounds are tabulated in Table 4.10, while Table 4.11 compares the measured and predicted results.

TABLE 4.10.--Depolarization Ratios of Ortho- and Para-chlorotoluene.

Compound	Temp. (°K)	ρ_v	ρ_u
o-chlorotoluene	298	0.418	0.588
	318	0.390	0.561
	338	0.359	0.528
	358	0.331	0.498
p-chlorotoluene	298	0.474	0.645
	318	0.441	0.612
	328	0.426	0.596
	338	0.408	0.579
	348	0.393	0.565
	358	0.385	0.554

TABLE 4.11.--Comparison of Theory and Experiment for the Toluene Derivatives

Compound	$\rho_V(298)$	$\alpha_T \times 10^3$*	$-Q(\log) \times 10^3$	$-Q(\mathrm{lin}) \times 10^3$	$-Q(2) \times 10^3$	% Error (log)	% Error (lin)
Toluene	0.321	0.9221	5.25	5.23	4.89	-7	-6
o-chloro-toluene	0.419	0.9008	3.80	3.46	3.76	-1	9
p-chloro-toluene	0.474		3.74	3.44			

*Reference (29)

A graph of the data has not been included, however, the fit is essentially as before, with the logarithmic and linear values of Q having approximately equal rms deviations. Unfortunately, reliable data with which to compute α_T for para-chlorotoluene are not available; however the excellent agreement between theory and experiment for ortho-chlorotoluene is apparent. It is also obvious that although the depolarization ratios of the two isomers are very different, there is no discernable difference in their values of Q. Hence, assuming essentially the same error for both isomers, we must expect para-chlorotholuene to have an $\alpha_T \geq 1.144$. Since this is a considerably different value than that for the ortho-isomer, it would seem to be of great interest to make the density measurements necessary to evaluate this parameter.

It is further of interest to note that the values of ρ_v are such that the smaller ρ_v corresponds to the smaller dipole moment, as was found to be the case in the previous sections. This indicates that the anisotropy is related to the "dipole induction" potential existing in the liquid state of polar molecules. Since the dipole induction potential is a low frequency interaction, it is apparent that it must interact with the hyperpolarizability terms which were ignored in the section on Theory of Rayleigh Depolarization (page 21). This is in qualitative agreement with the results of Buckingham and Stephen,[7] although no attempt has been made to quantitatively investigate the relationship.

Summary

The experimentally determined values of the depolarization ratio have been seen to bear a relationship to the dipole moment of the molecule, in addition to being related to the bulk physical properties of the fluid. Moreover, the slopes, Q, of $\ln \rho_v$ versus T have been seen to agree well with the predicted values when the dipole moment is non-zero. For molecules with no dipole moment, the dipole interaction in the fluid state is no longer the parameter responsible for determining the fluid properties, and the theory does not yield accurate results.

Tabulating the dielectric constants, ϵ, of some organic compounds as follows:

	ϵ
Cyclohexane	2.015*
Carbon Tetrachloride	2.228
Benzene	2.274
Toluene	2.379
Iodobenzene	4.630
Chloroform	4.806
Bromobenzene	5.400
Chlorobenzene	5.621
Methylene Chloride	9.080
Nitrobenzene	34.82

*Reference (30)

it seems that we may expect accurate predictions from the theory for liquids with dielectric constant greater than 2.3: that is

$$\epsilon \geq 2.3. \tag{4-3}$$

Using this number we may expect that water (ϵ = 78) would obey the theory, while carbon disulfide (ϵ = 2.6) would be on the borderline (i.e. although ϵ = 2.6, the dipole moment is zero) and may not obey the theory.

Of greater significance however, is the relationship of the symmetry of the molecule to the temperature dependence of the depolarization. Writing the induced moment in the molecule as

$$\overline{p}_i = \alpha_{ij}(F_j) + \frac{1}{2}\,\xi_{ijk}(F_jF_k) + \frac{1}{6}\,\gamma_{ijk\ell}(F_jF_kF_\ell) \tag{4-4}$$

where the subscripts refer to molecule fixed axes, the F_i are the field components due to both the external and internal fields, α_{ij} is the polarizability tensor, and the ξ_{ijk} and $\gamma_{ijk\ell}$ are the first- and second-order hyperpolarizabilities. We find that the tensors describing both the polarizability and hyperpolarizability are considerably simplified by symmetry. We may therefore specify the number of independent elements in each of the tensors, for the symmetry group corresponding to the molecule, as follows:

Molecule	Symmetry	Number of Constants		
		α_{ij}	ξ_{ijk}	$\gamma_{ijk\ell}$
Carbon Tetrachloride	Td	1	1	2
Chloroform	C_{3v}	2	3	4
Methylene Chloride	C_{2v}	3	3	6
Benzene	D_{6h}	2	0	3
Mono-substituted benzene derivatives	C_{2v}	3	3	6
Cyclohexane	D_{3d}	2	0	4
Hexane	D_{3h}	2	1	3

Apparently there are three trends in the data for these molecules: first, the agreement with theory is improved by increasing the number of polarizability elements; second, for a given number of α terms, the agreement improves with an increasing number of ξ terms; and finally, agreement improves as the number of γ terms decreases. These trends are not exact, since the data are also affected by the dipole moment in the case of the polar molecules, however, the following conclusions may be drawn:

(1) The hyperpolarizability interactions are significant in the liquid state.

(2) Due to the large "dipole induction" anisotropy, the temperature dependent hyperpolarizability terms do not affect the temperature dependence of ρ_v for polar molecules, even though they are significant in determining the anisotropy.

(3) Anisotropy induced through the γ terms is more temperature dependent than that due to ξ.

In the case of carbon tetrachloride, the α is isotropic, and the anisotropy is therefore determined by the ξ and γ terms. Buckingham and Stephen[7] showed that γ contributes as the difference in its terms, and is therefore small compared to ξ in this case. Thus, the approximation that the anisotropy is reasonably temperature independent should be valid even though agreement with the theory is very poor. For non-polar molecules, the Debye equation yields for the isotropic α,

$$\alpha = \frac{3}{4\pi N_o}\left[\frac{n^2 - 1}{n^2 + 2}\right]\overline{V} \qquad (4\text{-}5)$$

where n is the index of refraction. Then, assuming a temperature independent anisotropy, and using (4-2), and (2-128), we find that

$$Q = (\partial \ \ell n \ \rho_V/\partial T) = 2F\left[\alpha_T + \left(\frac{\partial n}{\partial T}\right)\left(\frac{6}{n^4 + n^2 - 2}\right)\right] \quad (4\text{-}6)$$

where F is defined in (4-1). Using the data for $CC\ell_4$, ($n = 1.455$, $dn/dT = .54 \times 10^{-3}$) we find that

$$-Q(CC\ell_4) = 3.80 \times 10^{-3}$$

Comparison with Table 4.8 shows that this result lies between the logarithmic and linear data, and therefore appears to be virtually exact. The implication is then, that in this case the γ terms in the hyperpolarizability interacted with the α evaluated in Chapter II in such a way as to decrease the temperature dependence. Moreover, this interpretation seems physically reasonable, and is in qualitative agreement with the other results.

Equations (4-5), and (4-6) may be expected to be valid only for non-polar molecules, of symmetry equal to, or greater than, that of carbon tetrachloride, and are therefore not adaptable to the previous results.

Binary Solutions

The results of the previous section show that we may expect good agreement with theory for liquids with dipole interactions. It is therefore interesting to inquire as to the agreement between theory and experiment for a binary solution in which one component has no dipole moment. In this section we shall make the necessary measurements on a series of benzene-nitrobenzene solutions, and, in addition, on a series of benzene-carbon tetrachloride solutions. The benzene-carbon tetrachloride solutions, having no permanent dipole interactions, may nonetheless interact due to the configurational differences between the tetrahedral and planar molecules.

Benzene-Nitrobenzene Mixtures

A series of five benzene-nitrobenzene solutions was prepared by weighing a quantity of nitrobenzene into a volumetric flask and diluting to volume. By making a final weighing, the densities and mole fractions of the solutions have been computed. Data for the calculation of the coefficient of thermal expansion, α_T, for the solutions were obtained from reference (29). Table 4.12 summarizes the data for α_T versus mole fraction, and compares the actual values with those computed from a linear relationship:

$$\alpha_T(\text{soln.}) = X_1\alpha_T(1) + X_2\alpha_T(2), \tag{4-7}$$

where X_1 and X_2 are the mole fractions of components 1 and 2 respectively, and $\alpha_T(1)$ and $\alpha_T(2)$ are the coefficients of thermal expansion of pure 1 and 2. It may be seen that (4-7) yields resonably good values of α_T for these solutions.

Table 4.13 is a tabulation of the measured values of the vertical depolarization ratios at various temperatures for the five solutions. Again, we may approximate the concentration dependence by a linear function: that is

TABLE 4.12.--Comparison of Theoretical and Experimental Values of α_T.

Mole Fraction Nitrobenzene	Density	$\alpha_T \times 10^3$ (Theor.)	$\alpha_T \times 10^3$ (exp)*
0.0	0.8787	1.237	1.237
0.224	0.9326	1.145	1.119
0.342	0.9972	1.097	1.068
0.464	1.0329	1.047	1.022
0.591	1.0669	0.995	0.973
0.722	1.1526	0.941	0.925
1.000	1.1984	0.828	0.828

*Experimental values obtained from density data Ref. (29)

TABLE 4.13.--Depolarization Ratios at Various Temperatures for Benzene-Nitrobenzene Mixtures.

Mole Fraction ϕ-NO_2 / (°K) Temp	0.224	0.342	0.464	0.591	0.722
298	0.354	0.410	0.464	0.503	0.548
308	0.339	0.392	0.444	0.488	0.531
318	0.324	0.373	0.427	0.469	0.520
328	0.311	0.354	0.410	0.459	0.502

$$\rho_V(\text{soln.}) = X_1\rho_V(1) + X_2\rho_V(2) \tag{4-8}$$

where the X_i is the mole fraction of component i, and $\rho_V(i)$ is the vertical depolarization ratio of pure i.

We may now construct Figure 4.5, which is a plot of the vertical depolarization ratio versus mole fraction (nitrobenzene) and compares the actual values with those computed from (4-8). Since (4-8) represents the relationship to be expected from dilution effects in an ideal solution of non-interacting molecules, we may consider it to define an "ideal" solution. The actual values in Table 4.13 then deviate slightly from ideality, due in this case, to an induction effect caused by the action of the permanent dipole of nitrobenzene on the polarizability of benzene.

Using (4-7) and (4-8) we find then, that for an "ideal" solution, (2-179) becomes

$$Q(\text{soln.}) = X_1Q(1) + X_2Q(2). \tag{4-9}$$

This may be corrected for non-ideality by using the measured depolarization ratio, rather than (4-8), in which case

$$Q(\text{soln.}) = 2F[1/T + X_1\alpha_T(1) + X_2\alpha_T(2)] \tag{4-10}$$

where, as before

$$F = (4\rho_V - 3)/3.$$

In the remainder of this study, (4-9) will be used to compute an "ideal" Q, while (4-10) will be used to obtain the "theoretical" Q.

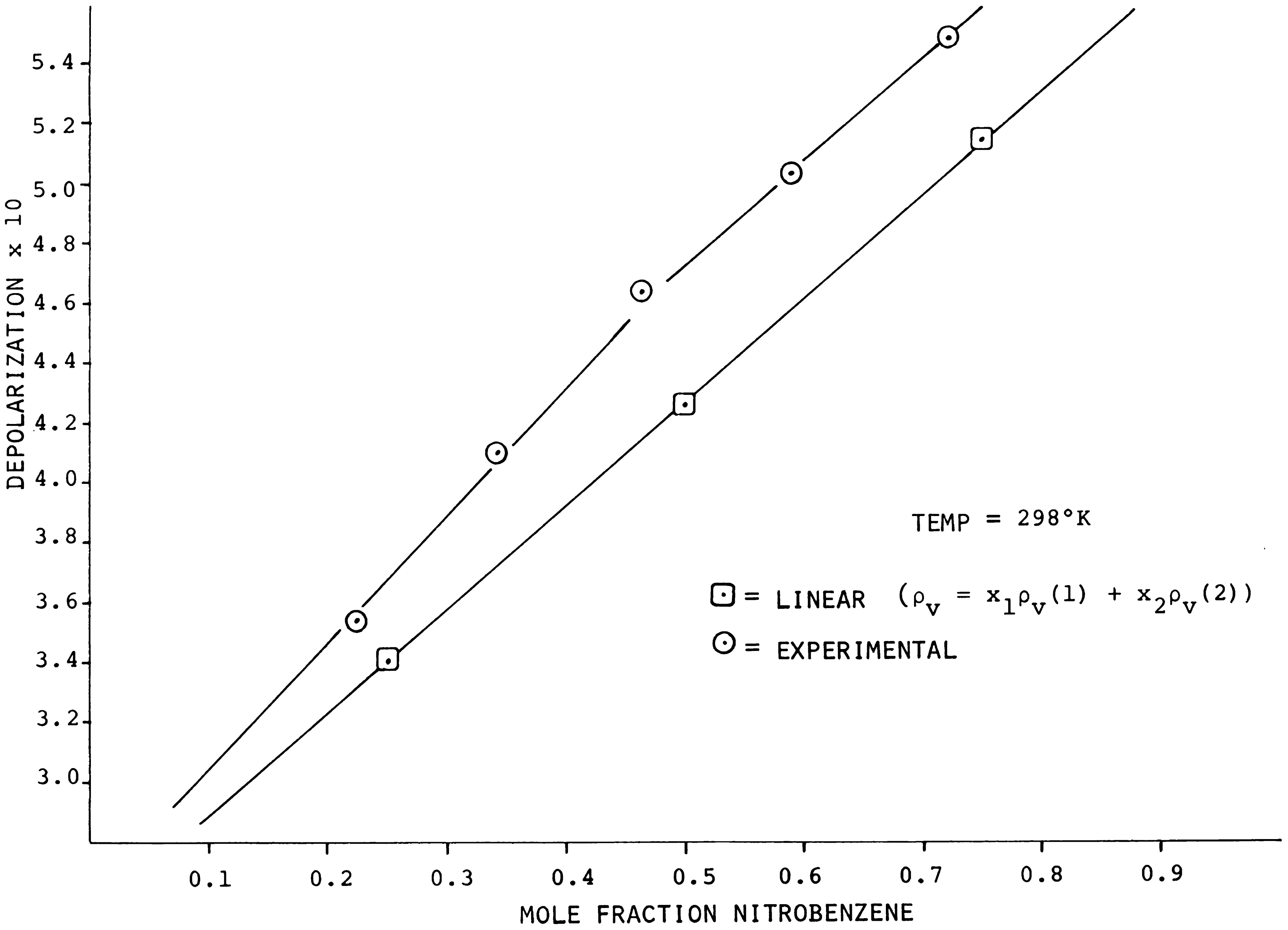

FIGURE 4.5.--Plot of the Depolarization Ratio Versus Mole Fraction for Benzene-Nitrobenzene Solutions.

The natural logarithm of the depolarization ratio has been plotted versus T for the five solutions in Figure 4.6, and the results obtained from Table 4.13 and Figure 4.6 are compiled in Table 4.14. It may be seen from the Table that the curvature of the actual slope, Q, is not large (approximately 3 percent) and that agreement with theoretical values, (4-10), is reasonably good.

TABLE 4.14.--Values of -Q for Benzene-Nitrobenzene Solutions

Mole Fraction Nitrobenzene →	0.224	0.342	0.464	0.591	0.722
$-Q(\text{logarithmic } \rho_v)\times10^3$	4.32	4.89	4.12	3.05	2.92
$-Q(\text{linear } \rho_v)\times10^3$	4.06	4.54	3.88	2.92	2.79
$-Q(\text{theoretical})\times10^3$	4.78	4.06	3.36	2.87	2.32
$-Q(\text{ideal})\times10^3$	4.05	3.67	3.30	2.90	2.52

Theoretical values from (4-10).
Ideal values from (4-9).

Figure 4.7 has been constructed from the results of Table 4.14. Several trends are apparent from this graph, and are worthy of note: the theoretical and experimental values agree well; the theoretical values are less than the actual values; and the non-linear, or "non-ideal" behavior is easily discerned. It may therefore be concluded that dipole induction interactions are causing the solutions to behave as predicted, and that the temperature dependent depolarization ratios may be used to study the behavior of these mixtures.

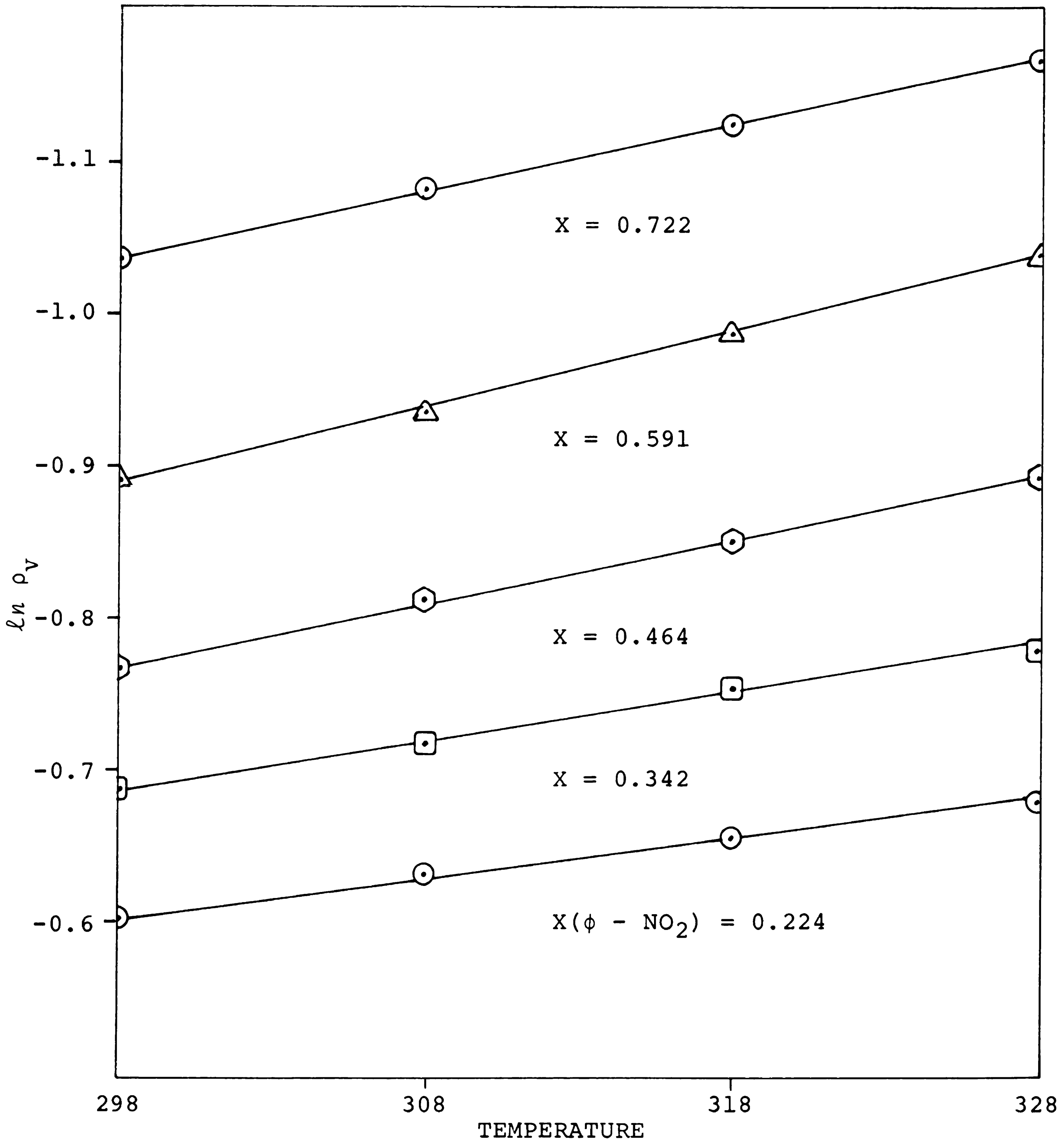

FIGURE 4.6.--Plot of $\ell n\ \rho_V$ Versus T for Benzene-Nitrobenzene Mixtures.

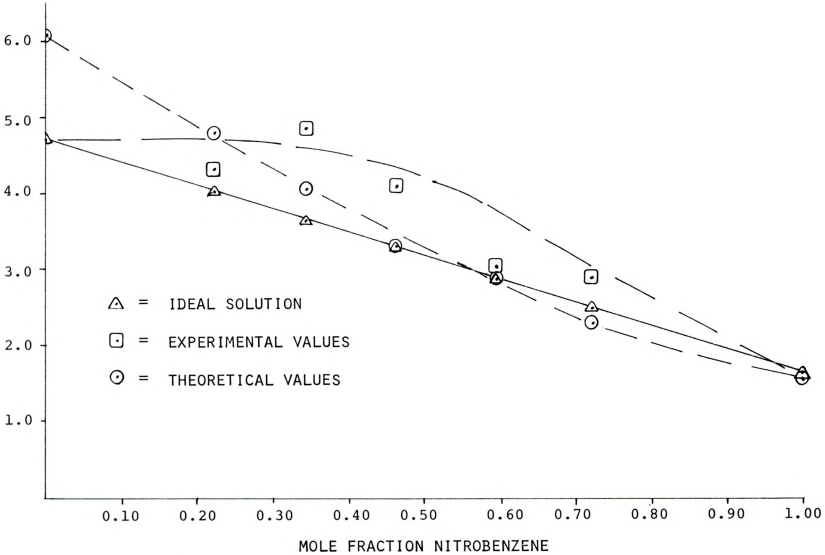

FIGURE 4.7.--Plot of -Q Versus Mole Fraction for Benzene-Nitrobenzene Mixtures.

Benzene-Carbon Tetrachloride Mixtures

A series of five solutions of varying concentrations of carbon tetrachloride in benzene was prepared by careful weighing into volumetric flasks. The mole fraction of carbon tetrachloride, density, and coefficient of thermal expansion of each solution is given in Table 4.15, along with values of α_T computed from (4-7).

TABLE 4.15.--Physical Properties of Benzene-Carbon Tetrachloride Solutions.

Mole Fraction Carbon Tetrachloride	Density	$\alpha_T \times 10^3$ (exp)	$\alpha_T \times 10^3$ (theor.)
0.000	0.8787	1.237	1.237
0.235	0.9657	1.236	1.237
0.356	1.0585	1.234	1.237
0.480	1.0912	0.243	1.237
0.610	1.2415	1.238	1.237
0.745	1.3418	1.236	1.237
1.000	1.5842	1.237	1.237

Theoretical values from (4-7)
Experimental values from Reference (29).

Unfortunately useful data could not be obtained for the two more concentrated solutions, however the temperature dependent depolarization ratios of the other three solutions are tabulated in Table 4.16.

TABLE 4.16.--Vertical Depolarization Ratios of Benzene-Carbon Tetrachloride Solutions at Various Temperatures.

Mole Fraction / (°K) Temp	0.235	0.356	0.480
298	0.212	0.191	0.167
308	0.204	0.183	0.158
318	0.192	0.173	0.147
328	0.180	0.162	0.137

The natural logarithms of these data have been used to construct a linear plot of vertical depolarization ratios versus temperature, in Figure 4.8.

Using Table 4.16 and Figure 4.8 we may now obtain the results compiled in Table 4.17, where, as in the previous section, the "ideal" Q has been computed using (4-9), and the "theoretical" Q has been obtained from (4-10).

TABLE 4.17.--Values of -Q for Benzene-Carbon Tetrachloride Mixtures

Mole Fraction $CC\ell_4$ →	0.000	0.235	0.356	0.480	1.000
$-Q \times 10^3$(log ρ_v)	4.72	5.45	5.49	6.60	4.24
$-Q \times 10^3$(lin ρ_v)	4.60	5.05	5.06	5.99	3.44
$-Q \times 10^3$(Theory)	6.04	6.60	7.03	7.14	8.98
$-Q \times 10^3$(Ideal)	4.72	4.60	4.54	4.48	4.25

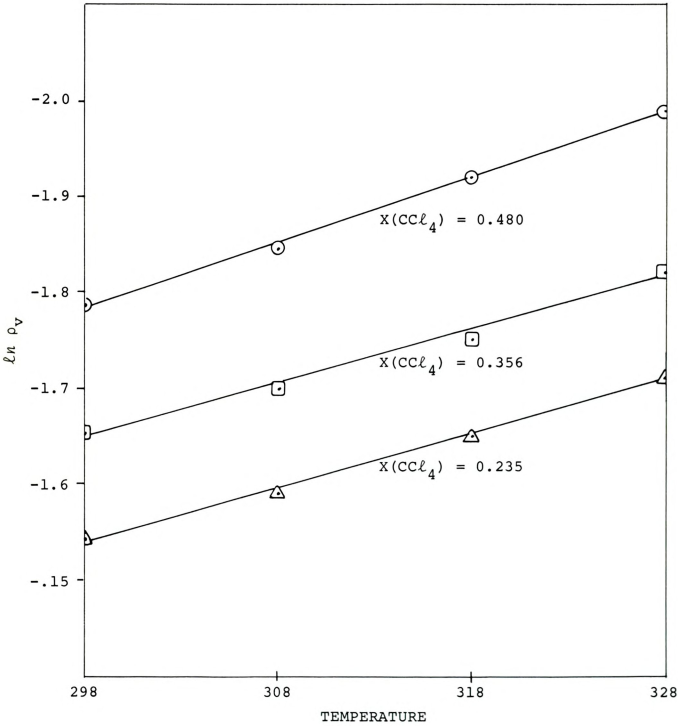

FIGURE 4.8.--Plot of $\ell n\ \rho_V$ Versus T for Benzene - CCℓ$_4$ Mixtures.

These results have been graphed in Figure 4.9, a plot of $-Q \times 10^3$ versus the mole fraction of carbon tetrachloride. The behavior in this case is more obvious than with the nitrobenzene-benzene solutions since the theory predicts a positive linear graph, while the linear extrapolation ("ideal" solution) yields a negative linear graph. The behavior of the measured Q shows that the dispersion and configuration interactions between the two species tend to make the measured values approach the theoretical. Since these forces are small compared to dipole-dipole, or inductive effects, the measured values are all smaller than the theoretical predictions. At some intermediate concentration, the interaction becomes a maximum, and subsequently the measured values fall off to intersect the linear "ideal" graph at a mole fraction of one. It is therefore obvious that this technique may be used to study short range interactions in the liquid state.

Summary

The data and results for benzene-nitrobenzene and benezene-carbon tetrachloride mixtures have been found to exhibit behavior indicating the existence of short-range interaction potentials in the liquid state. These forces may be expected to be functions of the polarizability and hyperpolarizability tensors discussed previously. Thus, the results show that binary solutions obey equation (2-179) reasonably well over intermediate concentration ranges, even though the pure liquids may exhibit appreciable error.

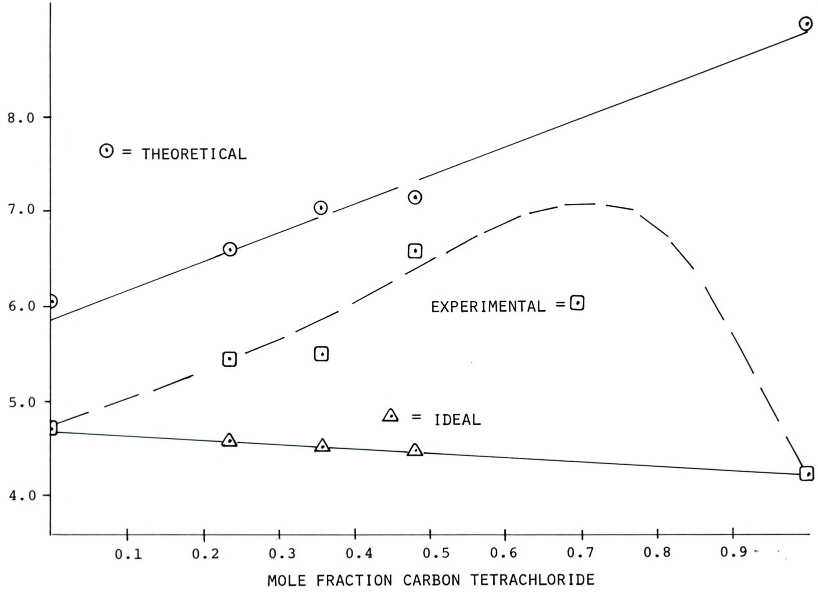

FIGURE 4.9.--Plot of -Q Versus Mole Fraction for Benzene-Carbon Tetrachloride Mixtures.

Perhaps the most significant conclusion that may be drawn from this section on Binary Solutions, is however, that the preponderance of evidence indicates that the intensity of the Rayleigh Wing (i.e. anisotropic scattering) is not a linear function of the concentration, and is influenced by the short-range configurational interactions.

Polymer Solutions

The theory of Chapter II is certainly not adequate to deal with the depolarization from polymer solutions; due to the assumptions regarding the form of the polarizability tensor, and the phase relationship between scattering centers at various parts of the polymer molecule. The vertical depolarization ratios of some polymer solutions have been measured however, to establish the magnitude of this quantity at the wavelength of the helium-neon laser (632.8 nm).

The samples measured were the National Bureau of Standards standard sample 706, polystyrene, and the Dow Chemical standard polystyrene sample, S11.

The samples were weighed into volumetric flasks, and solvent added to form a stock solution. More dilute samples were then obtained by successive dilutions.

Measurements were made in the photometer described in Chapter III, at a temperature of 25°C. The iris diaphragm in the shutter was closed to its smallest aperture to eliminate beam diameter effects due to multiple scattering.

The vertical depolarization ratio was measured for each concentration, and the difference between the depolarization ratio of the solvent and that of the solution was extrapolated to zero concentration. The extrapolation was achieved in two ways; graphically, and by a computer program. It was observed that the difference between ρ_V (solvent) and ρ_V (solution) was approximately logarithmic in the concentration range used. Therefore, the logarithm of the difference was plotted versus concentration to extrapolate graphically to zero. The computer extrapolation was achieved by fitting the data to an arbitrary polynomial by least squares techniques. The best polynomial was chosen by the "Gauss criterion of fit," the constant term of the expansion being the extrapolated difference in depolarization ratios.

The results obtained are summarized in Table 4.18,

TABLE 4.18.--Summary of Results for the Standard Polystyrene Samples

Solvent	Sample	ρ_V(graphical)	ρ_V(least-squares)
Benzene	706	0.038	0.015
Toluene	706	0.042	0.017
Benzene	S-11	0.012	0.007

where the physical properties of the polymers are as follows:

Polystyrene Standard Sample 706
Weight Average Molecular Weight - 257,800

Polystyrene Sample S-11
Weight Average Molecular Weight - 819,000

The results show that the least-squares fit to a polynomial yields considerably smaller depolarization ratios than the logarithmic plot. This is most probably due to the fact that the concentration range measured was quite high (i.e. .1 to 2 gm/ℓ) so that the final limiting slope had not been reached. The advantages of the polynomial fit are therefore obvious, since it is not necessary to establish the final limiting slope to get a good extrapolation.

The depolarization ratios obtained from the polynomial fit are probably as trustworthy as any available from data in benzene and toluene. However, the values measured in these solvents represent the difference between two relatively large numbers, and we must therefore expect a sizable absolute error. More accurate data may of course be obtained by using solvents with very small depolarization ratios, such as cyclohexane, and by working out to much lower concentration ranges.

In summary, although the results shown in Table 4.18 are not to be considered complete or definitive, they do establish the range within which the depolarization ratio of polystyrene lies at 632.8 nm.

CHAPTER V

CONCLUSIONS

The Present Study

The data and results presented in Chapter IV have been found to be in good agreement with the theory of Chapter II in the case of polar molecules. Agreement between theory and experiment has been found to within 5 percent for molecules with non-zero dipole moments. In the case of non-polar molecules, agreement is not as good, however there appears to be an inverse relationship between the sphericity of the molecule and the agreement with theory. For example, the results for hexane agree to within 4 percent despite the vanishing dipole moment, while the results for carbon tetrachloride exhibit an error greater than 100 percent. Hence, the theory of Chapter II does not adequately describe spherical systems. Perhaps the best explanation of this lies in the fact that the hyperpolarizability was ignored in the development of the theory. In a spherical system these terms would account for a large part of the intermolecular potential, whereas in non-spherical systems the polarizability interactions (that is interactions of the permanent dipoles with the polarizability) predominate.

It was reasoned then, that in binary solutions in which one component was of non-zero dipole moment, or in which the symmetry groups of the two species differ, the measurements should be more in accord with the theory, due to polarizability interactions causing an increased anisotropy. The results show that this is indeed the case, and, in addition, that the short-range interactions affect the Rayleigh Wing intensity more than the Rayleigh-Brillouin triplet. This is physically reasonable when it is recalled (i.e. Rayleigh Scattering (page 2)) that the Rayleigh Wing arises from scattering by orientation fluctuations in the liquid.

For non-polar molecules of high-symmetry, such as carbon tetrachloride, the Debye Equation for the polarizability yields an accurate value for the temperature dependence of the depolarization. This seems to indicate that the principal sources of deviation from the theory are the γ portion of the hyperpolarizability, which causes a decrease in the isotropic temperature dependence, and the interaction of the anisotropic polarizability with the hyperpolarizability to cause a temperature dependent anisotropic scattering.

In conclusion, we may note that the energy required to depolarize the scattered light can be estimated by approximating the depolarization ratio by

$$\rho_V = A \exp (\Delta E/RT) \qquad (5\text{-}1)$$

where A is an arbitrary constant, R, the gas constant, T the absolute temperature, and ΔE the energy barrier for depolarization. Differentiating yields

$$(\partial \ \ell n \ \rho_V/\partial T) = -\Delta E/RT^2 \tag{5-2}$$

or

$$\Delta E = -QRT^2 = (\partial \ \ell n \ \rho_V/\partial(1/T)) \tag{5-3}$$

Thus, we may obtain ΔE from a plot of $\ell n \ \rho_V$ versus 1/T, which is approximately linear at this temperature, or from the data obtained previously for Q. This energy value may be interpreted as indicating, by means of a Boltzmann factor, the number of interacting molecules in the vicinity of the scattering molecule. Thus, the smaller the energy barrier, the more interactions that are taking place within the liquid. Some representative values of ΔE are reported in Table 5.1, where the units are in calories per mole degree.

TABLE 5.1.--The Energy Barrier for Depolarization.

Molecule	ΔE(T = 298°K)
Benzene	835 cal/mole
Fluorobenzene	1030
Toluene	930
Chlorobenzene	718
Bromobenzene	664
Iodobenzene	494
Nitrobenzene	296
Carbon Tetrachloride	751
Chloroform	1405
Methylene Chloride	1345

These values indicate that, for the benzene derivatives, induced anisotropy due to intermolecular interactions is large, while in the methane derivatives the molecular anisotropy is predominant. Thus, despite similar symmetry, the actual mechanism of depolarization in methylene chloride must be quite different than that of the monosubstituted benzene derivatives.

Suggestions for Further Study

This study has demonstrated the feasibility of performing accurate measurements of the temperature dependence of the vertical depolarization ratio. It has also demonstrated the areas of uncertainty in the theory of Chapter II. Future studies should therefore be undertaken to extend the validity of both the theoretical and experimental results. Measurements should be made on other compounds, to determine the extent of validity of the conclusions drawn from this data; and in addition, the study of binary solutions should be continued.

Measurements on ortho, meta, and paradichlorobenzene would help establish the dipole moment dependence of the results (since p-dichlorobenzene has a vanishing moment), while measurements on water and salt solutions (dielectric constant > 78) would establish the dependence on the dielectric constant. In addition, water would be of interest due to its extremely small coefficient of thermal expansion $(\alpha_T - 0.207 \times 10^{-3})$.

Measurement of the temperature dependence of ρ_h, rather than ρ_v, may be found to yield data relating to the hyperpolarizability, since any temperature dependence in this quantity must be due to terms of higher order than the polarizability (i.e. according to the theory of Chapter II, ρ_h must be unity).

Measurement of the intensities and line widths of the resolved Rayleigh-Brillouin spectrum as a function of the temperature, may be expected to yield information concerning the precise mechanism of the temperature dependence. That is, the dependence of each component of the spectrum may be observed independently, thereby resolving any uncertainties as to which scattering processes are being affected. Moreover, the symmetry dependence of each component of the spectrum could be independently investigated.

BIBLIOGRAPHY

(1) J. B. Richter, U.d.n. Gegenstande der Chemie 11, 81 (1802).

(2) J. Tyndall, Phil. Mag. 37, 384 (1869).

(3) Lord Rayleigh, Phil Mag. 41, 447 (1871).

(4) A. Einstein, Ann. Phys. Lpz. 33, 1275 (1910).

(5) T. H. Maiman, Phys. Rev. 123, 1145 (1961).

(6) A. Javan, W. R. Bennett, Jr., and D. R. Herriott, Phys. Rev. Letters 6, 106 (1961).

(7) A. D. Buckingham and M. J. Stephen, Trans. Faraday Soc. 53, 884 (1957).

(8) H. C. Van de Hulst, "Light Scattering by Small Particles," John Wiley and Sons, Inc., New York, 1957.

(9) P. Doty, J. Polymer Sci., 3, 750 (1948).

(10) G. G. Stokes, Trans. Camb. Phil. Soc. 9, 399 (1852).

(11) R. C. Jones, J. Opt. Soc. Am. 46, 126 (1956).

(12) M. Born and E. Wolf, "Principles of Optics," Perogramon Press, New York, 1964.

(13) A. L. Schawlow and C. H. Townes, Phys. Rev. 112, 1940 (1958).

(14) P. W. Smith, J. Quantum Elec. 2, 62 (1966).

(15) P. W. Smith, J. Quantum Elec. 2, 77 (1966).

(16) K. Mielenz and K. F. Nefflen, Appl. Opt. 4, 565 (1965).

(17) A. Rousset, Ann. Phys. Paris 5, 5 (1936).

(18) P. J. W. Debye, J. Appl. Phys. 15, 338 (1944).

(19) H. Z. Cummins and R. W. Gammon, Appl. Phys. Letters 6, 171 (1965).

(20) K. A. Stacey, "Light Scattering in Physical Chemistry," Academic Press, New York, 1956.

(21) J. A. Osborn, Phys. Rev. 67, 351 (1945).

(22) A. Sommerfeld, "Electrodynamics," Academic Press, New York, 1952.

(23) Benoit and Stockmayer, J. Phy. Radium 17, 21 (1956).

(24) B. A. Brice, and M. Halwer, J. Opt. Soc. Am. 41, 1033 (1951).

(25) A. Kruis, Zeits, f. physik. Chemie B34, 13 (1936).

(26) International Critical Tables

(27) D. Tryer, J. Chem. Soc. 105, 2534 (1914).

(28) R. E. Gibson and O. H. Loeffler, J. Am. Chem. Soc. 61, 2515 (1939).

(29) Jean Timmermans, "The Physico-Chemical Constants of Binary Systems in Concentrated Solutions," Volume 1, Interscience Publishers, Inc., New York, 1959.

(30) C. P. Smyth, "Physical Methods of Organic Chemistry," Interscience Publishers, Inc., New York, 1946.

(31) R. C. C. Leite, R. S. Moore, and S. P. S. Porto, J. Chem. Phys. 40, 3741 (1964).

(32) J. Ehl, C. Loucheux, C. Reiss, and H. Benoit, Makromol. Chem. 75, 35 (1964).

APPENDIX

Divergence of the Laser Output

Since the beam divergence is a quantity of some importance in the analysis of the errors inherent in this system, a measurement was made of the divergence, in both single and multi-mode operation, of Lasers I and II described in Chapter III, the section on The Polarization Photometer (page 76).

Using Laser I, the system used in most of the work reported here, in the "semi"-confocal configuration, it was found that the beam diameter near the output mirror was slightly less than 0.25 inches with a multi-mode output. At 300 feet however, the output had diverged to approximately 12 inches, as shown in Figure 7.1:

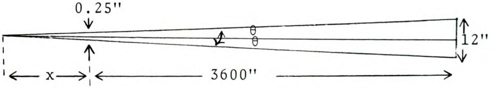

FIGURE 7.1.--The Laser Divergence

where θ is the divergence half-angle, and x is the distance to the point at which the radiation appears to be originating. Obviously, θ is given by

$$2\theta = 0.25/x = 12/(3600 + x) \tag{7-1}$$

and, rearranging, we obtain

$$x \simeq 75 \text{ inches} \tag{7-2}$$

so that

$$\theta \simeq 1.7 \times 10^{-3} \text{ radians.} \tag{7-3}$$

In single mode operation, the beam width near the output mirror, using this laser, became approximately 0.10 inch. At 300 feet, the width had diverged to about seven inches, yielding a divergence half-angle, θ, of

$$\theta \simeq 7/(3600 \times 2) \simeq 1 \times 10^{-3} \text{ radian.} \tag{7-4}$$

In this case, single mode operation was achieved by simply tilting the mirrors until the TEM_{oo} mode was made to oscillate due to the small mode volume within the device.

Using Laser II, it was found that at the surface of the output mirror the beam diameter was approximately 0.10 inch, while at 300 feet the diameter had diverged to about 28 inches. In this case, as before, the divergence half-angle is given by

$$2\theta \simeq 28/3600 \tag{7-5}$$

so that

$$\theta \simeq 4 \times 10^{-3} \text{ radians.} \tag{7-6}$$

Obviously this configuration is considerably more divergent than that of Laser I, and no attempt was made to measure the divergence in single mode operation.

Inherent Resolution of the Polaroid Filters

Since the polaroid filters are not ideal, they pass a small component of light polarized perpendicular to the plane of polarization of the filter. This inherent resolution may be considered to be an uncertainty in the alignment of the polaroid and may therefore be represented by the instrument operator $\overline{P}$, as shown in Table 2.1. Thus, when the polarizer is oriented parallel to the X-axis, that is so as to take the vertical polarization component, the instrument operator is given by

$$\overline{P}_v = \begin{bmatrix} 1 & \sin \epsilon \\ \sin & \sin^2 \epsilon \end{bmatrix} \tag{7-7}$$

where ϵ is the angle representing the misalignment, and the subscript v refers to the vertical orientation. When ϵ is small, as is the case, we may write

$$\overline{P}_v \simeq \begin{bmatrix} 1 & \epsilon \\ \epsilon & \epsilon^2 \end{bmatrix} \tag{7-8}$$

and, similarly for a horizontally polarized filter

$$\overline{P}_h = \begin{bmatrix} \epsilon^2 & \epsilon \\ \epsilon & 1 \end{bmatrix} \tag{7-9}$$

where the ϵ in both cases is the same since it is a function of the material only. Now, if two such polarizers are

oriented perpendicular to one another, we may generate the instrument operator of the combination as

$$\overline{P}_{\perp} = \overline{P}_v \overline{P}_h = 2\epsilon \begin{bmatrix} \epsilon & 1 \\ \epsilon^2 & \epsilon \end{bmatrix}; \qquad (7\text{-}10)$$

and illuminating the combination with unpolarized light, the coherence matrix of the light passing through the combination is given by

$$\overline{J}_{\perp} = 4\epsilon^2(1 + \epsilon^2) \begin{bmatrix} 1 & \epsilon \\ \epsilon & \epsilon^2 \end{bmatrix} \qquad (7\text{-}11)$$

From (7-11) we see that the intensity, $I_{\perp}$, of light transmitted by the combination is

$$I_{\perp} = \mathrm{Tr}\ \overline{J}_{\perp} = 4\epsilon^2(1 + \epsilon^2)^2 \simeq 4\epsilon^2. \qquad (7\text{-}12)$$

If the two polaroids are oriented with their axes parallel, the resulting operator is

$$\overline{P}_{||} = \overline{P}_v \overline{P}_v = (1 + \epsilon^2) \begin{bmatrix} 1 & \epsilon \\ \epsilon & \epsilon^2 \end{bmatrix}, \qquad (7\text{-}13)$$

and illuminating the combination with unpolarized light yields an output whose coherence matrix may be written as

$$\overline{J}_{||} = (1 + \epsilon^2)^3 \begin{bmatrix} 1 & \epsilon \\ \epsilon & \epsilon^2 \end{bmatrix}. \qquad (7\text{-}14)$$

The intensity of the transmitted light may now be seen to be

$$I_{||} = (1 + \epsilon^2)^4 \simeq 1. \qquad (7\text{-}15)$$

Combining (7-12) and (7-15) yields

$$I_{\perp}/I_{||} = 4\epsilon^2(1 + \epsilon^2)^2/(1 + \epsilon^2)^4 = 4\epsilon^2/(1 + \epsilon^2)^2$$

or

$$\epsilon \simeq \frac{1}{2}\sqrt{\frac{I_{\perp}}{I_{||}}} \qquad (7\text{-}16)$$

This is an extremely useful result, since it relates the inherent angular resolution of the polarizing elements to the easily measured raio of intensities with the polarizers crossed and the polarizers parallel. Measuring $I_{||}$ and $I_{\perp}$ using the photometer described in Chapter III, and a very intense tungsten lamp with a red filter as the light source, we obtained the results:

$$I_{\perp} \simeq 2 \times 10^{-5}$$

$$I_{||} = 0.7$$

so that

$$\epsilon = 0.0026 \text{ radians.}$$

Thus, the uncertainty in the plane of polarization of the polaroid is 2.6 milliradians.

Analysis of Errors in the Horizontal Depolarization Ratio

We have thus far concerned ourselves only with the measurement of the depolarization ratio for vetically polarized incident light. In the case of horizontally

polarized incident light, as was seen in Chapter II, the section on The Horizontal Depolarization Ratio (page 38), the total scattering is considerably reduced in intensity, and has a depolarization ratio of approximately unity. Since the deviation of the horizontal depolarization ratio, ρ_h, from unity may be a quantity of some interest (and more particularly, its temperature dependence) it is interesting to inquire with what accuracy we may measure this quantity using the photometer described earlier.

Approaching the problem in the same manner as in Chapter III, the section on Error Analysis and Total Accuracy (page 92), we shall consider the light scattering system as being oriented on the right-handed coordinate system of Figure 2.1, and shall observe the scattered light at some point along the Y-axis (the Z'-axis of the scattered field). Assuming, as before, that the system consists of a totally unpolarized light source, a polarizer, a scattering system, and a resolver, we may generate the instrument operator of the entire system as follows.

The polarizer (Brewster window) may be represented by the matrix $\overline{P}_h$, where the subscript h denotes the horizontal orientation, in the form

$$\overline{P}_h = \begin{bmatrix} \cos^2 \phi & \sin \phi \cos \phi \\ \sin \phi \cos \phi & \sin^2 \phi \end{bmatrix} \qquad (7\text{-}17)$$

where ϕ is the angle the polarizer makes with respect to the X-axis. Since in this case ϕ is approximately 90 degrees we may write

$$\overline{P}_h = \begin{bmatrix} \cos^2(90 \pm \Delta\phi) & \cos(90 \pm \Delta\phi) \\ \cos(90 \pm \Delta\phi) & 1 \end{bmatrix} \qquad (7\text{-}18)$$

where $\Delta\phi$ is the angular error due to misalignment and is assumed to be very small. (7-18) may be rewritten as

$$\overline{P}_h \simeq \begin{bmatrix} \sin^2 \Delta\phi & \sin \Delta\phi \\ \sin \Delta\phi & 1 \end{bmatrix} \qquad (7\text{-}19)$$

and dropping the Δ in the notation (bearing in mind that ϕ is now the error rather than the total angle) we see that

$$\overline{P}_h = \begin{bmatrix} \phi^2 & \phi \\ \phi & 1 \end{bmatrix}. \qquad (7\text{-}20)$$

The instrument operator for the scattering system is given as before by equation (3-9), that is

$$\overline{S}_{90°} = \begin{bmatrix} S_{XX} & S_{XY} \\ S_{XY}\,\Delta\theta - S_{XZ} & S_{YY}\,\Delta\theta - S_{YZ} \end{bmatrix} \qquad (3\text{-}9)$$

where $\Delta\theta$ is the error in alignment in the YZ plane (i.e. about the X-axis). The resolvers are, as before, represented by (3-11) and (3-12), that is

$$\overline{R}_v = \begin{bmatrix} 1 & \gamma \\ \gamma & \gamma^2 \end{bmatrix} \tag{3-11}$$

$$\overline{R}_h = \begin{bmatrix} \gamma^2 & \gamma \\ \gamma & 1 \end{bmatrix} \tag{3-12}$$

where the subscripts h and v refer to the horizontal and vertical components respectively, and the angle γ represents the error in alignment of the resolver (assumed to be small).

The instrument operators describing the entire system are then given by

$$\overline{L}_h = \overline{R}_h \ \overline{S} \ \overline{P}_h \tag{7-21}$$

and

$$\overline{L}_v = \overline{R}_v \ \overline{S} \ \overline{P}_h \tag{7-22}$$

or, substituting (7-20), (3-9), (3-11), and (3-12) into (7-21) and (7-22),

$$\overline{L}_h = \begin{bmatrix} \phi\gamma Q & \gamma Q \\ \phi Q & Q \end{bmatrix} \tag{7-23}$$

where

$$Q = \gamma\phi S_{XX} + \gamma S_{XY} + \theta\phi S_{XY} - \phi S_{XZ} + \theta S_{YY} - S_{YZ} \tag{7-24}$$

(and we have replaced $\Delta\theta$ by θ, remembering that θ is now a small error angle) and

$$\overline{L}_v = \begin{bmatrix} \phi W & W \\ \gamma\phi W & \gamma W \end{bmatrix} \tag{7-25}$$

where

$$W = \phi S_{XX} + S_{XY} + \theta\gamma\phi S_{XY} - \gamma\phi S_{XZ} + \theta\gamma S_{YY} - \gamma S_{YZ}. \tag{7-26}$$

Now, as was shown in Chapter II, in the section on Theory of Rayleigh Depolarization (page 21), the coherence matrix representation, $\overline{J}'$, of the light observed by the detector is given by

$$\overline{J}' = \overline{J}'_h + \overline{J}'_v = \overline{L}\ \overline{J}\ \overline{L}^\dagger \tag{7-27}$$

where

$$\overline{J}'_h = (1 + \phi^2)\begin{bmatrix} \gamma^2 Q^2 & \gamma Q^2 \\ \gamma Q^2 & Q^2 \end{bmatrix} \tag{7-28}$$

and

$$\overline{J}'_v = (1 + \phi^2)\begin{bmatrix} W^2 & \gamma W^2 \\ \gamma W^2 & \gamma^2 W^2 \end{bmatrix} \tag{7-29}$$

W and Q being given by (7-26) and (7-24). Thus, the intensities of the horizontal and vertical components of the scattered radiation are given by, respectively,

$$H_h = \mathrm{Tr}\ \overline{J}'_h = (1 + \phi^2)(1 + \gamma^2)Q^2 \tag{7-30}$$

$$V_h = \mathrm{Tr}\ \bar{J}_v' = (1 + \phi^2)(1 + \gamma^2)W^2 \tag{7-31}$$

where the subscript h refers to the horizontally polarized incident light. The depolarization ratio, ρ_h, for horizontally polarized incident light, is now found by combining (2-145), (7-30), and (7-31); that is,

$$\rho_h = V_h/H_h = W^2/Q^2 \tag{7-32}$$

where W and Q are as defined in (7-26) and (7-24). Performing the squaring operation, dropping cross products of off diagonal terms ($S_{MM'}$, $S_{NN'}$) which are zero according to (2-115) and (2-116), and dropping terms of fourth degree in ϕ, θ, and γ, (7-32) becomes

$$\rho_h = \frac{S_{XY}^2 + \phi^2 S_{XX}^2 + \gamma^2 S_{YZ}^2 + \phi\theta\gamma S_{XY}^2}{S_{YZ}^2 + \gamma^2 S_{XY}^2 + \phi^2 S_{XZ}^2 + \theta^2 S_{YZ}^2 + \phi\theta\gamma(S_{XX}S_{YY}^{*} + S_{XY}^2)} \tag{7-33}$$

Assuming now, that the third order terms, $\phi\theta\gamma$, are small compared to the second order terms, (7-33) becomes

$$\rho_h = \frac{S_{XY}^2 + \phi^2 S_{XX}^2 + \gamma^2 S_{YZ}^2}{S_{YZ}^2 + \gamma^2 S_{XY}^2 + \phi^2 S_{XZ}^2 + \theta^2 S_{YZ}^2}, \tag{7-34}$$

and recalling (2-115), that is

$$S_{NN'} = \left\{ \begin{array}{ll} \left[\dfrac{45\alpha^2 + 4\beta^2}{45}\right]\kappa & N = N' \\ \left[3\beta^2/45\right]\kappa & N = N' \end{array} \right\} \tag{2-115}$$

we have that

$$\rho_h = \frac{3\beta^2(1 + \gamma^2) + \phi^2(45\alpha^2 + 4\beta^2)}{3\beta^2(1 + \gamma^2 + \phi^2) + \theta^2(45\alpha^2 + 4\beta^2)} \tag{7-35}$$

or

$$\rho_h = \frac{1 + \gamma^2 + \phi^2/\rho_v}{1 + \gamma^2 + \phi^2 + \theta^2/\rho_v}, \tag{7-36}$$

where ρ_v is the vertical depolarization ratio.

The percentage error, PE, is given by

$$PE = \left[\frac{(\rho_h)_M - \rho_h}{\rho_h}\right] \times 100 \tag{7-37}$$

where $(\rho_h)_M$ is the measured value of ρ_h. Since the exact value of ρ_h is very near unity,

$$PE \simeq 100((\rho_h)_M - 1) \tag{7-38}$$

and combining (7-38) and (7-36) yields

$$\boxed{PE = 100 \frac{\phi^2(1 - \rho_v) - \theta^2}{\rho_v(1 + \gamma^2 + \phi^2) + \theta^2}} \tag{7-39}$$

This result, (7-39), is the solution to the percentage error in our measurement, as a function of the error angles, ϕ, θ, and γ, and may be used to quantitatively discuss the accuracy of a measurement of ρ_h.

At this point we shall examine the two limiting cases of (7-39), that is, the percentage error when ρ_v

is either unity or zero. When ρ_v is zero, we may write

$$PE = 100(\phi^2 - \theta^2)/\theta^2. \tag{7-40}$$

This result is rather interesting in that it predicts an increasing error as θ is reduced, when ϕ is larger than θ; and in that the error is independent of misalignment in the resolvers. A more realistic estimate of errors at small ρ_v is found by assuming a small, non-zero ρ_v so that (7-39) becomes

$$PE = 100(\phi^2 - \theta^2)/(\rho_v + \theta^2), \tag{7-41}$$

and the quantity ρ_v in the denominator limits the error when θ is reduced. Using the values found in Chapter III under Error Sources (page 100) for the error angles, we find that for ρ_v equal to zero

$$PE = -0.1135/.0018 = -63\% \tag{7-42}$$

that is, the measured horizontal depolarization ratio is 63 percent smaller than the actual value. Since the smallest ρ_v measurable with the photometer described previously is $\rho_v = 0.01$, we may ask with what accuracy we can measure ρ_h in this case. Using (7-41) we find that

$$PE = -0.1135/0.012 = -9.5\% \tag{7-43}$$

when $\rho_v = 0.01$.

In the case of large ρ_v we may rewrite (7-39) in the form,

$$PE = -100\ \theta^2/(1 + \theta^2 + \gamma^2 + \phi^2). \qquad (7\text{-}44)$$

This result is somewhat strange also, since increasing γ and ϕ tends to decrease the error. Substituting θ, ϕ, and γ in (7-44) yields for the large ρ_v,

$$PE = -0.16\%. \qquad (7\text{-}45)$$

Thus we have seen that misalignment errors do not affect ρ_h as seriously as they do ρ_v, and that the error due to beam parameters, θ, tends to reduce the value of ρ_h (assuming $\theta^2 > \phi^2$). Therefore, we may expect effects such as multiple scattering, increased beam diameter, and increased beam divergence to reduce ρ_h, whereas these same parameters tend to increase the measured ρ_v.

Substituting values for the error angles into (7-39) yields the numerical result,

$$PE = -\ (0.113 + 0.063\rho_v)/(\rho_v + 0.0018) \qquad (7\text{-}46)$$

which is graphed in Figure 7.2.

Calibration of the Differential Refractometer

In the measurement of the Rayleigh ratio of solutions, it is necessary to know the rate of change of refractive index with respect to concentration, dn/dc, very precisely. A number of instruments are available with which this quantity may be measured, however the differential refractometer is perhaps the most suitable choice. In

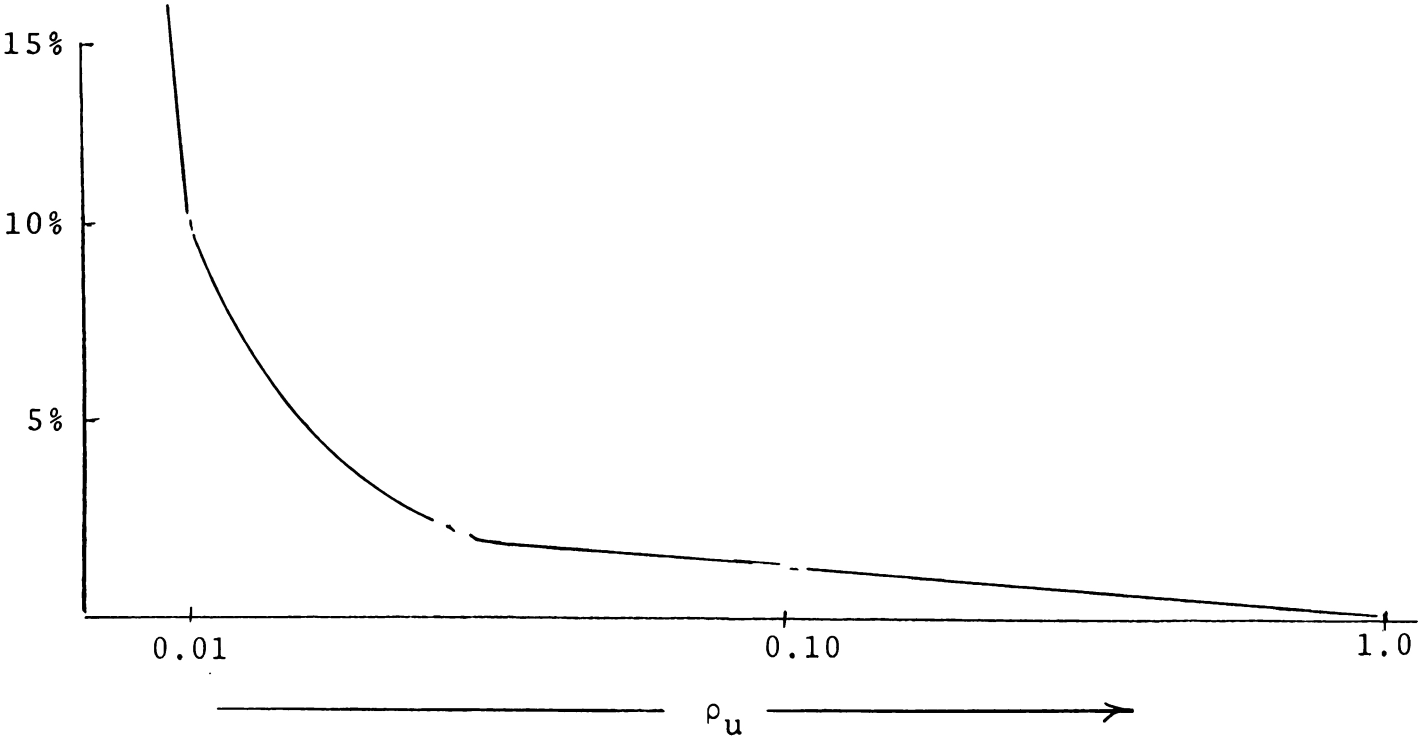

FIGURE 7.2.--Percentage Error in ρ_h as a Function of ρ_v.

this laboratory, a differential refractometer similar to the one described by Brice and Halwer[24] has been used to measure dn/dc at 632.8 nm.

Since it was necessary to obtain standards with which to calibrate the refractometer, the data of Kruis[25] were interpolated to obtain values at 632.8 nm. The interpolation was accomplished by using a least-squares fit of the data to a polynomial of degree n/2, in the wavelength; where n varied from one to (m-1), m being the number of data points. The best polynomial was chosen using the "Gauss criterion of fit," and was then used to calculate Δn at 632.8 nm. The results are presented in Table 7.1,

TABLE 7.1.--Difference in Refactive Index between Salt Solutions and Pure Water. (Temp. = 25°C)

Salt	Concentration(g/kg)	$\Delta n \times 10^5$
$K\,C\ell$	0.6986	9.510
NH_4NO_3	0.7905	9.687
$K\,C\ell$	1.0702	14.549
$Na\,C\ell$	0.9421	16.392
"	1.0371	18.064
NH_4NO_3	1.6775	20.497
$K\,C\ell$	2.8117	38.010
NH_4NO_3	3.4502	41.988
$Na\,C\ell$	3.3750	58.338
"	5.6274	96.750
NH_4NO_3	10.4082	125.07
$K\,C\ell$	10.8691	144.83
$Na\,C\ell$	6.9003	183.54
"	11.3107	192.60
"	20.5128	345.10
NH_4NO_3	29.4789	346.41
$Na\,C\ell$	37.8543	624.98
NH_4NO_3	60.7311	693.07
$Na\,C\ell$	69.0916	1107.62
"	108.9536	1688.20

and represent the difference in refractive index between the solution and pure solvent (water).

The results were checked by graphical interpolation and by measurement on the refractometer. The light source used in the measurements being the helium-neon laser described elsewhere in this work.

Comparison of Results

Comparison of the results reported here with those of other investigators is very difficult due to the differing conditions (i.e. wavelength, spatial characteristics of the source, sample purity, etc.), however Porto[31] has reported depolarization ratios measured with a helium-neon laser at a single temperature. Table 7.2 compares this data with those reported here, at the same temperature.

Comparison of Results

Molecule	Temp.	ρ_v (Porto)	ρ_v (this work)	Percent Diff.
Benzene	15°C	0.281	0.269	4
Toluene	15°C	0.359	0.336	6
Cyclohexane	≃25°C	0.0304	0.0188	50
$CC\ell_4$	≃25°C	0.0195	0.0166	14
$CHC\ell_3$	15°C	0.114	0.114	0

The results of this work are generally lower than those reported by Porto. Assuming no dust present in the samples, this indicates better alignment of the system in

our case. The only major difference is that of cyclohexane, however Porto did not specify a temperature for this data, and a valid comparison is therefore not possible.

Benoit and co-workers[32] have measured the depolarization of unpolarized light by Benzene at a number of temperatures. Although their data are not comparable due to the different wavelength, light source and instrument, it is interesting to note that their values of the depolarization ratio are larger than those reported here (calculated by assuming $\rho_h = 1$) as is to be expected, while the slope of their data is the same within experimental error.